

Sayak Roy

**Detailed Structural and Spectroscopic Studies on
Radical and Non-radical Ferrocenylcopper(I)
Complexes**

Detailed Structural and Spectroscopic Studies on Radical and Non-radical Ferrocenylcopper(I) Complexes

Von der Fakultät Chemie der Universität Stuttgart
Zur Erlangung der Würde eines
Doktors der Naturwissenschaften
(Dr. rer. nat.)
Genehmigte Abhandlung

vorgelegt von
Sayak Roy
aus Kalkutta (Indien)

Hauptberichter:

Prof. Dr. W. Kaim

Mitberichter:

Prof. Dr. Th. Schleid

Tag der mündlichen Prüfung

02.04.2009

Institut für Anorganische Chemie der Universität Stuttgart

2009

To my parents....

Acknowledgements

This work was completed from August 2005 to August 2008 at the Institute of Inorganic Chemistry, University of Stuttgart.

The completion of the work and the final writing would not have been possible without the help of various people. I would like to acknowledge all of them here.

First I would like to express my profound gratitude to my supervisor Prof. Dr. W. Kaim for giving me the opportunity and the facilities to carry out this thesis work in his group, for all his ideas and discussions and enormous encouragements.

Next I would like to thank Prof. Dr. Goutam Kumar Lahiri of Indian Institute of Technology, Bombay, India and Mr. Bholanath Mukherjee from Ramakrishna Mission Vivekananda Centenary College, Rahara, India for their continuous inspirations and motivation, Prof. Dr. Manish Bhattacharjee of Indian Institute of Technology, Kharagpur, India for helping me with the early lessons of chemistry and synthesis,

Dr. Biprajit Sarkar for his continuous help, encouragement and fruitful scientific discussions, Maa, baba for giving me the mental strength to face every single problem in life. Maa and Baba deserve special mention for their inseparable support and prayers. Words fail to express my appreciation to them.

I am particularly indebted to Pracheta for sharing every burdens, anxieties and pleasures of the study.

I would like to thank Dr. Carole Duboc from Grenoble High Magnetic Field Laboratory, France and once again to Dr. Biprajit Sarkar and for their enormous efforts in X-band and high field EPR measurements.

I am thankful to Ms. B. Förtsch for elemental analysis, Ms. K. Török for NMR measurements, Mr. J. Fiedler for spectroelectrochemical measurements and Dr. S. Zálíš for DFT calculation from the Heyrovský Institute of Physical Chemistry in Prague, Czech Republic,

Dr. F. Lissner, Dr. M. Niemeyer and Mr. Denis Bubrin from University of Stuttgart and Mr. S. Mobin from Indian Institute of Technology, Bombay, India for crystallographic data collection and solving crystal structures,

I convey my sincere thanks to Dr. Biprajit Sarkar once more for letting me know the basics of electrochemistry, EPR, spectroelectrochemistry and exposing me to various synthetic techniques, and for being an essential part of my thesis work.

Ms. Sumati Panicker-Otto and Ms. A. Winkelmann for helping me out with bureaucratic problems,

Mr. Ralf Hübner and again Dr. B. Schwederski for translating the summary,

Mr. Atanu Kumar Das (Universität Stuttgart, Germany), Dr. Poulomi Roy (Universität Erlangen-Nürnberg, Germany), Miss Tuli Dey (IIT, Kharagpur, India), Dr. Abhik Mukhopadhyay (Universidade Nova de Lisboa, Lisbon, Portugal) and Mr. Amit Kumar Roy (TU Chemnitz, Germany) to be there always as good friends,

Dr. Amarendranath Maity (Department of Physics, NDHU, Taiwan) for helping me initially with instrument handling and discussing scientific problems,

Orkan, Cüneat, Markus, Ralph, Johannes, Rajkumar and Hari for making my life much easier in Stuttgart with their support and help.

I also gratefully acknowledge Institut für Anorganische Chemie, Universität Stuttgart for financial support.

Finally I would like to thank all the past and present members of Prof. Kaim's and Dr. Sarkar's research group.

Contents

| | |
|--|-------|
| 1. Introduction | 1-6 |
| 2. The radical bridged Bis(ferrocenylcopper(I)) complexes with di-tertiarybutyl azodicarboxylate and di-isopropyl azodicarboxylate ligands: structural identity, multifrequency EPR, and spectroelectrochemistry. | 7-20 |
| 2.1 Introduction | 7 |
| 2.2 Synthesis and characterization | 9 |
| 2.3 Crystal structure | 10 |
| 2.4 Cyclic voltammetry | 12 |
| 2.5 UV-vis spectroelectrochemistry | 13 |
| 2.6 EPR spectroscopy | 15 |
| 2.7 Conclusion | 20 |
| 3. Establishing the chelating α-azocarbonyl function in π-acceptor ligands. | 21-33 |
| 3.1 Introduction | 21 |
| 3.2 Synthesis and characterization | 22 |
| 3.3 Crystal structure | 23 |
| 3.4 Cyclic voltammetry | 25 |
| 3.5 IR-spectroelectrochemistry | 28 |
| 3.6 UV-vis spectroelectrochemistry | 30 |
| 3.7 EPR spectroscopy | 32 |
| 3.8 Conclusion | 33 |
| 4. Mononuclear and dinuclear ferrocenylcopper complexes bridged by 2,2'-azobispyridine and its anion radical: structural electrochemical and spectroelectrochemical properties. | |
| 4.1 Introduction | 34 |
| 4.2 Synthesis and characterization | 35 |
| 4.3 Crystal structures | 37 |
| 4.4 Cyclic voltammetry | 42 |
| 4.5 UV-vis spectroelectrochemistry | 44 |
| 4.6 EPR spectroscopy | 48 |

| | |
|---|--------------|
| 4.7 Conclusion | 52 |
| 5. Stabilizing the elusive ortho-quinone/copper(I) oxidation state combination through π-π interaction in an isolated complex. | 53-63 |
| 5.1 Introduction | 53 |
| 5.2 Synthesis and characterization | 54 |
| 5.3 Crystal structure | 56 |
| 5.4 UV-vis spectroscopy | 58 |
| 5.5 Cyclic voltammetry | 58 |
| 5.6 EPR spectroscopy | 60 |
| 5.7 DFT and TD DFT calculation | 61 |
| 5.8 Conclusion | 62 |
| 6. Heterohexanuclear (Cu_3Fe_3) Complexes of Substituted Hexaazatrinaphthylene (HATN) Ligands: Twofold BF_4^- Association in the Solid and Stepwise Oxidation or Reduction to Spectroelectrochemically Characterized Species. | 64-81 |
| 6.1 Introduction | 64 |
| 6.2 Synthesis and characterization | 65 |
| 6.3 Crystal structure | 67 |
| 6.4 Cyclic voltammetry | 71 |
| 6.5 UV-vis-NIR spectroelectrochemistry | 74 |
| 6.6 EPR spectroscopy | 78 |
| 6.7 Conclusion | 81 |
| 7. Experimental section. | 82-98 |
| 7.1 Instrumentation | 82 |
| 7.2 Solvents and working conditions | 83 |
| 7.3 Syntheses | |
| 7.3.1 Synthesis of copper(I) precursors | 84 |
| 7.3.2 Synthesis of dinuclear Cu complex with adcOR ligands | 85 |
| 7.3.3 Synthesis of mono-nuclear Cu complexes with adc-NR ₂ ligands | 86 |
| 7.3.4 Synthesis of Cu complexes with abpy | 87 |
| 7.3.5 Synthesis of Cu complex with 9,10-phenanthroquinone | 89 |
| 7.3.6 Synthesis of tri-nuclear Cu complexes with different substituted diquinoxalino- | |

| | |
|---|---------|
| [2,3-a:2',3'-c]phenazine (dqp) ligands. | 89 |
| 7.4 Crystallography | |
| 7.4.1 $\{(\mu\text{-adcO}^t\text{Bu})[\text{Cu}(\text{dppf})]_2\}(\text{PF}_6)$ | 92 |
| 7.4.2 $[\text{Cu}^{\text{I}}(\text{adc-pip})(\text{dppf})](\text{BF}_4)$ | 93 |
| 7.4.3 $\{(\text{abpy})[\text{Cu}(\text{dppf})]\}\text{BF}_4$ | 94 |
| 7.4.4 $\{(\mu\text{-abpy})[\text{Cu}(\text{dppf})]_2\}(\text{BF}_4)$ | 95 |
| 7.4.5 $\{(\text{PhenQ})[\text{Cu}(\text{dppf})]\}\text{BF}_4$ | 96 |
| 7.4.6 $[(\mu_3\text{-dqp})\{\text{Cu}(\text{dppf})\}_3](\text{BF}_4)_3$ | 97 |
| 8. Summary | 99-107 |
| 9. Zusammenfassung | 108-116 |
| Appendix | |
| Bibliography | 117-124 |
| Abbreviations | 125-128 |
| Curriculum Vitae. | 129 |

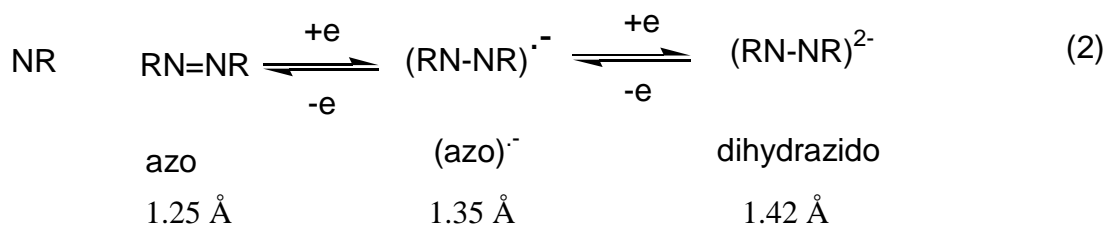
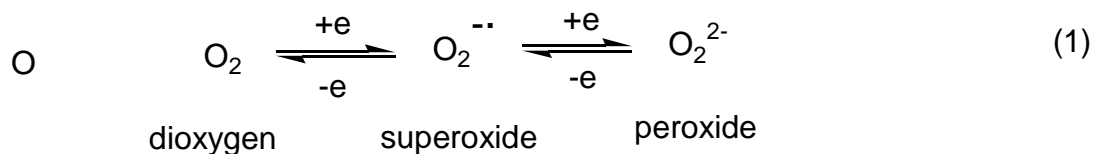
Chapter 1

Introduction.

Copper is an essential trace element in all living organisms. It is found in the active sites of several enzymes that catalyze biochemical reactions such as the oxidation of ascorbic acid, amino acids, phenols, amines, sugars and the ferrous ion.^{[1][2]} The role of copper as dioxygen carrier in arthropods and mollusks has also been well established. While surveying the known copper proteins and their functions in biology, it is found that copper can exist in two oxidation states, either as Cu^{I} (d^{10}) or Cu^{II} (d^9), which are interconvertible under physiological conditions. The ligand donors in proteins are mostly the imidazole group from histidine, the phenolic oxygen donor of tyrosine, or the sulfur donors from cysteine or methionine.

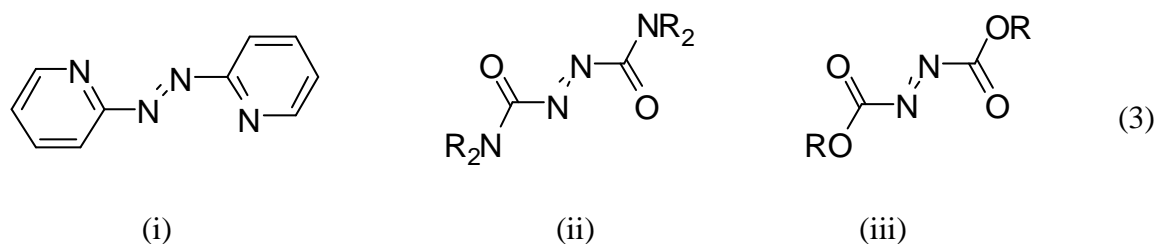
For several decades, the nature of copper containing active sites in proteins have been intensively studied by many research groups because of unusual coordination geometries and outstanding redox, absorption or electron paramagnetic resonance features.^[3-9] Based on structural and spectroscopic properties, at least three types of active sites are distinguished.^[10] The copper proteins which have the geometry in between that of Cu^{II} (square planar) and Cu^{I} (tetrahedral) and a set of cysteine ligands are in type 1, proteins with spectroscopic and structural features similar to typical Cu^{II} are in type 2, and two antiferromagnetically coupled bridged Cu^{II} centers coordinated by histidine are found in the class of type 3. Whereas the classical oxidation-reduction (i.e. 'redox') activity of the enzymes does indeed play a key role in enzyme activity, the exact role of copper and cuproenzymes in biological systems is not always well established. The redox activity of such enzymes is governed by the tuning of oxidation states ($\text{Cu}^{\text{I}}/\text{Cu}^{\text{II}}$) and ligands like O_2 ($\text{O}_2/\text{O}_2^-/\text{O}_2^{2-}$), NO ($\text{NO}/\text{NO}^\cdot/\text{NO}^-$), phenoxyl (phenoxyl/phenolate) or o-quinones (quinone/semiquinone/catecholate).^[11] As a result, 'model systems' in inorganic chemistry which are analogous to those enzymes always plays an important role in broadening our understanding.^[6,12]

In view of the capability of copper enzymes and cuproproteins to produce intermediate radical species,^[1,16] there is an interest in the exploration of the coordination chemistry of copper with azo ($-\text{N}=\text{N}-$) based ligands. Like dioxygen, the azo group can undergo successive two step one-electron reduction via the intermediacy of a radical species (1 and 2)^[3] due to its low

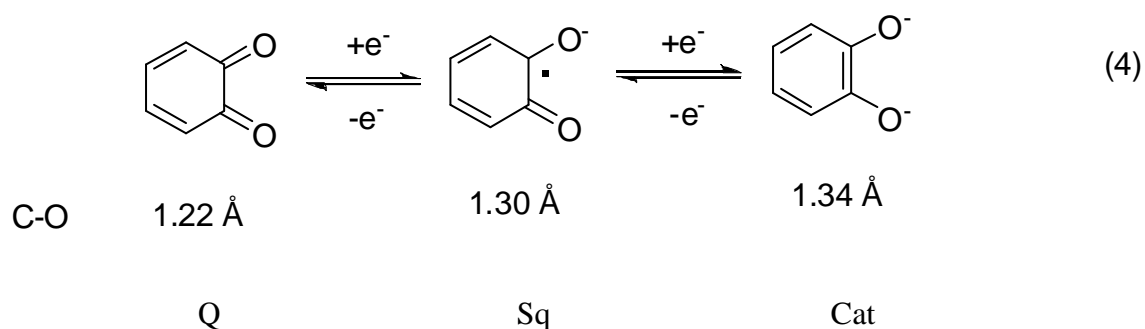


lying π^* orbital. The distinct change in the N-N distance on successive reduction facilitates the structural identification of the particular redox state of the azo group present in the complex.^[11]

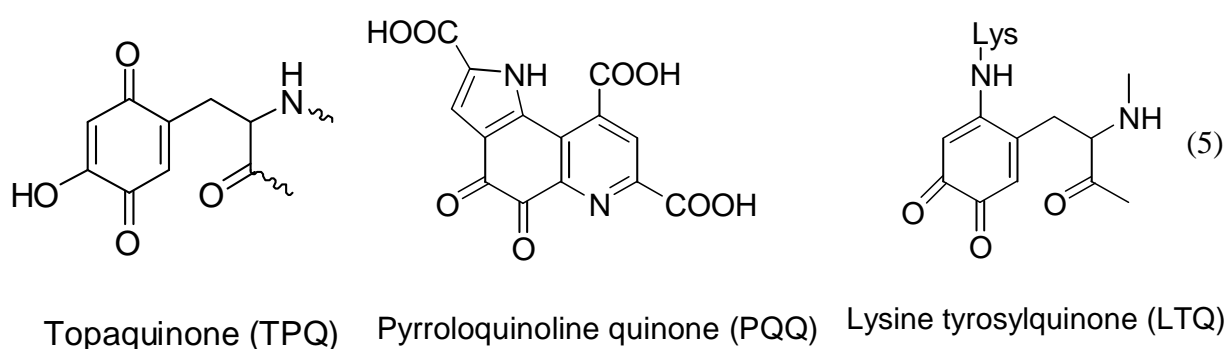
In this doctoral work the following azo-based ligands (3), (i) 2,2'-azobispyridine (abpy), (ii) esters of azodicarboxylic acids (adc-OR) and (iii) amides of azodicarboxylic acids (adc-NR₂) have been used in obtaining copper complexes. The S-frame bis-bidentate chelators (3) can bridge two metal complex fragments with small metal-metal distance ($\sim 5 \text{ \AA}$). The low-lying π^* orbitals of the azo functions in (i)-(iii) facilitate the stabilization of anion radical complexes.



Like dioxygen or the azo function, the binding ability of *o*-quinones (4) in different redox states^[11] (catecholate, Cat; semiquinone, Sq; quinone, Q) with the metal ions allows them to play an important role in biology. Copper containing oxidases

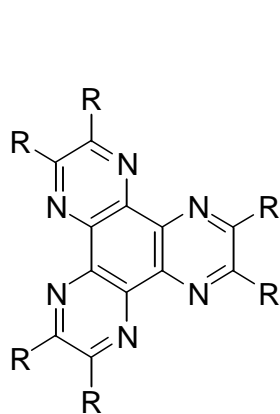


such as amine oxidase which catalyze oxidative deamination of primary amines to aldehydes, contain quinones as co-factors. For some time, this quinonoid co-factor has been assumed to be pyrroloquinoline quinone (PQQ),^[19,20] however, subsequent work has reformulated it as topaquinone (TPQ).^[21] Another copper enzyme, lysyl oxidase, uses a similar co-factor lysine tyrosylquinone (LTQ).^[19,20,21] A well studied cupro-enzyme, tyrosinase,^[22] which is very essential in bacteria, fungi, plants and animals, catalyzing hydroxylation of phenols to catechols (phenolase activity) and catechols to quinones (catecholase activity), also involves Cu-quinone type interaction. Moreover, the copper based catalytic oxidation of phenol under mild condition is of great interest for industrial and synthetic processes both from an economic and environmental point of view. It is widely used in dual objectives of removal of phenolic wastes in industrial effluents and surface water streams and secondly to achieve regioselective oxidation to useful products.^[23] Several mechanistic pathways have been proposed involving Cu-quinone intermediates. Hence, it is very important to study the Cu-quinone interaction, particularly for the better understanding of biochemical and chemical processes.



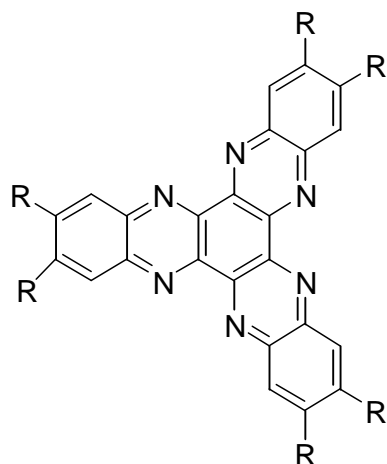
In this context, a number of examples of Cu^{I} -semiquinone^[24-27] or Cu^{II} -catecholate^[28,29] complexes have been described, however, an isolated and structurally characterized Cu^{I} -quinone combination is missing in the literature, possibly due to the fact of lower basicity of the oxygen donors in the fully oxidized quinone form.

The trinucleating nitrogen heterocyclic molecule 1,4,5,8,9,12-hexaazytriphenylene (HAT)^[30] and the related 1,6,7,12,13,18-hexaazatrinaphthylene (HATN)^[31] or its hexamethyl or hexachloro derivatives ($\text{R} = \text{H}, \text{Cl}, \text{Me}$) (6) have been studied in the context of their coordination to metal ions, of photo-physical properties, liquid crystalline ordering, light harvesting and DNA binding properties.^[32-36]



$\text{R} = \text{H}$

1,4,5,8,9,12-Hexaazatriphenylene (HAT)



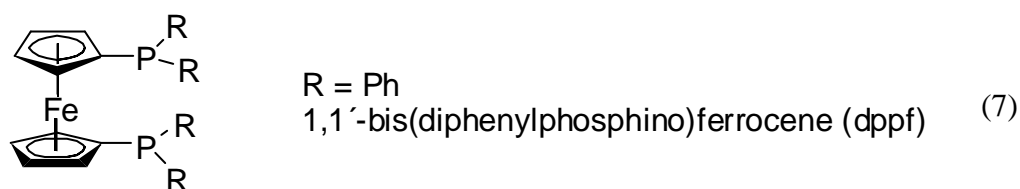
(6)

1,6,7,12,13,18-Hexaazatrinaphthylene
($\text{R} = \text{H}$, HATN; $\text{R} = \text{CH}_3$ HATN-Me₆; $\text{R} = \text{Cl}$ HATN-Cl₆)

However, these ligands have not yet been explored extensively like other nitrogen containing heterocycles (bipyridines, phenanthrolines), presumably due to their multistep synthetic procedure and poor solubility in common solvents. Despite the inherent problems some studies since the late 1980s have established the potential applications of HAT based ligands and the corresponding metal complexes in photochemical, supramolecular, magnetic and biochemical areas.^[37,38,39] The ruthenium, rhodium and rhenium complexes of HAT ligands are often used in photocytotoxicity, DNA binding and as staining agents.^[40,41] On the other hand the copper, cobalt and nickel complexes are used as supramolecular building blocks in coordination polymers.^[42-44] The primary reasons behind their application are: (i) availability of three chelating sites for the binding of several metal ions which can trigger the construction of metal-assembled systems, (ii) characteristic π -acceptor feature leading to low-energy

metal-ligand charge transfer transitions, and (iii) C_3 symmetry leading to degenerate orbitals.^[33(a)]

Furthermore, co-ligands also impart a significant role in tuning the overall electronic properties of the complexes. Thus, tertiary phosphines are known to be good co-ligands for stabilizing Cu^I .^[45,46] Therefore, a wide variety of tertiary mono- and di-phosphine based ligands have been used in synthesizing different Cu^I complexes. In the last years a new generation of phosphine ligands having a ferrocene backbone has become popular in chemistry (7). Bis(diphenylphosphine) containing ferrocene complexes are used quite often as ligands due to their tunable stereochemistry by appropriate ring tilting and twisting, variable co-ordination modes, electrochemical and catalytic properties.^[47]



Therefore, the primary intentions behind the use of dppf as co-ligand for the present study are: (i) stabilizing copper specifically in the +1 oxidation state within the complexes, (ii) extending greater stability to the complex molecules due to the small bite-angle, (iii) electron transfer properties available due to redox-active ferrocene moiety associated with the dppf unit which can be studied electrochemically and spectroscopically, and (iv) studying electronic communication between two or more ferrocene units in di-nuclear or poly-nuclear complexes.

In this doctoral work, several redox non-innocent ligands were used for binding with the ferrocenylcopper(I) centers. The new complexes thus synthesized (stated in subsequent chapters) were characterized by structural, spectroscopic and electrochemical techniques.

Chapter 2 describes the synthesis and characterization of dicopper(I) complexes, $[(\mu\text{-adcO}^t\text{Bu})\{Cu^I(\text{dppf})\}_2](PF_6)$ and $[(\mu\text{-adcO}^i\text{Pr})\{Cu^I(\text{dppf})\}_2](PF_6)$ where the bridging azodicarboxylic esters (adcO^tBu = di-tertbutyl azodicarboxylate and adcO^iPr = di-isopropyl azodicarboxylate) (3(iii)) exist in the radical state. The complexes have been characterized by standard analytical techniques and UV-vis spectroelectrochemical studies. The paramagnetic radical complexes have been investigated by X-band and high frequency EPR spectroscopy.

Chapter 3 deals with the complexation of $[\text{Cu}(\text{dppf})]^+$ with azodicarboximide ligands (3(ii)) which gives rise to mononuclear copper(I) species $[(\text{dppf})\text{Cu}^{\text{I}}(\text{adc-pip})](\text{BF}_4)$ and $[(\text{dppf})\text{Cu}^{\text{I}}(\text{adc-NMe}_2)](\text{BF}_4)$ (adc-pip = azodicarboxylic dipiperidide and adc-NMe_2 = N,N,N',N'-tetramethylazodicarboxamide). The complexes have been characterized by ^1H , ^{31}P NMR, X-ray crystallography and electrochemistry. The stabilization of the unusual non-reduced azodicarbonyl state of the ligands in the complexes has been investigated in details by IR-UV-vis spectroelectrochemistry and EPR in accessible redox states.

Chapter 4 describes the interaction of ferrocenylcopper(I) with the potentially dinucleating 2,2'-azobispyridine (abpy) ligand (3(i)) which leads to the formation of mononuclear copper(I) species, $[(\text{abpy})\{\text{Cu}^{\text{I}}(\text{dppf})\}]\text{BF}_4$ and dicopper(I) complexes, $[(\mu\text{-abpy})\{\text{Cu}^{\text{I}}(\text{dppf})\}_2](\text{BF}_4)_2$, bridged by the neutral abpy and $[(\mu\text{-abpy})^-\{\text{Cu}^{\text{I}}(\text{dppf})\}_2](\text{BF}_4)$ bridged by the radical state of abpy. The crystal structures of monocopper(I) and radical bridged dicopper(I) complexes have been determined. Moreover, spectroelectrochemical features of the complexes are studied in accessible redox states and the paramagnetic states are investigated by EPR.

Chapter 5 highlights the unusual stabilization of the Cu(I)-quinone combination in structurally and spectroscopically characterized $[(\text{dppf})\text{Cu}^{\text{I}}(o\text{-phenanthrenequinone})](\text{PF}_6)$. A deeper understanding of the interplay between copper ions and redox active phenol based ligands is important not only because this interaction is essential in enzymes but also because it is highly relevant for technical processes like hydroxylation of aromatic and other organic compounds. The stabilization of the elusive Cu^{I} -quinone state in the said complex has been established by experiment and theory.

Chapter 6 covers the isolation of hexanuclear complexes $[(\mu_3\text{-L})\{\text{Cu}(\text{dppf})\}_3](\text{BF}_4)_3$ where the three $\{\text{dppf}\text{Cu}^{\text{I}}\}$ units are bridged by hexaazatrinaphthylene (L, R=H, Me, Cl) (6). The crystal structure of the representative complex with R = H shows a 'Host-Guest' mode between the coordinated bridging ligand and the counter anions such that two BF_4^- anions are trapped on each side of the planar bridging ligand. Spectroelectrochemical aspects in accessible redox states and EPR of the paramagnetic states have been looked into.

Chapter 2

The radical bridged Bis(ferrocenylcopper(I)) complexes with di-tertiarybutyl azodicarboxylate and di-isopropyl azodicarboxylate ligands: structural identity, multifrequency EPR, and spectroelectrochemistry.

2.1 Introduction:

For many years the azodicarbonyl esters (adcOR) are well known organic reagents for Diels-Alder reaction,^[48] Click chemistry,^[49] Mitsunobu^[50] and Mitsunobu type of reactions. The molecule consists of a central azo (N=N) functional group flanked by two alkyl and aryl esters. The azodicarboxylic esters and related azodicarbonyl (adcR) molecules are part of a two-step redox series $\text{adcR}^{0/\bullet-/-2-}$ (Fig 2.1.1) which involves a unique combination of redox and coordination properties.^[17,51] Similarly as in quinones the oxidized form is a strongly π accepting but poorly σ donating form whereas the dianionic state is stabilized by a resonance situation. Of the just six conjugated π centers four can strongly interact with two bridged metals in a bis-chelate fashion while the remaining carbon atoms can be functionalized with donor/acceptor^[52] or coordinating^[53] substituents. The metals are held together in the $\text{adcR}^{0/\bullet-/-2-}$ bridged situation at a rather short distance of about 5 Å or less.^[55] The use of the $\mu\text{-adcR}^{0/\bullet-/-2-}$ system has been demonstrated for diruthenium,^[52,53] diosmium,^[54] dirhenium^[51] and also dicopper(I)^[55-58] complexes. The latter included EPR studies of the ¹⁴N, ³¹P, ⁶³Cu and ⁶⁵Cu hyperfine structure in radical complexes^[56] as formed by electron transfer assisted reactions from copper metal,^[55] a high-frequency EPR investigation^[57] and a detailed DFT study have also been reported^[58]. A structure determination confirmed the “inverse cryptate” situation for the radical cation $\{(\mu\text{-adcO}^t\text{Bu})[\text{Cu}(\mu\text{-bdph})]_2\}^+$, bdph = 1,6-bis(diphenylphosphino)hexane, where the radical center appears to be shielded by the long chain diphosphines and the metals instead of the nitrogen atoms serve as bridgeheads.^[55]

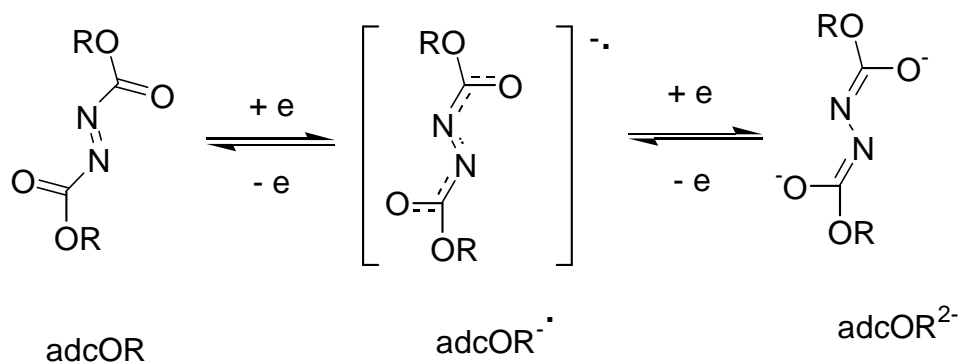


Fig 2.1.1: Stepwise one electron reduction of azodicarbonyl esters (adcOR).

Functionalized ferrocene derivatives have frequently been employed as redox-active terminal groups.^[47,59-61] The well established^[61] 1,1'-bis(diphenylphosphinoferrocene) ligand (dppf) and other ferrocene end groups have thus been used to probe intramolecular electronic communication across organic or organometallic species in molecular arrays, including light induced processes^[47,59], in addition to their structure-determining function for organic catalysis.^[61]

This chapter describes the result of combining dppf with two other components of metallasupramolecular^[64] species, viz., copper(I) as π -electron donating metal centers for connecting chelating π acceptor ligands,^[66-68] and a non-innocent bridging ligands, di-*tert.*-butylazodicarboxylic ester (adcO^tBu) or di-*iso.*-propylazodicarboxylic ester (adcOⁱPr). The synthesis, molecular structure and the spectroelectrochemical characterization of $\{(\mu\text{-adcO}^t\text{Bu})[\text{Cu}(\text{dppf})]_2\}(\text{PF}_6)$ and $\{(\mu\text{-adcO}^i\text{Pr})[\text{Cu}(\text{dppf})]_2\}(\text{PF}_6)$ are reported in this chapter. The paramagnetic compounds have been studied using both conventional X band EPR at 9.5 GHz and high-frequency EPR at 285 GHz.^[57] Cyclic voltammetry and UV/Vis/NIR spectroelectrochemistry using an OTTLE cell^[69] are being used to elucidate the site of oxidation processes, this being the first structurally characterized example involving such different oxidizable groups ($2 \times \text{Fc}$, $2 \times \text{Cu}^{\text{I}}$, and an organic radical anion) in close proximity.

2.2 Synthesis and characterization:

The complexes were synthesized through a general procedure by reacting activated Cu powder, dppf and azodicarboxylic esters in methanol (2% water) in air. This is apparently water and O₂-requiring reaction yielded radical bridged heterotetranuclear radical complexes $\{(\mu\text{-adcO}^t\text{Bu})[\text{Cu}(\text{dppf})]_2\}(\text{PF}_6)$ and $\{(\mu\text{-adcO}^i\text{Pr})[\text{Cu}(\text{dppf})]_2\}(\text{PF}_6)$ (Fig 2.2.1).

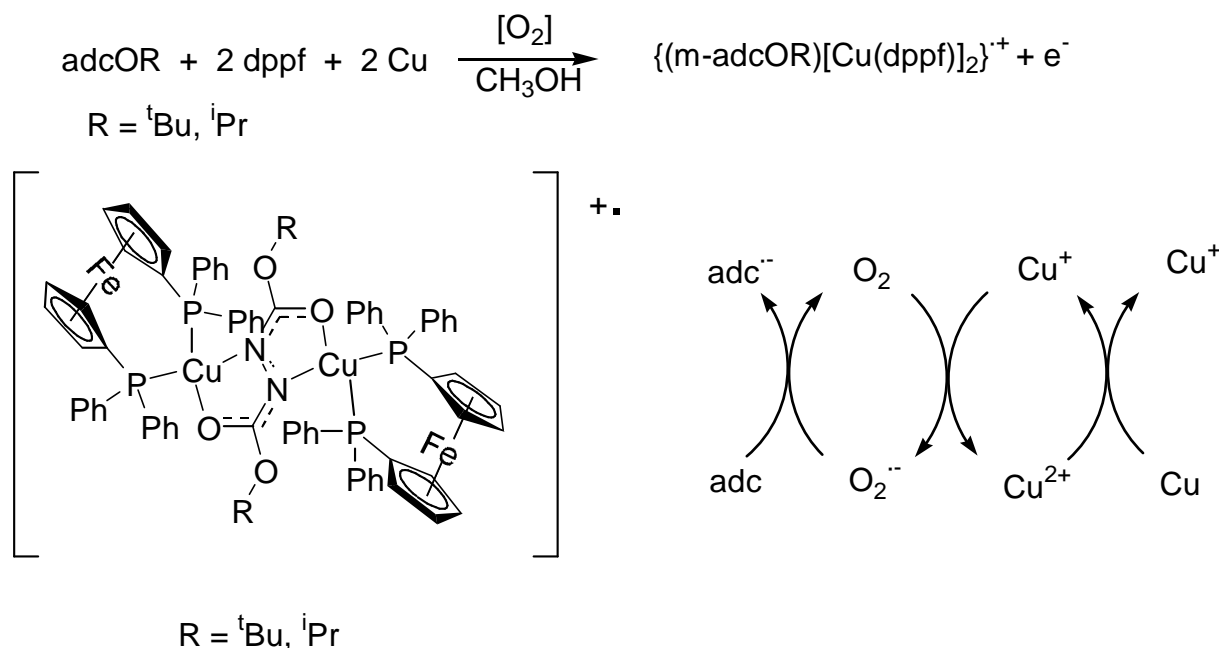


Figure 2.2.1: General reaction scheme and mechanism.

Due to paramagnetism a ¹H NMR spectrum was not obtained. The compounds were initially characterized by elemental analysis and IR spectroscopy. Single crystal of $\{(\mu\text{-adcO}^t\text{Bu})[\text{Cu}(\text{dppf})]_2\}(\text{PF}_6)$ for X-ray diffraction was obtained from CH₂Cl₂/hexane at 4°C. IR spectrum in CH₂Cl₂ solution shows C-O stretching at 1597 and 1579 cm⁻¹ for $\{(\mu\text{-adcO}^t\text{Bu})[\text{Cu}(\text{dppf})]_2\}(\text{PF}_6)$ and $\{(\mu\text{-adcO}^i\text{Pr})[\text{Cu}(\text{dppf})]_2\}(\text{PF}_6)$ respectively where as for the free ligands adcO^tBu and adcOⁱPr, the ν_{C=O} are 1760 and 1755 cm⁻¹ (Tab 2.2.1).

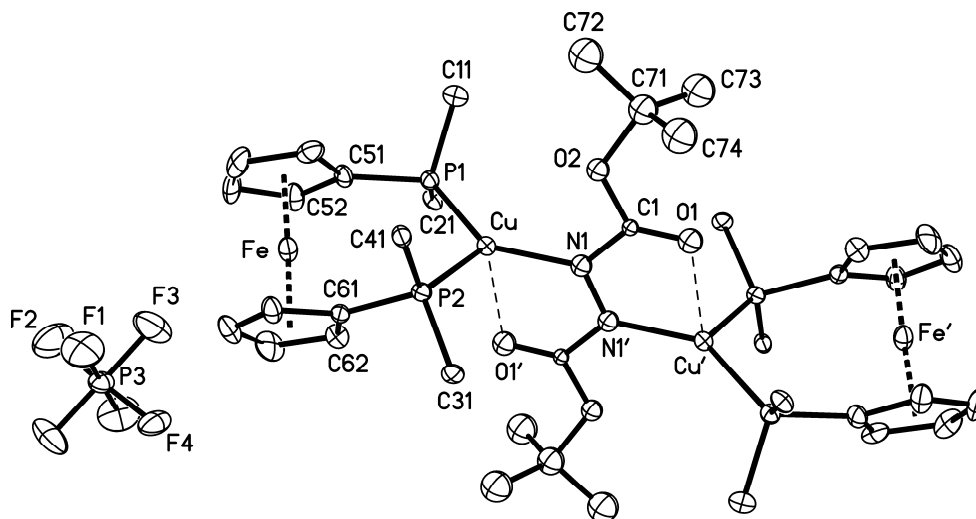
Tab 2.2.1: IR data^{a)} for the ligands and complexes.

| Compound | ν _{C=O} / cm ⁻¹ |
|---|-------------------------------------|
| adcO ^t Bu | 1760 |
| $\{(\mu\text{-adcO}^t\text{Bu})[\text{Cu}(\text{dppf})]_2\}(\text{PF}_6)$ | 1597 |
| adcO ⁱ Pr | 1755 |
| $\{(\mu\text{-adcO}^i\text{Pr})[\text{Cu}(\text{dppf})]_2\}(\text{PF}_6)$ | 1579 |

^{a)}in CH₂Cl₂ solution

2.3 Crystal Structure:

Deep blue prism-shaped crystals could be obtained by slow diffusion of diethyl ether in the solution of CH_2Cl_2 at 4°C . This crystal was measured at 173 K. The complex $\{(\mu\text{-adcO}^t\text{Bu})[\text{Cu}(\text{dppf})]_2\}(\text{PF}_6)$ was crystallized in $P2_1/m$ space group. The molecular structure of the complex is shown in the Fig 2.3.1. Even the limited structural information due to severe disorder reveals an anion radical formulation for the central adcO^tBu bridge. N-N (azo) distance is 1.28-1.38 Å. The metal-metal distances are 4.78 Å (Cu-Cu) and 12.55 Å (Fe-Fe). The ferrocene axes are oriented at 40.5° relative to the central CuOCNNCOCu plane. The molecular structure of the complex is shown in fig 2.3.1 and important bond lengths and bond angles are tabulated in tab 2.3.1



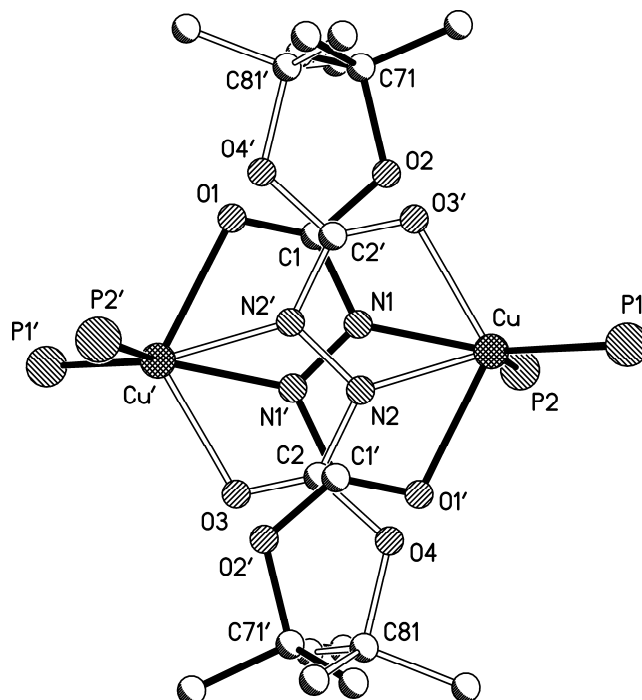


Figure 2.3.1: (top) Molecular structure of $\{(\mu\text{-adcO}^t\text{Bu})[\text{Cu}(\text{dppf})]_2\}\text{PF}_6$ in crystal; (bottom) central part of the molecular structure of $\{(\mu\text{-adcO}^t\text{Bu})[\text{Cu}(\text{dppf})]_2\}^+$ showing the disorder in azocarboxylate moiety

Table 2.3.1: Important bond lengths (\AA) and bond angles ($^\circ$) for complex $\{(\mu\text{-adcO}^t\text{Bu})[\text{Cu}(\text{dppf})]_2\}\text{PF}_6$

| Bond lengths (\AA) | | Bond angles ($^\circ$) and dihedral angles | |
|-------------------------------|------------|--|-----------|
| Cu-N1 | 1.965(12) | P1-Cu-P2 | 112.16(7) |
| Cu-N2 | 1.971(10) | P1-Cu-N1 | 135.0(3) |
| Cu-P1 | 2.2374(18) | P1-Cu-N2 | 135.3(3) |
| Cu-P2 | 2.263(2) | P2-Cu-N2 | 107.9(3) |
| Cu-O1' | 2.309(11) | P2-Cu-N1 | 112.0(3) |
| Cu-O3' | 2.209(10) | N1-Cu-O1' | 74.2(4) |
| N1-N1' | 1.31(2) | P1-Cu-O1' | 110.1(3) |
| N2-N2' | 1.40(2) | P2-Cu-O1' | 95.1(3) |
| C1-N1 | 1.42(3) | N2-Cu-O3' | 76.1(4) |
| C1-O1 | 1.214(19) | P1-Cu-O3' | 109.7(2) |
| C1-O2 | 1.35(2) | P2-Cu-O3' | 106.4(2) |
| C2-N2 | 1.38(3) | | |
| C3-O3 | 1.195(18) | | |
| C2-O4 | 1.37(2) | | |

2.4 Cyclic voltammetry

Because of the presence of three kinds of oxidizable centers in the complexes $\{(\mu\text{-adcO}^t\text{Bu}^{\bullet-})[\text{Cu}^{\text{I}}(\text{dppf})_2]\}(\text{PF}_6)$ and $\{(\mu\text{-adcO}^i\text{Pr})[\text{Cu}(\text{dppf})_2]\}(\text{PF}_6)$, i.e. iron(II), copper(I) and $\text{adcOR}^{\bullet-}$, cyclic voltammetry is employed to check the electrochemical feature. The already reported Cu(I) complexes with adcO^tBu , $\{(\mu\text{-adcO}^t\text{Bu})[\text{Cu}(\text{bdph})_2]\}^+$ and $\{(\mu\text{-adcO}^t\text{Bu})[\text{Cu}(\text{bdpp})_2]\}^+$ ($\text{bdpp} = 1,5\text{-bis}(\text{diphenylphosphino})\text{pentane}$) were also isolated in the radical bridged form.^[55,56] Hence it could be oxidised electrochemically by removing one e^- from singly occupied π^* level and reduced by putting one extra e^- to the singly occupied π^* level. In $\text{CH}_2\text{Cl}_2/0.1 \text{ M Bu}_4\text{NPF}_6$ the first oxidation process is represented by a separated one-electron wave at $+0.22 \text{ V}$ vs. $\text{Fc}^{+/0}$; which is attributed to the transition $\text{adcO}^t\text{Bu}^{(\bullet-)\rightarrow(0)}$ in $\{(\mu\text{-adcO}^t\text{Bu})[\text{Cu}(\text{dppf})_2]\}^{(+)\rightarrow(2+)}$. The next oxidation wave at 0.51 V exhibits twice the current (Fig 2.4.1) but shows a slightly non-Nernstian behaviour on the reverse scan. This feature is associated with the oxidation of two widely separated (12.55 \AA) and not conjugatively coupled ferrocene moieties. Other oxidation waves corresponding to the copper(I/II) conversion or phosphine oxidation were not observed below 1.3 V , presumably due to the accumulated high charge. One-electron reduction was possible at -0.85 V , a process associated again with the electroactive bridge $\text{adcO}^t\text{Bu}^{(\bullet-)\rightarrow(2-)}$.

Similarly in the complex $\{(\mu\text{-adcO}^i\text{Pr})[\text{Cu}(\text{dppf})_2]\}(\text{PF}_6)$, a quasi-reversible oxidation at $+0.32 \text{ V}$ ($\text{adcO}^i\text{Pr}^{(\bullet-)\rightarrow(0)}$), an irreversible reduction at -0.70 V ($\text{adcO}^i\text{Pr}^{(\bullet-)\rightarrow(2-)}$) and one reversible two electron ferrocene ancillary based oxidation at 0.534 V vs. $\text{Fc}^{0/+}$ were observed.

The cyclic voltammogram of $\{(\mu\text{-adcO}^t\text{Bu})[\text{Cu}(\text{dppf})_2]\}\text{PF}_6$ is shown in fig 2.4.1 and the potentials for $\{(\mu\text{-adcO}^t\text{Bu})[\text{Cu}(\text{dppf})_2]\}\text{PF}_6$ and $\{(\mu\text{-adcO}^i\text{Pr})[\text{Cu}(\text{dppf})_2]\}(\text{PF}_6)$ are tabulated in tab 2.4.1.

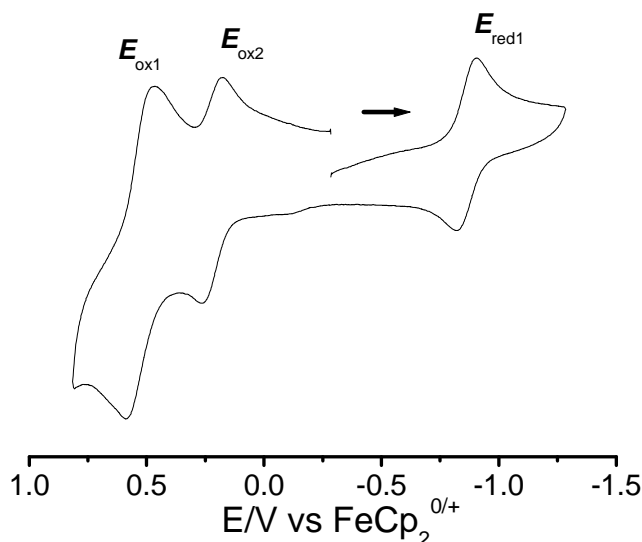


Figure 2.4.1: Cyclic voltammogram of $\{(\mu\text{-adcO}^t\text{Bu})[\text{Cu}(\text{dppf})]_2\}^+$ in CH_2Cl_2 / 0.1 M Bu_4NPF_6 at room temperature (scan rate 100 mV/s)

Tab 2.4.1: Electrochemical Data^{a)}:

| Compound | E_{ox1} | E_{ox2} | E_{red1} |
|---|--------------------|---------------------|---------------------|
| $(\text{adcO}^t\text{Bu})^-$ ^[11] | - | -1.13 ^{b)} | -1.84 ^{b)} |
| $\{(\mu\text{-adcO}^t\text{Bu})[\text{Cu}(\text{bdph})]_2\}^+$ ^[54] | - | 0.29 ^{c)} | -0.87 ^{c)} |
| $\{(\mu\text{-adcO}^t\text{Bu})[\text{Cu}(\text{bdpp})]_2\}^+$ ^[54] | - | 0.5 ^{c)} | -0.87 ^{c)} |
| $\{(\mu\text{-adcO}^t\text{Bu})[\text{Cu}(\text{PPh}_3)_2]_2\}^+$ ^[63] | - | 0.25 ^{c)} | -0.74 ^{c)} |
| $\{(\mu\text{-adcO}^t\text{Bu})[\text{Cu}(\text{dppf})]_2\}^+$ ^[70] | 0.51 ^{c)} | 0.22 ^{c)} | -0.85 ^{c)} |
| $\{(\mu\text{-adcO}^i\text{Pr})[\text{Cu}(\text{dppf})]_2\}^+$ | 0.53 ^{c)} | 0.32 ^{c)} | -0.70 ^{b)} |

^{a)} In CH_2Cl_2 / 0.1 M Bu_4NPF_6 at RT. Potentials in V vs. Fc/Fc^+ ; ^{b)} cathodic peak potentials corresponding to irreversible peak; ^{c)} half-wave potential corresponding to reversible step.

2.5 UV-vis Spectroelectrochemistry

UV-vis spectroelectrochemistry of $\{(\mu\text{-adcO}^t\text{Bu})[\text{Cu}(\text{dppf})]_2\}\text{PF}_6$ and $\{(\mu\text{-adcO}^i\text{Pr})[\text{Cu}(\text{dppf})]_2\}\text{PF}_6$ were performed using Optically Transparent Thin Layer Electrochemical (OTTLE) cell. The spectroelectrochemical oxidation for complex $\{(\mu\text{-adcO}^t\text{Bu})[\text{Cu}(\text{dppf})]_2\}\text{PF}_6$ and $\{(\mu\text{-adcO}^i\text{Pr})[\text{Cu}(\text{dppf})]_2\}(\text{PF}_6)$ are shown in Fig 2.5.1 and 2.5.2 and the absorption data of all redox steps for complexes $\{(\mu\text{-adcO}^t\text{Bu})[\text{Cu}(\text{dppf})]_2\}\text{PF}_6$ and $\{(\mu\text{-adcO}^i\text{Pr})[\text{Cu}(\text{dppf})]_2\}\text{PF}_6$ are summarized in Tab 2.5.1.

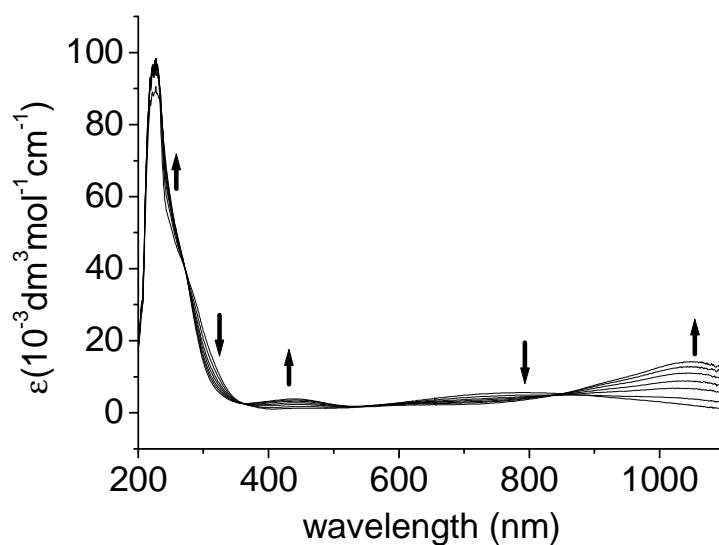


Figure 2.5.1: Spectroelectrochemical oxidation of $\{(\mu\text{-adcO}^t\text{Bu})[\text{Cu}(\text{dppf})]_2\}(\text{PF}_6)$ in $\text{CH}_2\text{Cl}_2/0.1$ M Bu_4NPF_6 .

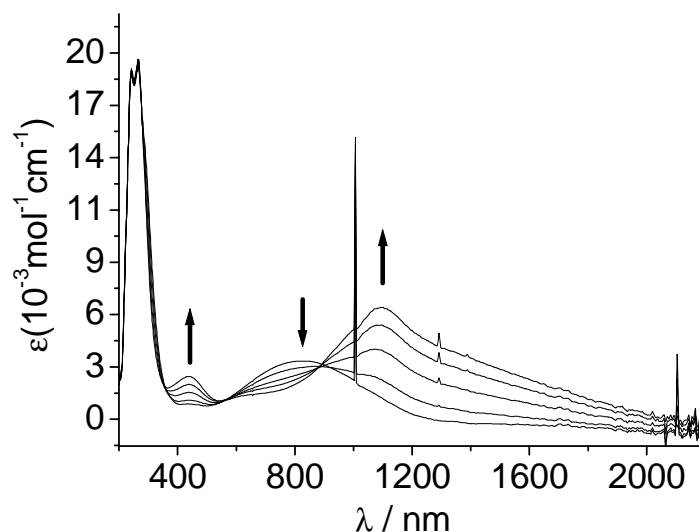


Figure 2.5.2: Spectroelectrochemical oxidation of $\{(\mu\text{-adcO}^t\text{Pr})[\text{Cu}(\text{dppf})_2]\}(\text{PF}_6)$ in $\text{CH}_2\text{Cl}_2/0.1 \text{ M Bu}_4\text{NPF}_6$.

Table 2.5.1: UV-vis-NIR Spectroelectrochemical Data^{a)}:

| Compound | $\lambda_{\text{max}}^{\text{b)}} (\epsilon \times 10^{-3} \text{ M}^{-1} \text{ cm}^{-1})^{\text{c)}}$ |
|--|---|
| $\{(\mu\text{-adcO}^t\text{Bu})[\text{Cu}(\text{bdph})_2]\}^{2+}$ [54] | 1100 |
| $\{(\mu\text{-adcO}^t\text{Bu})[\text{Cu}(\text{bdpp})_2]\}^{\cdot+}$ [54] | 700 |
| $\{(\mu\text{-adcO}^t\text{Bu})[\text{Cu}(\text{dppf})_2]\}^{4+}$ [70] | 440(4.11) |
| $\{(\mu\text{-adcO}^t\text{Bu})[\text{Cu}(\text{dppf})_2]\}^{2+}$ [70] | 248(sh), 440(4.11), 1043(10.43) |
| $\{(\mu\text{-adcO}^t\text{Bu})[\text{Cu}(\text{dppf})_2]\}^{\cdot+}$ [70] | 798(4.04) |
| $\{(\mu\text{-adcO}^t\text{Bu})[\text{Cu}(\text{dppf})_2]\}^{[70]}$ | 368(sh) |
| $\{(\mu\text{-adcO}^t\text{Pr})[\text{Cu}(\text{dppf})_2]\}^{4+}$ | 424(5.00) |
| $\{(\mu\text{-adcO}^t\text{Pr})[\text{Cu}(\text{dppf})_2]\}^{2+}$ | 438(2.35), 1091(6.13) |
| $\{(\mu\text{-adcO}^t\text{Pr})[\text{Cu}(\text{dppf})_2]\}^{\cdot+}$ | 824(3.22) |
| $\{(\mu\text{-adcO}^t\text{Pr})[\text{Cu}(\text{dppf})_2]\}$ | 397(sh) |

^{a)} from spectroelectrochemistry in OTTLE cell in $\text{CH}_2\text{Cl}_2 / 0.1 \text{ M Bu}_4\text{NPF}_6$. ^{b)} wavelengths in nm. ^{c)} molar extinction coefficient in $\text{M}^{-1} \text{ cm}^{-1}$

The blue radical complex exhibits a very broad long-wavelength band at about 800 nm absorption maximum ($\epsilon = 4000 \text{ M}^{-1} \text{ cm}^{-1}$). The band is attributed to a metal-to-ligand charge transfer (MLCT) transition $d(\text{Cu}^{\text{I}}) \rightarrow \pi^*(\text{adcO}^t\text{Bu}^{\cdot-})$ involving the two copper(I) donors and the π accepting radical anion $\text{adcO}^t\text{Bu}^{\cdot-}$ with its half-empty π^* orbital. On reversible one-electron oxidation that band intensifies and shifts to 1043 nm maximum ($\epsilon = 10400 \text{ M}^{-1} \text{ cm}^{-1}$, Figure 2.5.1). It still represents the $d(\text{Cu}^{\text{I}}) \rightarrow \pi^*(\text{adcO}^t\text{Bu})$ MLCT transition, however, the π^*

MO is now completely depopulated and energetically destabilized which explains both the intensity increase and the bathochromic shift. A weaker, probably second MLCT band emerges in the visible, at 440 nm with $\epsilon = 4100 \text{ M}^{-1} \text{ cm}^{-1}$. It is possible, on the other hand, to investigate the reversible reduction of the radical complex to the neutral form $\{(\mu\text{-adcO}^t\text{Bu})[\text{Cu}(\text{dppf})]_2\}^{(+)\rightarrow(0)}$. This process resulted in the complete disappearance of the long-wavelength MLCT bands because of the complete filling of the $\pi^*(\text{adcO}^t\text{Bu})$ orbital, some intensity was increasing in the UV region at about 370 nm as a shoulder.

The complex $\{(\mu\text{-adcO}^i\text{Pr})[\text{Cu}(\text{dppf})]_2\}^{+}$ shows a broad MLCT based transition band at 824 nm which upon first oxidation shifts to 1090 nm (Fig 2.5.2). The reduction of $\{(\mu\text{-adcO}^i\text{Pr})[\text{Cu}(\text{dppf})]_2\}^{+}$ can not be studied due to irreversibility.

These spectroelectrochemical data are almost identical with the complexes reported in earlier work.^[54] Oxidised species $\{(\mu\text{-adcO}^t\text{Bu})[\text{Cu}(\text{bdph})]_2\}^{2+}$ shows an absorption band at 1100 nm due to $d(\text{Cu}^I) \rightarrow \pi^*(\text{adcO}^t\text{Bu})$ transition and isolated radical bridged species $\{(\mu\text{-adcO}^t\text{Bu})[\text{Cu}(\text{bdpp})]_2\}^{+}$ shows a 700 nm band which is attributed to MLCT transition from $d(\text{Cu}^I)$ to π^* of $(\text{adcO}^t\text{Bu}^\bullet)$ (Tab 2.5.1).

The two electron oxidation of ferrocenyl ancillaries in the complexes $\{(\mu\text{-adcO}^t\text{Bu})[\text{Cu}(\text{dppf})]_2\}^{4+}$ and $\{(\mu\text{-adcO}^i\text{Pr})[\text{Cu}(\text{dppf})]_2\}^{4+}$ can not be studied spectroelectrochemically because of the disintegration of the complexes.

2.6 EPR spectroscopy:

3.5.1. Theory

Electron Paramagnetic Resonance (EPR) is the ideal spectroscopic method for identification and characterization of radicals and metal-centred spin. In the present case the paramagnetic species are radical complexes where an anion radical ligand is bound to diamagnetic transition metals (Cu^I). EPR gives three sources of information.

The isotropic g value: Deviations of g from the free electron value g_e can be attributed to the contribution of other excited states with non-zero angular momentum to the radical ground state. They arise from spin-orbit interactions which are proportional to the spin-orbit coupling constants of the involved atoms which increases with the atomic number as Z^5 . The sign of the deviation is indicative of the frontier orbital situation according to Stone's approximation (Eq. 3.5.1.1.).

$$g = g_e - \frac{2}{3} \sum_i \sum_n \sum_{kj} \frac{\langle \Psi_0 | \xi_k L_{ik} \delta_k | \Psi_n \rangle \langle \Psi_n | L_{ij} \delta_j | \Psi_0 \rangle}{E_n - E_0} = g_e + \Delta g_s$$

$$g_e = 2.0023$$

Ψ_0 : MO of the unpaired electron in the ground state

Ψ_n : all other MOs

ξ_k : spin-orbit coupling constant

$L_{ik/ij}$: angular momentum operator for AO at nucleus k, j

$L_{ik} \delta_k = 0$ except at atom k

E_0 : energy of a singly occupied molecular orbital (SOMO)

E_n : energies of empty or doubly occupied molecular orbitals (LUMO or HOMO)

Considering the denominator of the equation, only the neighboring levels have a significant contribution to Δg . This means that heavy atoms which are bound near the radical center have a large effect on the g value. However, two cases are possible:

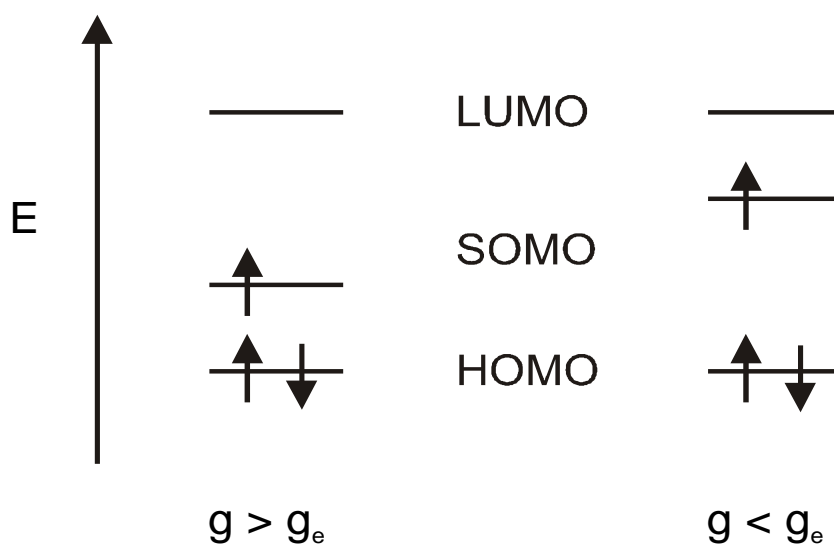


Fig. 3.5.1.1.: Energy level diagram.

If $E_0 > E_n$, a deviation to higher values than g_e is to be expected. This means that the SOMO lies closer to the HOMO than to the LUMO.

If $E_0 < E_n$, the SOMO lies closer to LUMO than to the HOMO.

Even though anion radical complexes of transition metal fragments usually display rather small deviations of g_{iso} from g_e ($\Delta g_s \leq \pm 0.02$) because the spin is mainly delocalized over the light atoms from the ligand with small spin-orbit coupling constants, the characteristic

changes on going from the ligand anion radical to the complexes can provide valuable information on the orbital ordering.

The g anisotropy ($\Delta g = g_1 - g_3$) from measurements of powders or glassy frozen solutions is largely a result of contributions from elements with high spin-orbit coupling constants. In the EPR spectra of transition metal complexes where the spin is predominantly on the metal centre, the g -anisotropy is usually quite large. However, in the case of transition metal complexes with anion radical ligands the g anisotropy is generally small, even in species which contain 5d metal centers like osmium or rhenium. Moreover, the broadness of the lines, sometimes in adjunction with insufficiently resolved metal hyperfine splitting, can preclude the determination of the expected g anisotropy for complexes with heavy transition metal elements at conventional EPR frequencies (X band). Thus, it is often necessary to go to high fields / high frequencies (≥ 95 GHz) to resolve it.

The hyperfine coupling between the unpaired electron and the various nuclei of the radical species is another most informative source of insight from EPR. Ideally, all nuclei with non-zero nuclear spins should couple to a certain extent with the unpaired electron and thus reveal the nature of the SOMO. Unfortunately, it is not always possible to obtain such information from conventional EPR experiments: the intrinsic line-width may be too large for the resolution of the hyperfine structure, the dominant metal hyperfine splitting can obscure the hyperfine splitting from the spin-bearing ligand atoms, and the low natural abundance and / or low nuclear magnetic moment of isotopes can lead to undetectable hyperfine coupling.

Results:

The complexes being discussed in this chapter are all stable radical. Hence these paramagnetic complexes are the origin for EPR signal in native state. At X-band (9.5 GHz) in CH_2Cl_2 solution the complexes show a typical line-rich spectrum at $g_{\text{iso}} = 2.0112$ for $\{(\mu\text{-adcO}^t\text{Bu})[\text{Cu}(\text{dppf})]_2\}^{\cdot+}$ and 2.0117 for $\{(\mu\text{-adcO}^i\text{Pr})[\text{Cu}(\text{dppf})]_2\}^{\cdot+}$ (fig 2.6.1 and 2.6.2). In both the cases the hyperfine coupling from two $^{63,65}\text{Cu}$, two ^{14}N and four ^{31}P were observed which is very much comparable to $\{(\mu\text{-adcO}^t\text{Bu})[\text{Cu}(\text{PPh}_3)_2]_2\}^{\cdot+}$, $\{(\mu\text{-adcO}^t\text{Bu})[\text{Cu}(\text{bdpp})]_2\}^{\cdot+}$ and $\{(\mu\text{-adcO}^t\text{Bu})[\text{Cu}(\text{bdph})]_2\}^{\cdot+}$.^[9,10] To determine the g anisotropy the high frequency EPR (285 GHz) was measured at 5 K which revealed the three g components in glassy or frozen solution (fig 2.6.1 and 2.6.2). The rhombic g splitting is very typical to this kind of azo radical anion compounds involving Cu(I). The small g anisotropy confirms the predominant localization of spin in the bridging ligand. Hyperfine coupling constants and anisotropic g tensors are tabulated below in Tab 2.6.1.

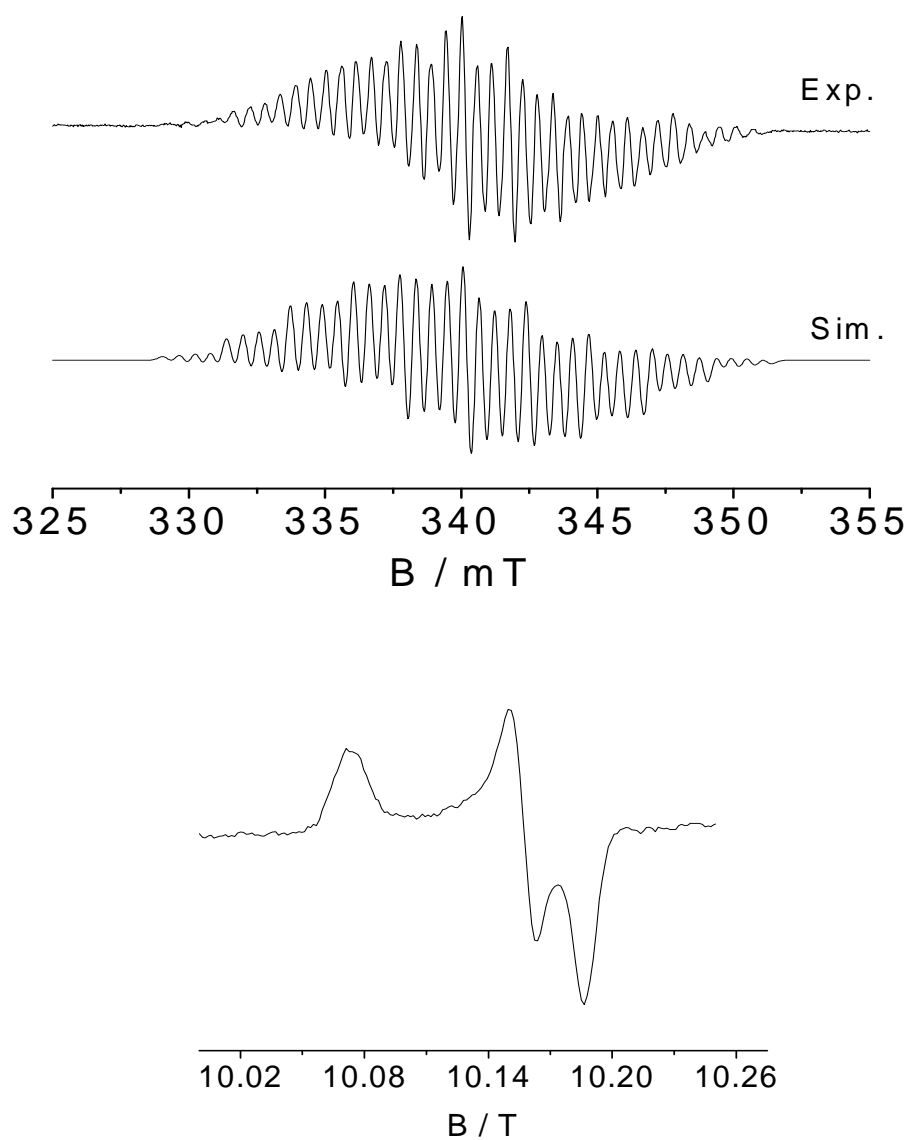


Figure 2.6.1: X-band EPR spectrum of $\{(\mu\text{-adcO}^t\text{Bu})[\text{Cu}(\text{dppf})]_2\}^+$ at 298 K in CH_2Cl_2 (top); High field EPR spectrum (285 GHz) at 5 K in MeCN / n-PrCN (1:1) (bottom)

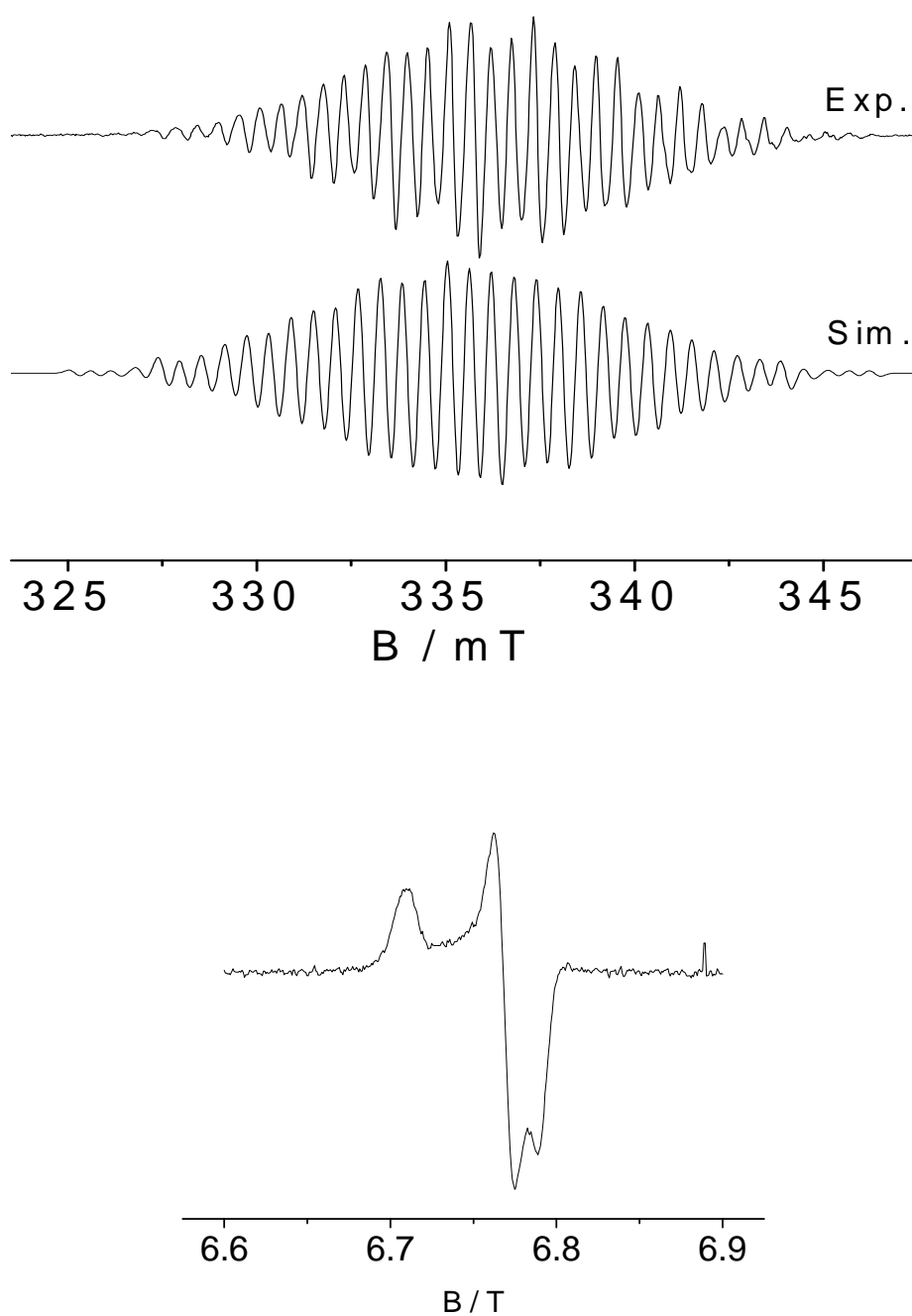


Figure 2.6.2: X-band EPR spectrum of $\{(\mu\text{-adcO}^i\text{Pr})[\text{Cu}(\text{dppf})_2]\}^+$ at 298 K in CH_2Cl_2 (top); High field EPR spectrum (285 GHz) at 5 K in MeCN / n-PrCN (1:1) (bottom)

Table 2.6.1: EPR data

| Compound | $g_1^a)$ | $g_2^a)$ | $g_3^a)$ | $g_{iso}^b)$ | $a(^{63/65}\text{Cu})^c)$ | $a(^{14}\text{N})^c)$ | $a(^{31}\text{P})^c)$ |
|--|----------|----------|----------|--------------|---------------------------|-----------------------|-----------------------|
| $(\text{adcO}^t\text{Bu})^-$ | - | - | - | - | - | 0.478 | - |
| $\{(\mu\text{-adcO}^t\text{Bu})[\text{Cu}(\text{dppf})_2]^+\}^{[70]}$ | 2.022 | 2.005 | 1.999 | 2.011 | 1.675 | 0.573 | 2.35 |
| $\{(\mu\text{-adcO}^t\text{Pr})[\text{Cu}(\text{dppf})_2]^+\}$ | 2.022 | 2.005 | 2.002 | 2.011 | 1.76 | 0.54 | 2.38 |
| $\{(\mu\text{-adcO}^t\text{Bu})[\text{Cu}(\text{PPh}_3)_2]^+\}^{[55]}$ | d) | d) | d) | 2.0102 | 1.607, 1.721 | 0.640 | 1.872 |
| $\{(\mu\text{-adcO}^t\text{Bu})[\text{Cu}(\text{bdpp})_2]^+\}^{[55]}$ | d) | d) | d) | 2.0098 | 1.570 | 0.634 | 1.856 |
| $\{(\mu\text{-adcO}^t\text{Bu})[\text{Cu}(\text{bdph})_2]^+\}^{[55]}$ | 2.022 | 2.009 | 2.002 | 2.0104 | 1.681 | 0.64 | 1.85 |

^{a)}from High field EPR measurements at 5 K in MeCN / n-PrCN (1:1); ^{b)} from X-band EPR measurements at 298 K in CH₂Cl₂; ^{c)}hyperfine coupling constants in mT; ^{d)} not measured.

2.7 Conclusion:

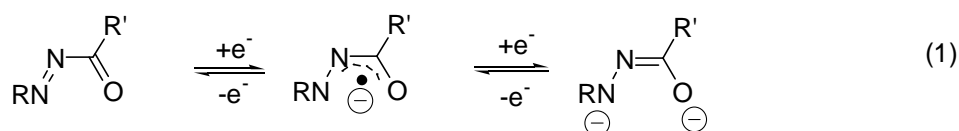
In this chapter structural and spectroscopic feature of stable dicopper(I) radical bridged complexes with the esters of azodicarboxylic acids as bridging ligand and ferrocenylphosphine as ancillary ligands is demonstrated. Due to native state paramagnetism the compounds show well resolved EPR spectrum in X-band having hyperfine coupling from two Cu, two N and four P. High field EPR measurement shows typical rhombic g-anisotropy of the spectrum. Ligand centered one electron oxidation and reduction was monitored by electrochemistry and corresponding spectral change was examined in UV-vis spectroelectrochemistry. The redox feature of the ferrocenyl ancillaries were also observed electrochemically and spectroelectrochemically. The large separation between the two ferrocenyl ancillaries (12.55 Å) is responsible for poor communication between them.

Chapter 3

Establishing the chelating α -azocarbonyl function in π -acceptor ligands.

3.1 Introduction

Four-center two-step redox systems (1) with coordinating heteroatoms in 1,4-positions have long played a prominent role in coordination chemistry as potentially non-innocent ligands (eq. 1).^[71] The combination RNNC(R')O, coupling π electron deficient^[72] carbonyl and azo functions, has been observed and structurally established in doubly and singly reduced form,^[52,55,56,70] however, the unreduced group N=N-C=O was not yet described as part of a metal chelate system. As for example in the earlier chapter (Chapter 2) isolation and spectroscopic characterization of the compounds, having singly reduced chelate with ferrocenylcopper(I) moiety, is described.



In contrast to the earlier work, in this chapter, the first structurally isolated such hetero-dinuclear compounds with unreduced N=N-C=O group are reported.^[73] The ligands azodicarboxylic dipiperidide (adc-pip) and N,N,N',N'-tetramethylazodicarboxamide (adc-NMe₂) (Fig: 3.1.1) having identical chelating sites and similar redox nature like other azodicarbonyl compounds, are chosen to serve the purpose of non-innocent ligands.

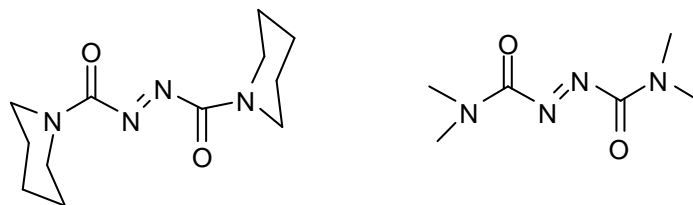


Fig: 3.1.1: Ligands azodicarboxylic dipiperidide (adc-pip) and N,N,N',N'-tetramethylazodicarboxamide (adc-NMe₂)

These complexes were characterized by ^1H , ^{31}P NMR, IR spectroscopy, elemental analysis and X-ray crystal structure diffraction.^[73] The spectral properties of in situ generated species were studied by UV-vis-IR and EPR spectroelectrochemistry.

3.2 Synthesis and characterization

The complexes $[\text{Cu}^{\text{I}}(\text{adc-pip})(\text{dppf})](\text{BF}_4)$ and $[\text{Cu}^{\text{I}}(\text{adc-NMe}_2)(\text{dppf})](\text{BF}_4)$ were synthesized by following a general procedure described for one of the complexes (Fig 3.2.1). The precursor complex $[\text{Cu}(\text{dppf})(\text{CH}_3\text{CN})_2]\text{BF}_4$ were made according to the literature procedure.^[74] Stirring the mixture of 1 equiv. of $[\text{Cu}(\text{dppf})(\text{CH}_3\text{CN})_2]\text{BF}_4$ and 1 equiv of adc-pip in dry CH_2Cl_2 at room temperature for 8 h gives a dark violet solution which on removal of solvent, produces dark violet crystalline solid $[\text{Cu}^{\text{I}}(\text{adc-pip})(\text{dppf})](\text{BF}_4)$. The complexes were initially characterized by ^1H (Tab 3.2.1), ^{31}P NMR. Mass spectroscopy dose not give any useful information due to fragmentation during ionization process.

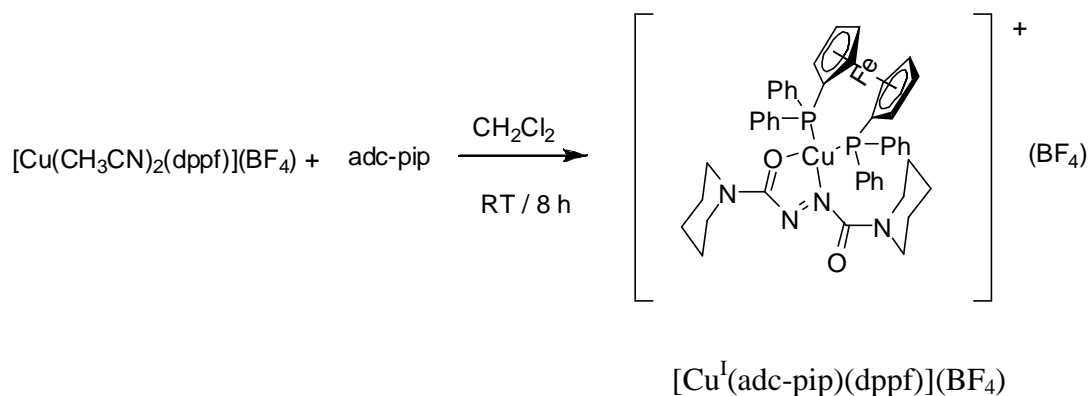


Fig 3.2.1: general reaction scheme for the synthesis of $[\text{Cu}^{\text{I}}(\text{adc-pip})(\text{dppf})](\text{BF}_4)$.

Table 3.2.1: NMR data^{a)} for the complexes.

| Compound | δ / ppm |
|--|---|
| adc-pip | 1.63(m, 3H), 3.41(m, 1H), 3.70(m, 1H) |
| $[\text{Cu}^{\text{I}}(\text{adc-pip})(\text{dppf})](\text{BF}_4)$ | 1.61-1.82(m, pip), 3.42(m, pip), 3.75(m, pip), 4.32(s, 4H, Cp), 4.52(s, 4H, Cp), 7.35 (m, 20H, Ph). |
| adc-NMe ₂ | 3.0(s,6H), 3.15(s,6H) |
| $[\text{Cu}^{\text{I}}(\text{adc-NMe}_2)(\text{dppf})](\text{BF}_4)$ | 2.98(s, 6H, CH ₃), 3.16(s, 6H, CH ₃) 4.32(s, 4H, Cp), 4.40(s, 4H, Cp), 7.42 (m, 20H, Ph). |

^{a)} in CD_2Cl_2 at RT

IR spectrum for $[\text{Cu}^{\text{I}}(\text{adc-pip})(\text{dppf})](\text{BF}_4)$ gives two sharp $\nu_{\text{C=O}}$ at 1672 cm^{-1} , for coordinated carbonyl and at 1703 cm^{-1} , for non-coordinated C=O. Similarly for $[\text{Cu}^{\text{I}}(\text{adc-NMe}_2)(\text{dppf})](\text{BF}_4)$, bands in the IR region appear at 1680 (coordinated C=O) and 1713 (non-coordinated C=O) cm^{-1} (Tab 3.2.2). The free ligand shows only one carbonyl stretching band because of symmetry. The appearance of two C=O bands for the complexes is an identification of metal coordination at only one of the carbonyl groups. The elemental analysis data is given in experimental section.

Table 3.2.2: IR data^{a)} for the ligands and complexes.

| Compound | $\nu_{\text{C=O}} / \text{cm}^{-1}$ |
|--|--|
| adc-pip | 1694 |
| $[\text{Cu}^{\text{I}}(\text{adc-pip})(\text{dppf})](\text{BF}_4)$ | 1672 (metal coordinated), 1703 (non-coordinated) |
| adc-NMe ₂ | 1695 |
| $[\text{Cu}^{\text{I}}(\text{adc-NMe}_2)(\text{dppf})](\text{BF}_4)$ | 1680 (metal coordinated), 1713 (non-coordinated) |

^{a)} in solid

3.3 Crystal structure

The dark-violet crystal of $[\text{Cu}^{\text{I}}(\text{adc-pip})(\text{dppf})](\text{BF}_4)$ was grown by slow diffusion of hexane in CH_2Cl_2 at 4°C . It was crystallized in monoclinic $P2_1/n$ space group. One molecule of H_2O was found as a solvent of crystallization. The molecular structure shows how one of the N=N-C=O functions chelates the copper(I) center of heterodinuclear $[\text{Cu}(\text{dppf})]^+$ without being reduced to the monoanionic (radical) or dianionic form. This assignment follows not only from the composition of the material but also from the analysis of the strongly alternating interchelate bonds with lengths $d_{\text{N=N}} = 1.258(7) \text{ \AA}$, $d_{\text{C-N}} = 1.466(8) \text{ \AA}$, and $d_{\text{C=O}} = 1.234(7) \text{ \AA}$. Apparently there is relatively little π back donation from this form of copper(I), which might otherwise lengthen the double bonds and shorten the single bond or even cause an eventual reduction of the ligand. With $d_{\text{Cu-N}} = 1.990(5) \text{ \AA}$ and $d_{\text{Cu-O}} = 2.170(4) \text{ \AA}$ the metal chelation is rather asymmetric, in agreement with the different basicities of N and O; the dihedral angle between the P1-Cu-P2 and O1-Cu-N2 planes is 87.14° so that the configuration at the metal can be described as distorted tetrahedral. The stability of the situation with unreduced N=N-C=O is probably favoured by the rigidity of heterodinuclear $[\text{Cu}(\text{dppf})]^+$ complex fragment.

The non-coordinated C=O bond length is 1.216(7) Å. Important bond lengths and bond angles are given in the Tab 3.3.1. The distance between Cu...Fe is 4.048 Å.

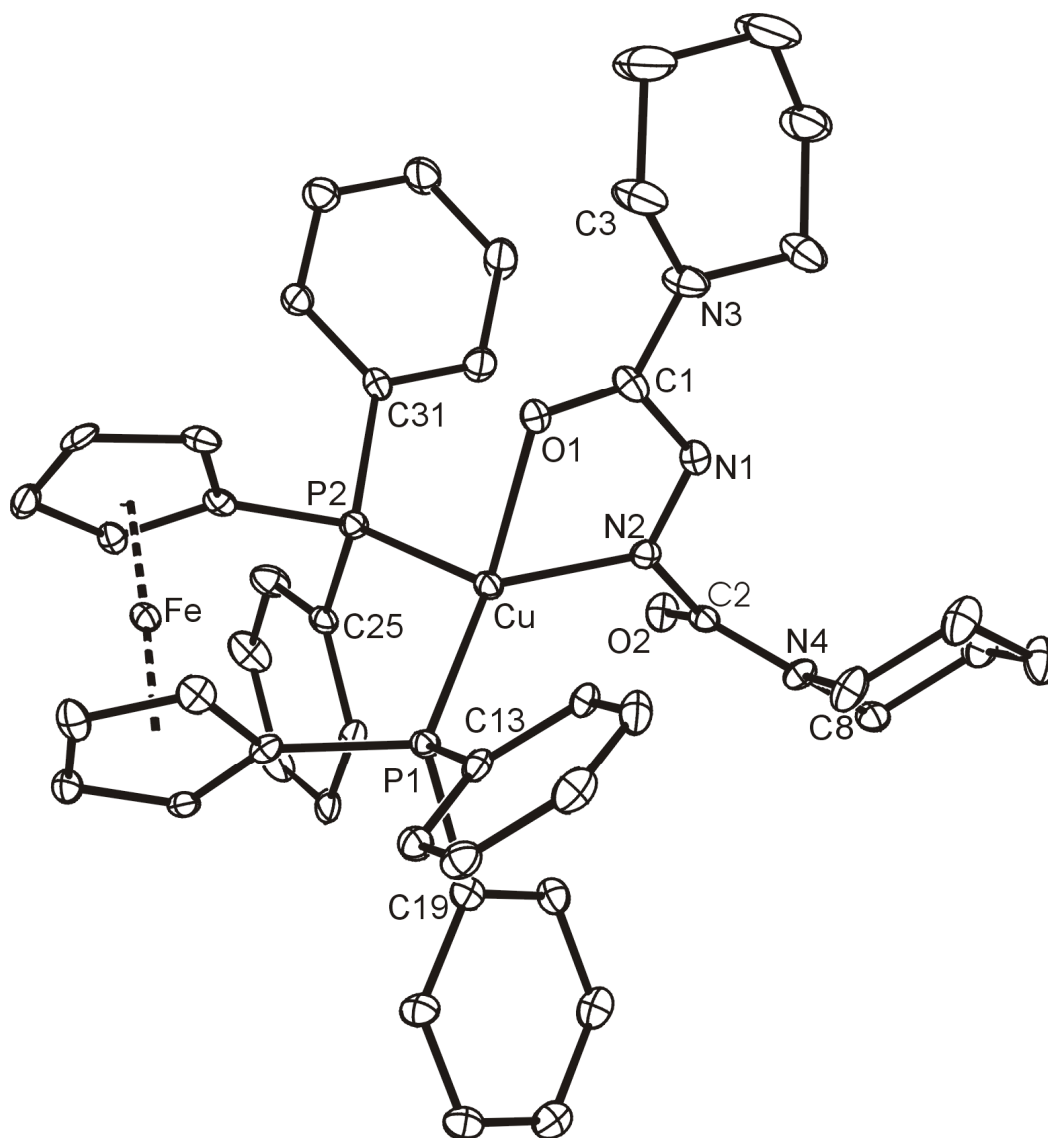


Fig 3.3.1: Molecular structure of $[\text{Cu}^{\text{I}}(\text{adc-pip})(\text{dppf})](\text{BF}_4^-)$ in crystal. H atoms and BF_4^- (counter anion) are removed for clarity.

Table 3.3.1: Important bond lengths (Å) and bond angles (°).

| Bond lengths (Å) | | Bond angles (°) and dihedral angles | |
|------------------|----------|-------------------------------------|-------------|
| Cu-O1 | 2.170(4) | P1-Cu-P2 | 109.85(6) |
| Cu-N2 | 1.990(5) | P1-Cu-N2 | 128.01(15) |
| Cu-P1 | 2.228(2) | P1-Cu-O1 | 116.66(12) |
| Cu-P2 | 2.254(2) | P2-Cu-O1 | 104.02(12) |
| C1-O1 | 1.234(7) | P2-Cu-N2 | 115.71(14) |
| C2-O2 | 1.216(7) | O1-C1-N1-N2 | - 4.8 (8) |
| C1-N1 | 1.466(8) | N1-N2-C2-O2 | - 103.4 (6) |
| C2-N2 | 1.470(7) | | |
| N1-N2 | 1.258(7) | | |

3.4 Cyclic voltammetry

At room temperature $[\text{Cu}^{\text{I}}(\text{adc-pip})(\text{dppf})](\text{BF}_4)$ shows an irreversible reduction at -1.02 V in CH_2Cl_2 / 0.1 M Bu_4NPF_6 with respect to $\text{Fc}^{0/+}$. On lowering the temperature to -70°C the reduction becomes reversible with potential shifted to -0.87 V. The second reduction occurs at -1.76 V. Both the reductions occur on the azodicarbonyl moiety. There is a reversible one electron oxidation at 0.37 V. The complex has two oxidizable parts, one is ferrocenylphosphino co-ligand and the Cu(I) center. The oxidation of Cu(I) usually does not occur at such low potential in related complexes and hence this oxidation is assigned to the ferrocenyl co-ligand. At higher temperature the cyclic voltammetric wave is distorted through conformational changes involving the uncoordinated carboxamido function. For the complex $[\text{Cu}^{\text{I}}(\text{adc-NMe}_2)(\text{dppf})](\text{BF}_4)$ reversibility of the 1st reduction process does not improve even at lower temperature. In this case the ferrocenyl co-ligand based oxidation is observed at 0.44 V.

The cyclic voltammogram of $[\text{Cu}^{\text{I}}(\text{adc-pip})(\text{dppf})](\text{BF}_4)$ at RT and -70°C are shown in Fig 3.4.1 and 3.4.2 respectively and for $[\text{Cu}^{\text{I}}(\text{adc-NMe}_2)(\text{dppf})](\text{BF}_4)$ at RT is shown in Fig 3.4.3 and the potentials are tabulated in Tab 3.4.1.

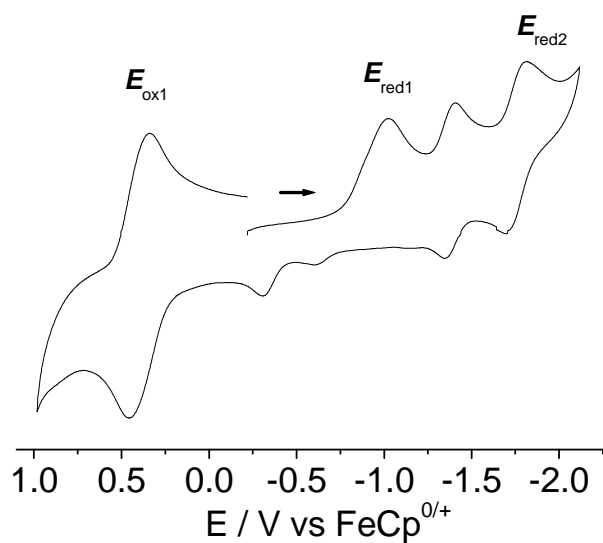


Fig 3.4.1: Cyclic voltammogram of $[\text{Cu}^{\text{I}}(\text{adc-pip})(\text{dppf})](\text{BF}_4)$ at RT in CH_2Cl_2 / 0.1 M Bu_4NPF_6 (scan rate 100 mV / s)

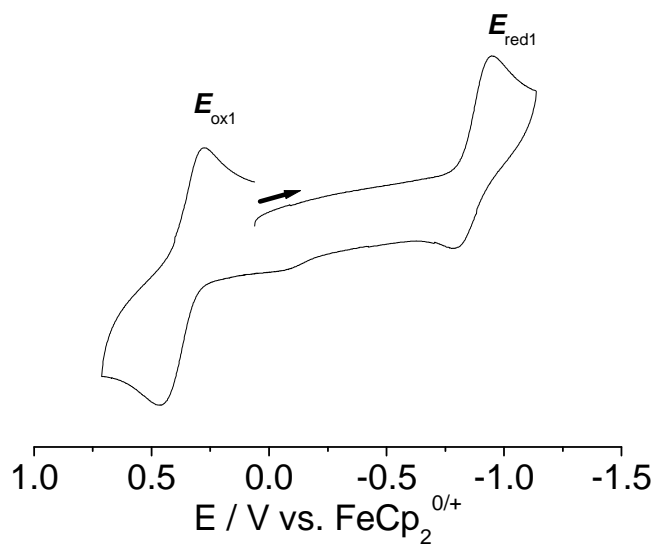


Fig 3.4.2: Cyclic voltammogram of $[\text{Cu}^{\text{I}}(\text{adc-pip})(\text{dppf})](\text{BF}_4)$ at -70°C in CH_2Cl_2 / 0.1 M Bu_4NPF_6 (scan rate 100 mV / s)

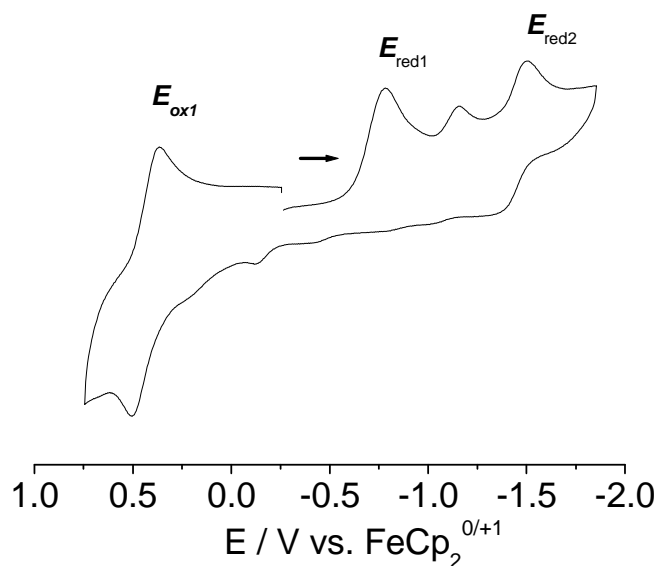


Fig 3.4.3: Cyclic voltammogram of $[\text{Cu}^{\text{I}}(\text{adc-NMe}_2)(\text{dppf})](\text{BF}_4)$ at RT in CH_2Cl_2 / 0.1 M Bu_4NPF_6 (scan rate 100 mV / s)

Table 3.4.1: Electrochemical potential^{a)} from cyclic voltammetry.

| Compound | E_{ox1} | E_{red1} | E_{red2} |
|--|-----------------------------|---|---|
| adc-pip | - | - 2.33 ($E_{\text{pc}}^{\text{b)}$, RT) | - |
| adc-NMe ₂ | - | - 2.38 ($E_{\text{pc}}^{\text{b)}$, RT) | - |
| $[\text{Cu}^{\text{I}}(\text{adc-pip})(\text{dppf})](\text{BF}_4)$ | 0.39 (RT) 0.37 (- 70° C) | - 1.02 ($E_{\text{pc}}^{\text{b)}$, RT) - 0.87 (- 70° C) | - 1.76 (RT) - 1.68 (- 70° C) |
| $[\text{Cu}^{\text{I}}(\text{adc-NMe}_2)(\text{dppf})](\text{BF}_4)$ | 0.44 (RT) | - 0.78 ($E_{\text{pc}}^{\text{b)}$, RT) | - 1.50 ($E_{\text{pc}}^{\text{b)}$, RT) |

^{a)} Potentials E in V vs $\text{FeCp}_2^{0/+}$ in CH_2Cl_2 / 0.1 M Bu_4NPF_6 (scan rate 100 mV / s); ^{b)} cathodic peak potentials corresponding to irreversible peak;

3.5 IR spectroelectrochemistry

The IR spectroelectrochemical investigation was performed in OTTLE cell. The measurements were done to investigate the change of coordinated and non-coordinated carbonyl stretching frequencies on reduction and oxidation processes. The range chosen in these measurements was the typical carbonyl stretching region.

The changes in the carbonyl stretching bands of the complex $[\text{Cu}^{\text{I}}(\text{adc-pip})(\text{dppf})](\text{BF}_4)$ during reduction are shown in Fig 3.5.1 and 3.5.2 and the results for the $[\text{Cu}^{\text{I}}(\text{adc-pip})(\text{dppf})](\text{BF}_4)$ and $[\text{Cu}^{\text{I}}(\text{adc-NMe}_2)(\text{dppf})](\text{BF}_4)$ complexes are summarized in Tab 3.5.1.

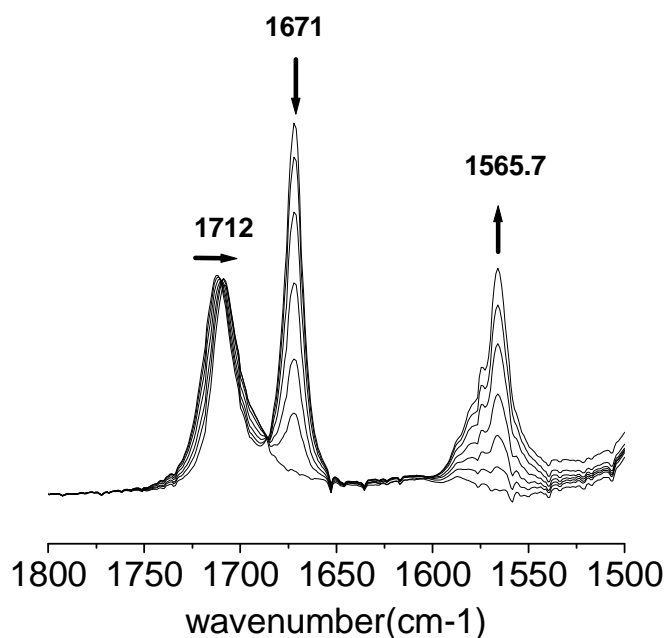


Fig 3.5.1: Spectroelectrochemical reduction of $[\text{Cu}^{\text{I}}(\text{adc-pip})(\text{dppf})]^+$ to $[\text{Cu}^{\text{I}}(\text{adc-pip})(\text{dppf})]^0$ at RT in $\text{CH}_2\text{Cl}_2 / 0.1 \text{ M Bu}_4\text{NPF}_6$.

On first reduction of $[\text{Cu}^{\text{I}}(\text{adc-pip})(\text{dppf})]^+ \rightarrow [\text{Cu}^{\text{I}}(\text{adc-pip})(\text{dppf})]^0$, $\nu_{\text{C=O}}$ for non-coordinated carbonyl has very negligible shift from 1712 to 1708 cm^{-1} where as the coordinated carbonyl stretch has shifted from 1671 to 1566 cm^{-1}

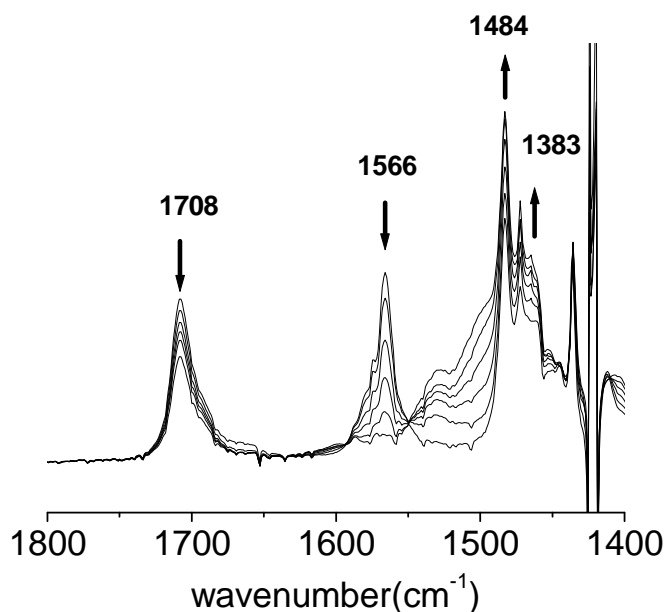


Fig 3.5.2: Spectroelectrochemical reduction of $[\text{Cu}^{\text{I}}(\text{adc-pip})(\text{dppf})]^0$ to $[\text{Cu}^{\text{I}}(\text{adc-pip})(\text{dppf})]^{-}$ at RT in $\text{CH}_2\text{Cl}_2 / 0.1 \text{ M Bu}_4\text{NPF}_6$.

Even upon 2nd reduction at -1.76 V the non-coordinated carbonyl stretching remains unchanged and the coordinated carbonyl is shifted to much lower energy at 1482 cm^{-1} . This indicates that both the reduction processes occur on the chelate ring ($\text{N}=\text{N}-\text{C}=\text{O}$). Oxidation has no effect on the carbonyl stretching frequencies as it takes place on ferrocenyl group.

$[\text{Cu}^{\text{I}}(\text{adc-NMe}_2)(\text{dppf})](\text{BF}_4)$ shows similar changes in stretching frequencies but the processes are not reversible.

Tab 3.5.1: IR vibrational data obtained from spectroelectrochemistry for the complexes.^{a)}

| Compound | $\nu_{\text{C=O}} / \text{cm}^{-1}$ |
|---|-------------------------------------|
| $[\text{Cu}^{\text{I}}(\text{adc-pip})(\text{dppf})]^+$ | 1712, 1671 |
| $[\text{Cu}^{\text{I}}(\text{adc-pip})(\text{dppf})]^0$ | 1708, 1566 |
| $[\text{Cu}^{\text{I}}(\text{adc-pip})(\text{dppf})]^{-}$ | 1708, 1482 |
| $[\text{Cu}^{\text{I}}(\text{adc-NMe}_2)(\text{dppf})]^+$ | 1716, 1685 |
| $[\text{Cu}^{\text{I}}(\text{adc-NMe}_2)(\text{dppf})]^0$ | 1713, 1583 (irreversible) |
| $[\text{Cu}^{\text{I}}(\text{adc-NMe}_2)(\text{dppf})]^{-}$ | irreversible |

^{a)}From spectroelectrochemistry in an OTTLE cell in $\text{CH}_2\text{Cl}_2 / 0.1 \text{ M Bu}_4\text{NPF}_6$;

3.6 UV-vis-NIR spectroelectrochemistry

$[\text{Cu}^{\text{I}}(\text{adc-pip})(\text{dppf})](\text{BF}_4)$ shows a metal to ligand charge transfer (MLCT, $d(\text{Cu}^{\text{I}}) \rightarrow \pi^*$) band at 520 nm ($\epsilon = 2550 \text{ M}^{-1} \text{ cm}^{-1}$). On 1st reduction this MLCT band is shifted to 640 nm ($\epsilon = 1400 \text{ M}^{-1} \text{ cm}^{-1}$). 2nd reduction results complete disappearance of MLCT band due to full occupancy of the π^* level. Since the oxidation occurs on the ferrocene moiety, the appearance of a characteristic band at 770 nm and shift in MLCT band to lower wavelength ($520 \rightarrow 462$ nm, $\epsilon = 3170 \text{ M}^{-1} \text{ cm}^{-1}$) is observed.

Complex $[\text{Cu}^{\text{I}}(\text{adc-NMe}_2)(\text{dppf})](\text{BF}_4)$ shows similar type of absorption behaviour. It has the MLCT band at 522 nm ($\epsilon = 1200 \text{ M}^{-1} \text{ cm}^{-1}$) which is shifted bathochromically to 654 nm ($\epsilon = 592 \text{ M}^{-1} \text{ cm}^{-1}$) on 1st electron uptake. On 2nd reduction like earlier case the MLCT disappears. Oxidation gives ferrocenium based absorption shoulder at 780 nm and hypsochromic shift in MLCT band ($522 \rightarrow 470$ nm, $\epsilon = 1400 \text{ M}^{-1} \text{ cm}^{-1}$).

Spectral changes associated with reductions and oxidations of $[\text{Cu}^{\text{I}}(\text{adc-pip})(\text{dppf})](\text{BF}_4)$ are shown in Fig 3.6.1 – 3.6.3 and the absorption data for $[\text{Cu}^{\text{I}}(\text{adc-pip})(\text{dppf})](\text{BF}_4)$ and $[\text{Cu}^{\text{I}}(\text{adc-NMe}_2)(\text{dppf})](\text{BF}_4)$ are tabulated in Tab 3.6.1.

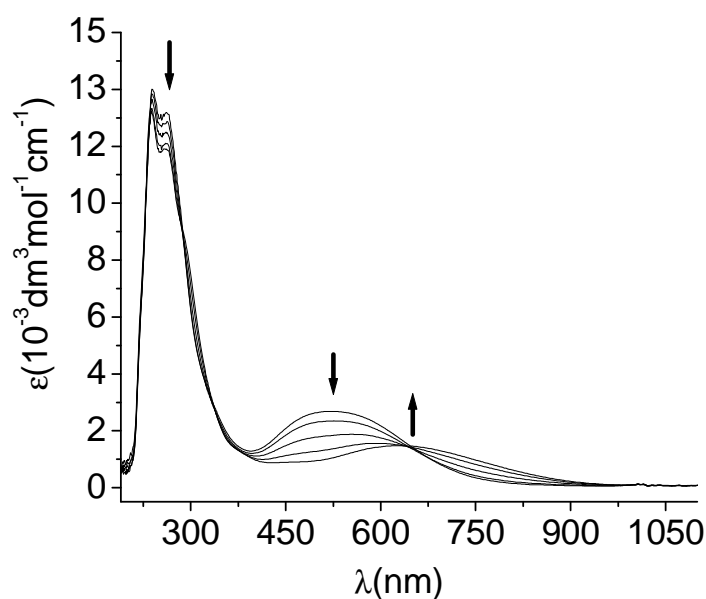


Fig 3.6.1: Spectroelectrochemical reduction of $[\text{Cu}^{\text{I}}(\text{adc-pip})(\text{dppf})]^+$ to $[\text{Cu}^{\text{I}}(\text{adc-pip})(\text{dppf})]^0$ at RT in $\text{CH}_2\text{Cl}_2 / 0.1 \text{ M Bu}_4\text{NPF}_6$.

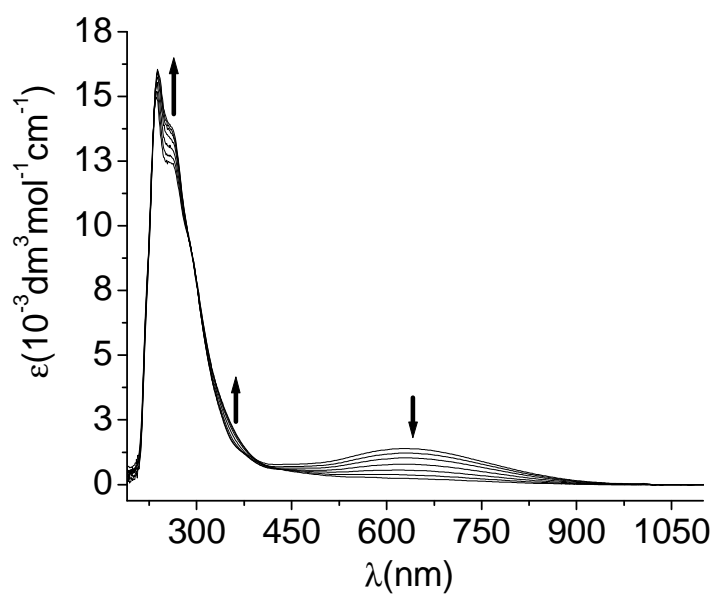


Fig 3.6.2: Spectroelectrochemical reduction of $[\text{Cu}^{\text{I}}(\text{adc-pip})(\text{dppf})]^0$ to $[\text{Cu}^{\text{I}}(\text{adc-pip})(\text{dppf})]^{-}$ at RT in $\text{CH}_2\text{Cl}_2 / 0.1 \text{ M Bu}_4\text{NPF}_6$

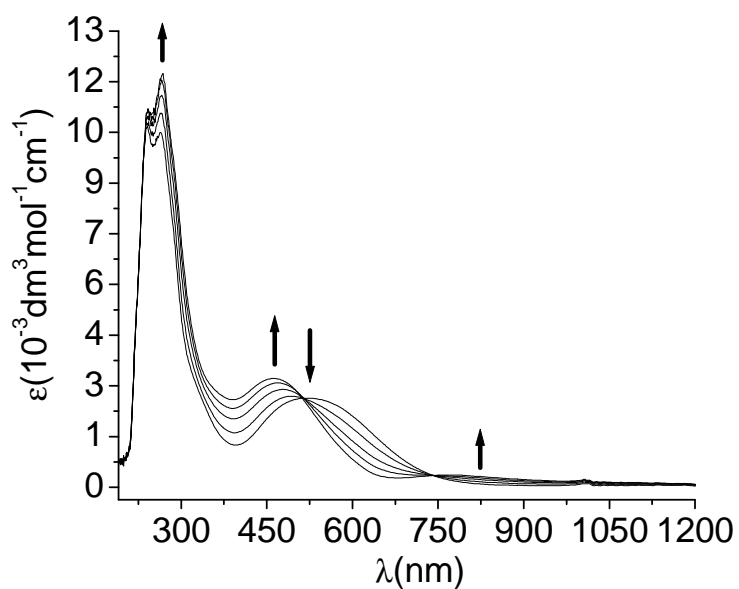


Fig 3.6.3: Spectroelectrochemical oxidation of $[\text{Cu}^{\text{I}}(\text{adc-pip})(\text{dppf})]^+$ to $[\text{Cu}^{\text{I}}(\text{adc-pip})(\text{dppf})]^{2+}$ at RT in $\text{CH}_2\text{Cl}_2 / 0.1 \text{ M Bu}_4\text{NPF}_6$

Tab 3.6.1: Absorption data from spectroelectrochemistry.^{a)}

| Compound | L = adc-pip | L = adc-NMe ₂ |
|---|--------------------------------|-------------------------------|
| L | 295 (2.26), 435 (0.05) | 288 (1.5), 438 (0.037) |
| [Cu ^I (L)(dppf)] ²⁺ | 264(12.18), 460(3.17), 770(sh) | 268(4.63), 473(1.43), 780(sh) |
| [Cu ^I (L)(dppf)] ⁺ | 261(12.65), 520(2.55) | 269(4.47), 522(1.22) |
| [Cu ^I (L)(dppf)] ⁰ | 635(1.41) | 654(0.59) |
| [Cu ^I (L)(dppf)] ⁻ | 261(13.3), 358 (sh) | 287(sh), 361(sh) |

^{a)} From spectroelectrochemistry in an OTTLE cell in CH₂Cl₂ / 0.1 M Bu₄NPF₆; wavelengths in nm; molar extinction coefficient (ϵ) in 10⁻³ dm³mol⁻¹cm⁻¹

3.7 EPR spectroscopy

It was possible to study the in-situ generated one electron reduced paramagnetic form [Cu^I(adc-pip)(dppf)]⁻ and [Cu^I(adc-NMe₂)(dppf)]⁻ by EPR spectroscopy. The EPR spectra measured at 298 K is shown in Fig 3.7.1.

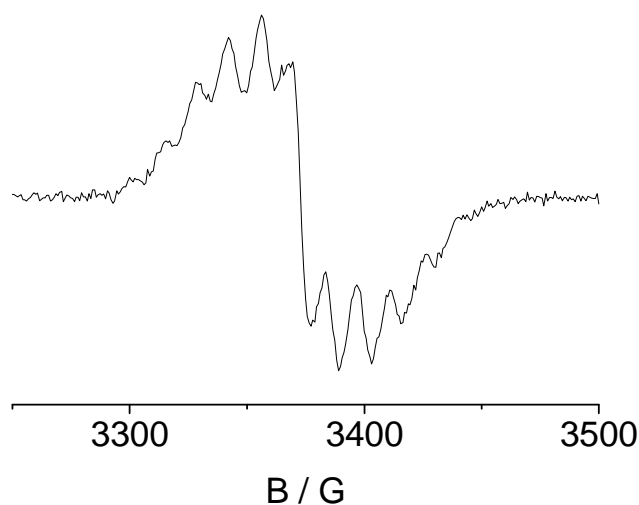


Fig 3.7.1. X-band EPR spectrum of [Cu^I(adc-pip)(dppf)]⁻ obtained by insitu electrolysis at 298 K in CH₂Cl₂ / 0.1 M Bu₄NPF₆.

The insitu generated one electron reduced species showed partially resolved EPR spectrum at 298 K. However, due to poor resolution it was not possible to obtain hyperfine data completely. The isotropic *g* values are at 2.0079 for [Cu^I(adc-pip)(dppf)]⁻ and 2.0078 for [Cu^I(adc-NMe₂)(dppf)]⁻ with approximately 16 mT of total spectral width. The isotropic *g*

values are rather high compared to the free electron g value of 2.0023 due to the high spin-orbit coupling constants of Cu and P.

3.7 Conclusion

From the examples discussed in this chapter it is seen that the heterodinuclear complex ion $[\text{Cu}^{\text{I}}(\text{dppf})]^+$, $\text{dppf} = 1,1'$ -bis(diphenylphosphino)ferrocene, coordinates to azodicarboxylic acid diamides without reduction of the chelating $\text{N}=\text{N}-\text{C}=\text{O}$ group ($d_{\text{N}=\text{N}} = 1.258(7) \text{ \AA}$, $d_{\text{C}-\text{N}} = 1.466(8) \text{ \AA}$, $d_{\text{C}=\text{O}} = 1.234(7) \text{ \AA}$ for $[\text{Cu}(\text{adc-pip})(\text{dppf})](\text{BF}_4)$). With electrochemistry and EPR, IR and UV-vis spectroelectrochemistry, the stepwise reduction on the chelate ring ($\text{N}=\text{N}-\text{C}=\text{O}$) keeping another carbonyl of the ligand completely redox insensitive, is monitored. All effort to synthesise dinuclear Cu complex were unsuccessful because of steric hindrance. Herein the spectroscopic and structural evidence for first such cases of the heterodinuclear compounds with completely unreduced $\text{N}=\text{N}-\text{C}=\text{O}$ group are reported.

Chapter 4

Mononuclear and dinuclear ferrocenylcopper complexes bridged by 2,2'-azobispyridine and its anion radical: structural electrochemical and spectroelectrochemical properties.

4.1 Introduction

The ligand 2,2'-azobispyridine (abpy) has adopted a special position in coordination chemistry for studying metal-metal interaction due to its ability of binding two metal centers at a distance of 5 Å in a bis-chelate fashion, due to the small size of its π system and because of its low energy π^* orbital.^[17] This ligand was first introduced to coordination chemistry by Baldwin, Lever and Parish.^[75] The ligand abpy can be synthesized conveniently by oxidative coupling of 2-aminopyridine and has potential for different coordination modes to metals.^[17,75] The structurally established alternatives include mono- and di-nuclear coordination situations by formation of five-membered chelate rings NNCNM (A and B Fig. 4.1.1) and also a rare $\mu, \eta^2: \eta^1$ coordination mode (C).^[75-80]

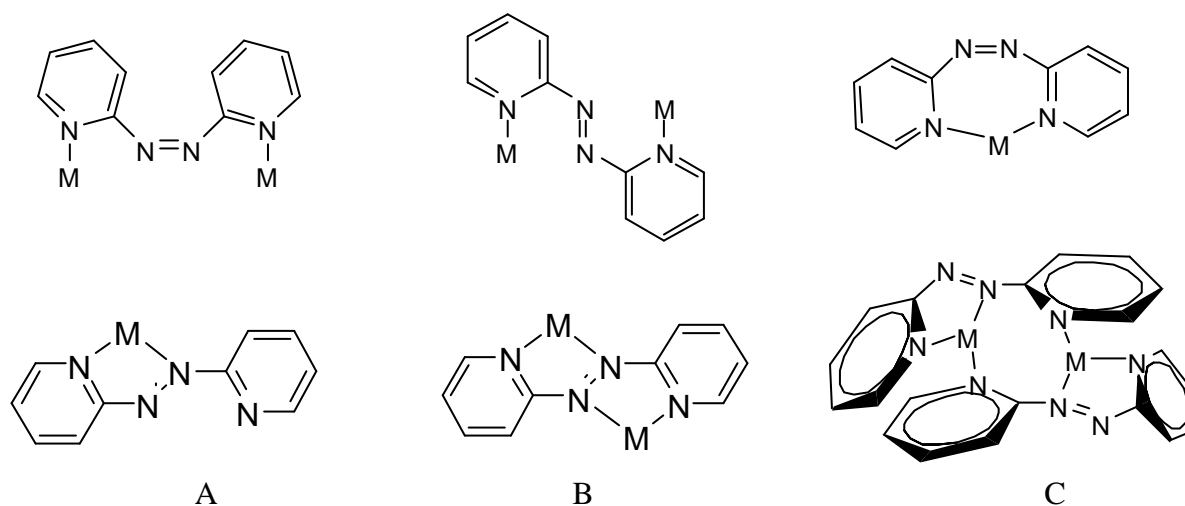


Fig. 4.1.1: Different coordination modes of abpy.^[75-80]

Due to the availability of a low-lying π^* orbital, abpy can be reduced by two successive one-electron steps (Fig 4.1.2). The change in N=N bond length on successive reduction is indeed a characteristic property to determine the oxidation state of such ligands.

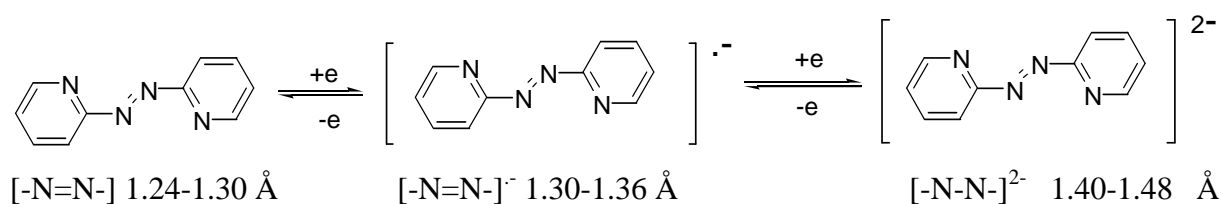


Fig 4.1.2: Stepwise reduction of abpy.^[76-81]

In this chapter the redox system abpy/abpy^{•-} has been used to form heterodinuclear and heterotetranuclear complexes with [Cu(dppf)]⁺. The structural and spectroscopic properties of these complexes are described in details.

4.2 Synthesis and characterization

The heterodinuclear complex [(abpy)Cu(dppf)](BF₄) was synthesized by stirring the mixture of 1 equiv. of abpy and 1 equiv. of the precursor complex [Cu(dppf)(CH₃CN)₂](BF₄)^[74] in dry CH₂Cl₂ at room temperature. The solvent was removed under vacuum to obtain a dark violet solid which was washed several times with dry hexane and was recrystallized from CH₂Cl₂ / hexane (1/3). The complex was characterized by ¹H, ³¹P NMR and elemental analysis. Due to the fluxional behavior of the molecule at room temperature, signals from abpy were broad. Because of the free coordination site on abpy the [Cu(dppf)]⁺ shuttles from one side to another. The ¹H and ³¹P NMR spectra were measured at 223 K. The mass spectroscopic results were not conclusive due to fragmentation.

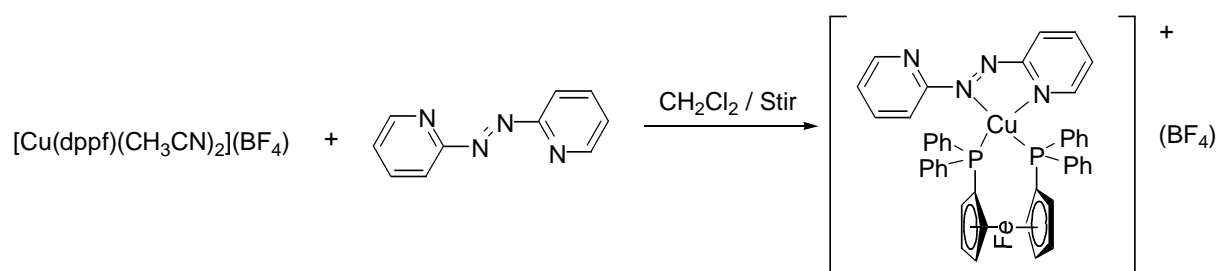


Fig 4.2.1: Synthetic scheme for [(abpy)Cu(dppf)](BF₄).

The heterotetranuclear complex bridged by neutral abpy, {(μ-abpy)[Cu(dppf)]₂}(BF₄)₂, was synthesized from the mononuclear complex [(abpy)Cu(dppf)](BF₄). Reaction of one equiv. of [(abpy)Cu(dppf)](BF₄) with 1 equiv. of [Cu(dppf)(CH₃CN)₂](BF₄)^[74] at RT under argon atmosphere in dry CH₂Cl₂ resulted in the heterotetranuclear diamagnetic compound {(μ-

abpy)[Cu(dppf)]₂}(BF₄)₂. Characterization of the complex was done by ¹H and ³¹P NMR spectroscopy, elemental analysis and mass spectroscopy.

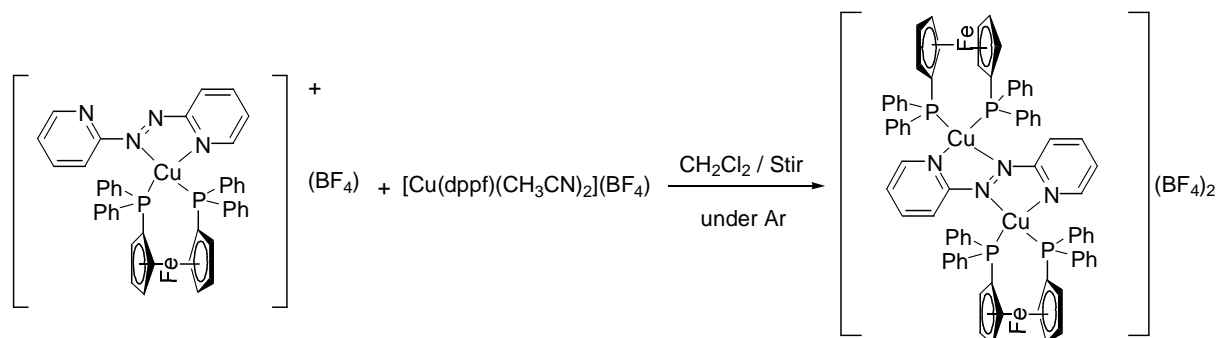


Fig 4.2.2: Synthetic scheme for {(μ-abpy)[Cu(dppf)]₂}(BF₄)₂.

The radical anion-bridged {(μ-abpy)[Cu(dppf)]₂}(BF₄) is synthesized by a different route, i. e. by stirring the mixture of activated Cu powder, Cu(BF₄)₂·H₂O, abpy and dppf in dry CH₂Cl₂ at RT. Cu⁰ and Cu^{II} salt comproportionate to give Cu^I, which self-assembles with bridging abpy and dppf ancillaries to yield the radical-bridged heterotetranuclear complex {(μ-abpy)[Cu(dppf)]₂}(BF₄). The wine-red solution was filtered off from Cu powder and the solvent was removed under reduced pressure. The dark red solid is washed and recrystallized to get the pure paramagnetic complex {(μ-abpy)[Cu(dppf)]₂}(BF₄).

Due to native state paramagnetism, the ¹H NMR spectrum was broad. The compound was characterized initially by elemental analysis and mass spectroscopy.

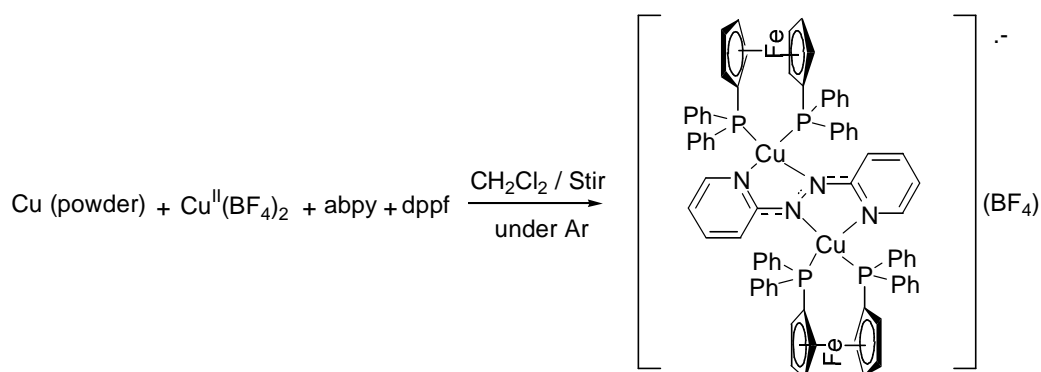


Fig. 4.2.3: Synthetic scheme for {(μ-abpy)[Cu(dppf)]₂}(BF₄).

Table 4.2.1: ¹H and ³¹P NMR data^{a)} for the complexes.

| Compound | δ / ppm for ¹ H NMR | δ / ppm for ³¹ P NMR |
|----------|---|---------------------------------|
| abpy | 8.76 (2H, H ^{6,6'}); 7.94 (2H, H ^{4,4'}); 7.86 (2H, H ^{3,3'}); 7.48 (2H, H ^{5,5'}) | - |

| | | |
|--|--|-------|
| $[(\text{abpy})\text{Cu}(\text{dppf})](\text{BF}_4)^{\text{b)}}$ | 4.26-4.69 (8H, Cp); 6.96-7.45 (m, 20H, (Ph-H)); 7.42(d,1H, J = 6.6 Hz); 7.62 (t, 1H, J = 6.7 Hz); 7.82 (m, 2H); 8.17 (d, 1H, J = 4.1 Hz); 8.35 (t, 1H, J = 7.6 Hz); 8.55 (d, 2H, J = 7.1 Hz) | -3.76 |
| $\{(\mu\text{-abpy})[\text{Cu}(\text{dppf})_2]\}(\text{BF}_4)_2$ | 4.46-4.78 (16H, Cp); 6.96-7.45 (m, 40H, (Ph-H)); 7.58(t, 2H, H ^{5,5'}); 8.00 (t, 2H, H ^{3,3'}); 8.39 (d, 2H, J = 8.0 Hz, H ^{4,4'}); 8.51 (d, 2H, J = 5.0 Hz, H ^{6,6'}) | -0.82 |

^{a)} in CD₂Cl₂; ^{b)} at 223 K

The ¹H NMR signal for the heterodinuclear complex $[(\text{abpy})\text{Cu}(\text{dppf})](\text{BF}_4)$ shows the expected higher number of peaks from the abpy ligand than the heterotetranuclear $\{(\mu\text{-abpy})[\text{Cu}(\text{dppf})_2]\}(\text{BF}_4)_2$ (Tab 4.2.1). Due to paramagnetism the complex $\{(\mu\text{-abpy})[\text{Cu}(\text{dppf})_2]\}(\text{BF}_4)_2$ shows broad NMR signals which could not be assigned.

4.3 Crystal structures

4.3.1 Crystal structure of $[(\text{abpy})\text{Cu}(\text{dppf})](\text{BF}_4)$

Dark-violet crystals of $[(\text{abpy})\text{Cu}(\text{dppf})](\text{BF}_4)$ were grown by slow diffusion of n-hexane into CH₂Cl₂ at 4°C. It crystallizes in the monoclinic $P2_1/n$ space group. The molecular structure of the compound is shown in Fig 4.3.1.1, selected bond lengths and bond angles are tabulated in Tab 4.3.1.1.

The intra-chelate bond lengths are N1-N2 = 1.274(3) Å, Cu-N1 = 2.045(2) Å, Cu-N3 = 2.079(2) Å, N2-C6 = 1.417(4) Å and N3-C6 = 1.347(4) Å. The relative lengthening of the azo (N1-N2) bond distance when compared to free abpy, is due to π back donation from (d¹⁰)Cu^I to the π^* orbital of the ligand. The relatively shorter Cu-N_{azo} bond length over Cu-N_{py} justifies higher basicity on N_{azo} than N_{py}. The phosphinoferrrocene co-ligand binds Cu with almost equal bond lengths of Cu-P2 = 2.257(9) Å and Cu-P1 = 2.262(9) Å respectively. The distance between Cu--Fe is 4.076 Å. The elongation of Cu-P1 bond over Cu-P2 and deviation in the bond angles, small P1(ax)-Cu-N1 (105.01°(7)) and N1-Cu-N3 (76.77°(10)) over large P2(eq)-Cu-N3 (114.50°(7)), are implying the distorted tetrahedral coordination. This kind of distortion is also known from biology.

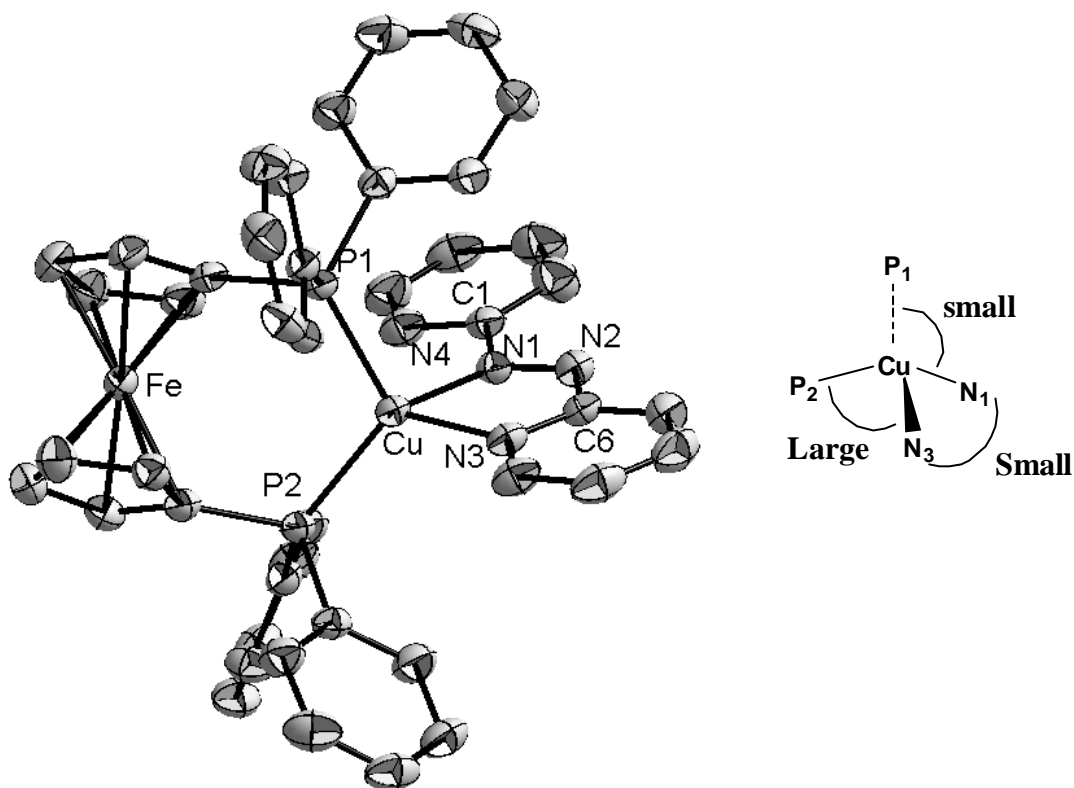


Fig 4.3.2.1: Molecular structure of $[(abpy)Cu(dppf)]^+$ in crystal of $[(abpy)Cu(dppf)](BF_4)$, trigonal pyramidal (3+1) coordination of Cu (right).

Table 4.3.1.1: Important bond lengths (Å) and bond angles ($^\circ$) for $[(abpy)Cu(dppf)]^+$ in crystal of $[(abpy)Cu(dppf)](BF_4)$.

| Bond lengths (Å) | | Bond angles ($^\circ$) and dihedral angles | |
|------------------|----------|--|------------|
| Cu-N1 | 2.045(2) | P1-Cu-P2 | 111.96(3) |
| Cu-N3 | 2.079(2) | P1-Cu-N3 | 113.64 (7) |
| Cu-P1 | 2.262(9) | P1-Cu-N1 | 105.01(7) |
| Cu-P2 | 2.257(9) | P2-Cu-N1 | 130.53(7) |
| C6-N3 | 1.347(4) | P2-Cu-N3 | 114.50(7) |
| C6-N2 | 1.417(4) | N1-Cu-N3 | 76.77(10) |
| N1-N2 | 1.274(3) | N3-C6-N1-N2 | - 1.7 (4) |
| C1-N1 | 1.448(4) | N4-C1-N1-N2 | 175.8(2) |

| | | | |
|-------|----------|--|--|
| C1-N4 | 1.329(4) | | |
|-------|----------|--|--|

4.3.2 Crystal structure of $\{(\mu\text{-abpy})[\text{Cu}(\text{dppf})_2]\}(\text{BF}_4)$

The dark red block-shaped crystals for X-ray measurements of $\{(\mu\text{-abpy})[\text{Cu}(\text{dppf})_2]\}(\text{BF}_4)$ were grown via the diffusion technique using dry n-hexane diffusing into a CH_2Cl_2 solution at 4°C . The complex crystallizes in the monoclinic space group ($P2_1/c$). The molecular structure of the compound is shown in Fig 4.3.2.2 and selected bond lengths and bond angles are tabulated in Tab 4.3.2.1.

The azo bond length ($d_{\text{N1-N2}}$) is 1.317(5) Å in the complex $\{(\mu\text{-abpy})[\text{Cu}(\text{dppf})_2]\}(\text{BF}_4)$, which is longer than the values for $[(\text{abpy})\text{Cu}(\text{dppf})](\text{BF}_4)$ (1.274 Å) and for the earlier reported dicopper complex $\{(\mu\text{-abpy})[\text{Cu}(\text{PPh}_3)_2]_2\}(\text{BF}_4)_2$ (1.248 Å).^[81] The structure of another unusually stable radical dinuclear Cu^{I} complex with abcp (azo-bis(5-chloropyrimidine), $\{(\mu\text{-abcp})[\text{Cu}(\text{PPh}_3)_2]_2\}(\text{PF}_6)$, revealed a considerably lengthened N-N distance of 1.345(7) Å.^[82] Still the structural results of $\{(\mu\text{-abpy})[\text{Cu}(\text{dppf})_2]\}(\text{BF}_4)$ support the formation of bond order 1.5 by lengthening of the central N1-N2 bond, which lies in between that of a double bond, 1.25 Å, and of a single bond, 1.45 Å.^[81] The N-N bond lengths in different Cu^{I} complexes with abpy or abcp ligands are tabulated in Tab 4.3.2.2. The complex exhibits an S-frame dicopper coordination by abpy with an intermetallic Cu--Cu distance of 4.825 Å. The intermetallic intramolecular Fe--Fe distance involving the two ferrocenyl ancillaries is 12.651 Å. The presence of only one counter-anion BF_4 justifies the formation of a radical anion containing complex.

The shorter Cu-N_{azo} distances (2.042(3) Å) over Cu-N_{py} (2.065(4) Å) is not very uncommon which was earlier observed in the complex $\{(\mu\text{-abcp})[\text{Cu}(\text{PPh}_3)_2]_2\}(\text{PF}_6)$ ^[82,85] suggesting higher electron density on azo N compared to N of pyridine ring in mono-reduced form. This observation was also reproduced by DFT approach on both abcp^- (Fig 4.3.2.1) and $\{(\mu\text{-abcp})[\text{Cu}(\text{PPh}_3)_2]_2\}(\text{PF}_6)$ ^[85]. However, the Cu-N_{azo} and Cu-N_{py} bond lengths (2.101(6) and 2.095(6) Å respectively) are almost same in neutral abpy bridge dinuclear copper(I) complex $\{(\mu\text{-abpy})[\text{Cu}(\text{PPh}_3)_2]_2\}(\text{BF}_4)_2$.^[81]

In $\{(\mu\text{-abpy})[\text{Cu}(\text{dppf})_2]\}(\text{BF}_4)$, the P atoms of ferrocenylphosphine co-ligands bind Cu^{I} in almost equal distances of 2.26 Å which is because of no $\pi/\pi/\pi$ type interaction involving the bridging ligand.

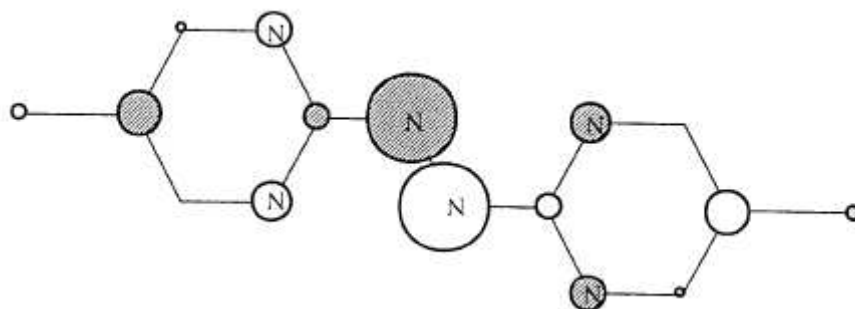


Fig 4.3.2.1: π -LUMO presentation of abcpc from DFT.

The geometry around the copper centers is distorted due to small N-Cu-N bite of $77.60^\circ(14)$ and $78.27^\circ(14)$ and relatively large N-Cu-P angles. The smaller bite-angle of ferrocenylphosphine co-ligands over other chelate phosphines is justified by P-Cu-P bond angle of about 111° where as hexaPhos binds Cu^{I} with an angle of 122° . The PPh_3 binds Cu^{I} in the complexes $\{(\mu\text{-abcpc})[\text{Cu}(\text{PPh}_3)_2]_2\}(\text{PF}_6)$ ^[82,85] and $\{(\mu\text{-abpy})[\text{Cu}(\text{PPh}_3)_2]_2\}(\text{BF}_4)_2$ ^[81,83] with $124.13(5)^\circ$ and $120.0(1)^\circ$ respectively.

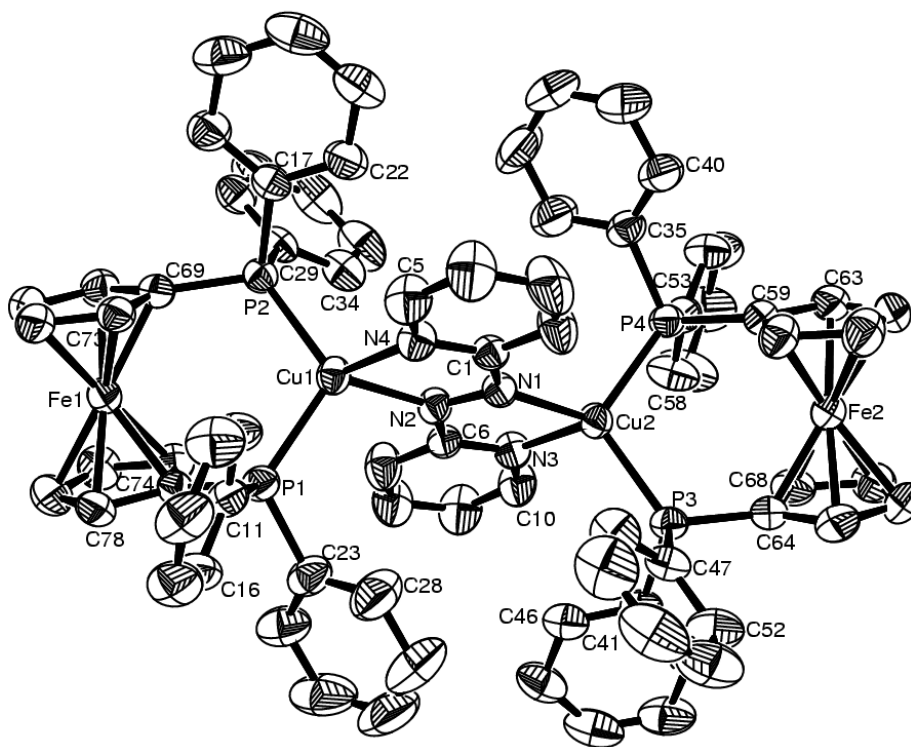


Fig 4.3.2.2: Molecular structure of $\{(\mu\text{-abpy})[\text{Cu}(\text{dppf})]_2\}^+$ in crystal of $\{(\mu\text{-abpy})[\text{Cu}(\text{dppf})]_2\}(\text{BF}_4)$.

Table 4.3.2.1: Important bond lengths (Å) and bond ang ($^\circ$) for $\{(\mu\text{-abpy})[\text{Cu}(\text{dppf})]_2\}^+$ in crystal of $\{(\mu\text{-abpy})[\text{Cu}(\text{dppf})]_2\}(\text{BF}_4)$

| Bond lengths (Å) | | Bond angles ($^\circ$) and dihedral angles | |
|------------------|----------|--|------------|
| Cu1-N2 | 2.052(3) | N2-Cu1-N4 | 77.60(14) |
| Cu1-N4 | 2.058(4) | N2-Cu1-P1 | 110.30(10) |
| Cu1-P1 | 2.265(1) | N4-Cu1-P1 | 118.17(10) |
| Cu1-P2 | 2.265(1) | N2-Cu1-P2 | 123.58(10) |
| Cu2-N1 | 2.042(3) | N4-Cu1-P2 | 111.66(10) |
| Cu2-N3 | 2.065(4) | P1-Cu1-P2 | 111.93(4) |
| Cu2-P3 | 2.251(1) | N1-Cu2-N3 | 78.27(14) |
| Cu2-P4 | 2.264(1) | N1-Cu2-P4 | 112.10(9) |
| N1-N2 | 1.317(5) | N3-Cu2-P4 | 117.58(10) |
| C6-N2 | 1.382(5) | N1-Cu2-P3 | 123.39(10) |
| C6-N3 | 1.345(5) | N3-Cu2-P3 | 110.71(10) |
| C1-N1 | 1.379(5) | P4-Cu2-P3 | 111.34(4) |
| C1-N4 | 1.343(5) | N3-C6-N2-N1 | -6.2(5) |
| | | N4-C1-N1-N2 | 3.5(5) |
| | | C1-N1-N2-C6 | 179.1(3) |

Tab 4.3.2.2: Bond lengths (Å) in Cu^{I} -complexes with abpy and related azo ligands.

| Compound | $d(\text{NN})$ | $d(\text{CuN}_{\text{azo}})$ | $d(\text{CuN}_{\text{py}})$ | $d(\text{MM})$ |
|---|----------------|------------------------------|-----------------------------|----------------|
| abpy ^[9] | 1.246(2) | - | - | - |
| abcp ^[14] | 1.230(2) | - | - | - |
| $[(\text{abpy})\text{Cu}(\text{dppf})](\text{BF}_4)$ | 1.274(3) | 2.045(2) | 2.079(2) | - |
| $\{(\mu\text{-abpy})[\text{Cu}(\text{dppf})]_2\}(\text{BF}_4)$ | 1.317(5) | 2.052(3); 2.042(3) | 2.058(4); 2.065(4) | 4.825 |
| $\{(\mu\text{-abpy})[\text{Cu}(\text{PPh}_3)_2]_2\}(\text{BF}_4)_2$ ^[51] | 1.248(11) | 2.101(6) | 2.095(6) | 4.937 |
| $\{(\mu\text{-abcp})[\text{Cu}(\text{PPh}_3)_2]_2\}(\text{PF}_6)$ ^[71] | 1.345(7) | 2.043(3) | 2.096(3) | 4.866 |

4.4 Cyclic voltammetry

Through cyclic voltammetry the redox properties of the complexes can be studied. The cyclic voltammogram of $[(\text{abpy})\text{Cu}(\text{dppf})](\text{BF}_4)$ is shown in Fig 4.4.1 and the results are summarized in Tab. 4.4.1. The heterodinuclear complex shows reversible electrochemical reduction at -0.98 V and an irreversible wave at -1.76 V in $\text{CH}_2\text{Cl}_2 / 0.1$ M Bu_4NPF_6 at RT vs. $\text{FeCp}_2^{0/+}$. The reductions are attributed to successive one-electron uptake by the π^* level of abpy.

The complex shows reversible one-electron oxidation for the ferrocenyl ancillary at 0.43 V vs. $\text{FeCp}_2^{0/+}$. The oxidation of copper(I) to copper(II) can not be detected in the solvent range of CH_2Cl_2 (1.6 V vs. $\text{FeCp}_2^{0/+}$).

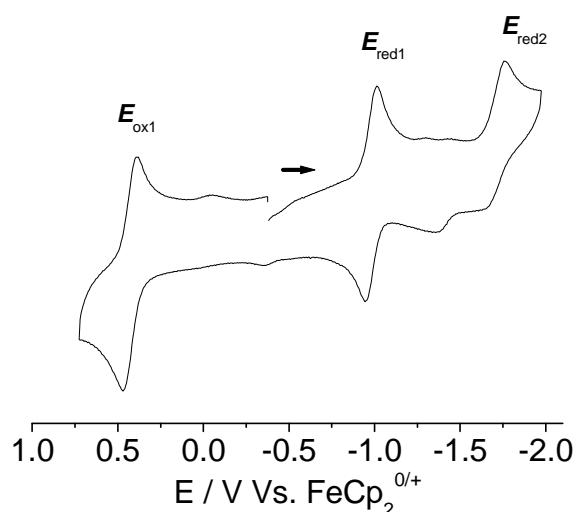


Fig. 4.4.1: Cyclic voltammogram of $[(\text{abpy})\text{Cu}(\text{dppf})](\text{BF}_4)$ in $\text{CH}_2\text{Cl}_2 / 0.1$ M Bu_4NPF_6 at RT with scan rate of 100 mV/s.

The cyclic voltammogram of $\{(\mu\text{-abpy})[\text{Cu}(\text{dppf})]_2\}(\text{BF}_4)$ is shown in Fig 4.4.2 and the results are tabulated in Tab. 4.4.1. Since the complex $\{(\mu\text{-abpy})[\text{Cu}(\text{dppf})]_2\}(\text{BF}_4)$ is isolated in the one-electron reduced form, the ligand abpy^- in the complex can be oxidized and reduced reversibly by one electron. Indeed, the cyclic voltammogram the complex shows a one electron reversible oxidation wave at -0.38 V for the step $(\text{abpy})^- \rightarrow (\text{abpy})$, and one-electron reversible reduction wave at -1.37 V vs. $\text{FeCp}_2^{0/+}$ which is assigned to the formation of doubly reduced $(\text{abpy})^{2-}$. The substantial amount of shift in reduction potential of $\{(\mu\text{-$

abpy)[Cu(dppf)]₂}(BF₄) compared to the heterodinuclear complex [(abpy)Cu(dppf)](BF₄) (-0.98 V) and that of free abpy (-1.46 V vs. FeCp₂^{0/+}) can be attributed to the chelation of two [Cu(dppf)]⁺ units, causing the lowering of the π* level of abpy. The dicopper complex of abcp, {(μ-abcp)[Cu(PPh₃)₂]₂}²⁺, shows the abcp based reduction at much lower potential (+0.06 V vs. FeCp₂^{0/+}) due to the presence of chloride substituents and additional nitrogen functionalities in bridging azo ligand.^[82] The rather negative-shift in reduction potential of {(μ-abpy)[Cu(dppf)]₂}(BF₄) compared to {(μ-abpy)[Cu(PPh₃)₂]₂}(BF₄)₂ and {(μ-abpy)[Cu(diPhos)₂]₂}(BF₄)₂ can be justified by greater σ-donor ability of phosphines with ferrocene back-bone.^[83] The Cu^I/Cu^{II} and the phosphine oxidations are not observed in solvent range of CH₂Cl₂ (1.6 V vs. Fe^{0/+}).

The complex {(μ-abpy)[Cu(dppf)]₂}(BF₄) can be reversibly oxidized in a second time by two electrons at 0.45 V vs. FeCp₂^{0/+} due to the redox-active ferrocenyl ancillaries which oxidize at the same potential (no detectable splitting of the wave).

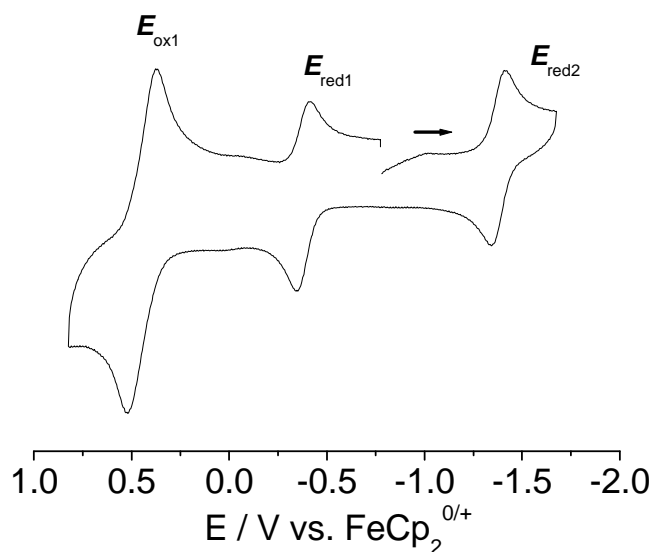


Fig. 4.4.2: Cyclic voltammogram of {(μ-abpy)[Cu(dppf)]₂}(BF₄) in CH₂Cl₂ / 0.1 M Bu₄NPF₆ at RT with scan rate of 100 mV/s.

The heterotetranuclear diamagnetic species {(μ-abpy)[Cu(dppf)]₂}(BF₄)₂ with the neutral abpy bridge shows identical redox behaviour as {(μ-abpy)[Cu(dppf)]₂}(BF₄), two one-electron reductions and one two-electron oxidation from. This is expected because the two compounds differ only in the oxidation state of abpy.

Tab. 4.4.2 Comparison of the potentials^{a)} obtained from cyclic voltammetry^{b)}.

| Compound | $E_{\text{ox1}}^{\text{c)}$ | $E_{\text{red1}}^{\text{c)}$ | E_{red2} |
|---|-----------------------------|------------------------------|---------------------|
| abpy | - | -1.46 | -2.04 |
| $[(\text{abpy})\{\text{Cu}(\text{dppf})\}](\text{BF}_4)$ | 0.43 | -0.98 | -1.76 ^{d)} |
| $\{(\mu\text{-abpy})[\text{Cu}(\text{PPh}_3)_2]_2\}(\text{BF}_4)_2$ ^[83] | 1.75 ^{e)} | 0.18 | -0.46 |
| $\{(\mu\text{-abpy})[\text{Cu}(\text{diPhos})_2]_2\}(\text{BF}_4)_2$ ^[83] | 1.33 ^{e)} | 0.06 | -0.45 |
| $\{(\mu\text{-abpy})[\text{Cu}(\text{pentaPhos})_2]_2\}(\text{BF}_4)_2$ ^[89] | 1.06 ^{e)} | -0.48 | -1.45 |
| $\{(\mu\text{-abpy})[\text{Cu}(\text{hexaPhos})_2]_2\}(\text{BF}_4)_2$ ^[89] | 1.26 ^{e)} | -0.35 | -1.38 |
| $\{(\mu\text{-abpy})[\text{Cu}(\text{dppf})]_2\}(\text{BF}_4)$ | 0.45 | -0.38 | -1.37 |
| abcp ^[77,88] | - | -1.01 | -1.49 |
| $\{(\mu\text{-abcp})[\text{Cu}(\text{PPh}_3)_2]_2\}(\text{PF}_6)$ ^[82,88] | 1.42 ^{e)} | 0.06 | -0.75 |

^{a)}Potentials E in V vs. $\text{FeCp}_2^{0/+}$; ^{b)}at 100 mV/s scan rate in CH_2Cl_2 / 0.1 M Bu_4NPF_6 ; ^{c)}half wave potential corresponding to reversible step; ^{d)}cathodic peak potential corresponding to an irreversible reduction; ^{e)}anodic peak potential corresponding to an irreversible oxidation.

4.5 UV-vis-NIR spectroelectrochemistry

The spectroelectrochemistry experiments of the complexes $[(\text{abpy})\text{Cu}(\text{dppf})](\text{BF}_4)$ and $\{(\mu\text{-abpy})[\text{Cu}(\text{dppf})]_2\}(\text{BF}_4)$ were performed in an OTTLE cell.

The complex $[(\text{abpy})\text{Cu}(\text{dppf})](\text{BF}_4)$ shows a band at 531 nm with a shoulder at 630 nm due to the MLCT transition from $d^{10}(\text{Cu}^{\text{I}})$ to $\pi^*(\text{abpy})$. Another sharp band at 350 nm is assigned to a typical abpy-based intra-ligand transition. (Fig. 4.5.1)

Upon reversible one-electron reduction the band at 530 nm grows while the shoulder moves to c.a. 860 nm. Some NIR intensity at 1600 nm is observed due to transition involving electron from half-filled π^* orbital. The intra-ligand transition band shows a characteristic shift to 389 nm (at 408 nm in free abpy^-) (Fig. 4.5.1).

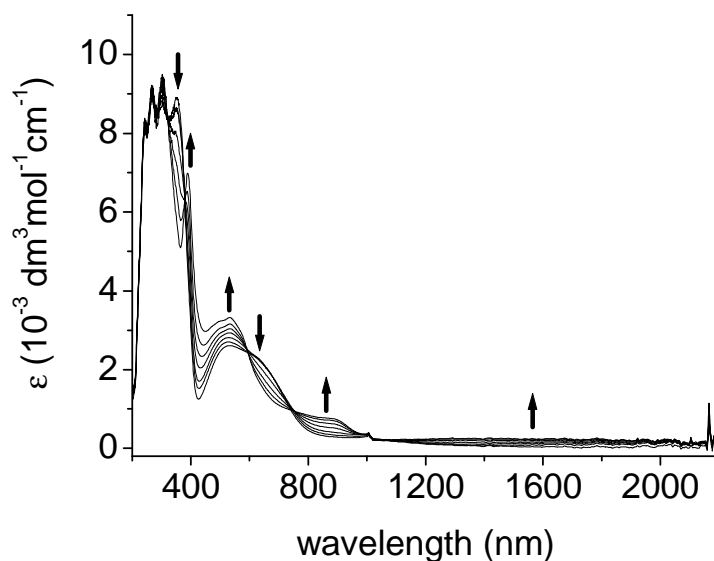


Fig. 4.5.1: Spectroelectrochemical reduction of $[(\text{abpy})\text{Cu}(\text{dppf})]^+$ to $[(\text{abpy})\text{Cu}(\text{dppf})]$ in $\text{CH}_2\text{Cl}_2 / 0.1 \text{ M Bu}_4\text{NPF}_6$

The oxidation at $0.43 \text{ V vs. FeCp}_2^{0/+}$ shows a growing shoulder at 850 nm for the weak long wavelength transition of ferrocenium. Furthermore, the oxidation shifts the MLCT band to 480 nm with the disappearance of the shoulder (Fig 4.5.2).

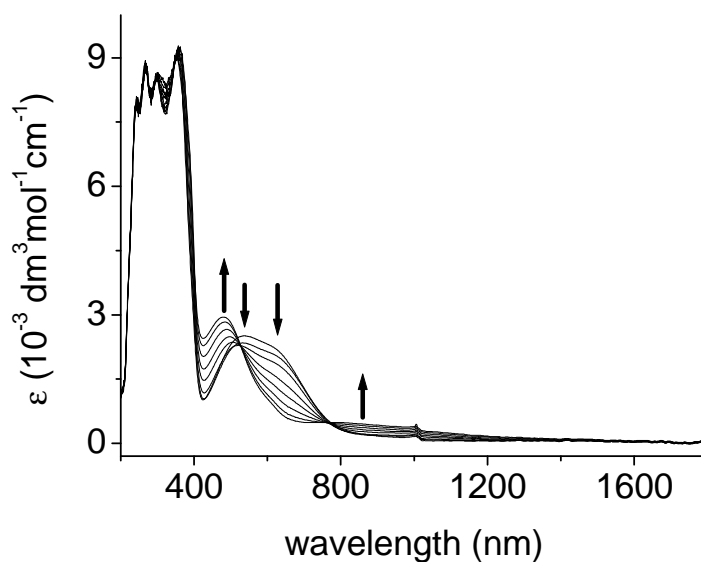


Fig. 4.5.2: Spectroelectrochemical oxidation of $[(\text{abpy})\text{Cu}(\text{dppf})]^+$ to $[(\text{abpy})\text{Cu}(\text{dppf})]^{2+}$ in $\text{CH}_2\text{Cl}_2 / 0.1 \text{ M Bu}_4\text{NPF}_6$

The heterotetranuclear complex $\{(\mu\text{-abpy})[\text{Cu}(\text{dppf})_2](\text{BF}_4)\}$ exhibits a slightly structured MLCT band at 530 nm corresponding to a $(d_\pi)\text{Cu}^{\text{I}} \rightarrow \pi_1^*(\text{abpy})^-$ transition. The di-nuclear complex of abcp, $\{(\mu\text{-abcp})[\text{Cu}(\text{PPh}_3)_2]_2\}^{+\cdot}$, shows characteristic MLCT band at 700 and 560 nm^[7,10] and a band at 510 nm appears for electrochemically generated one electron reduced species $\{(\mu\text{-abpy}^-)[\text{Cu}(\text{PPh}_3)_2]_2\}^{\cdot+}$.^[83] Like all cases a typical sharp intra-ligand abpy-based transition band is seen at 390 nm.^[81(b)]

The electrochemical reduction $\{(\mu\text{-abpy})[\text{Cu}(\text{dppf})_2]\}^{\cdot+ \rightarrow 0}$, at -1.37 V (vs. $\text{Fc}^{0/+}$), results in the appearance of a MLCT band at 484 nm which is tentatively assigned to charge transfer from Cu^{I} to π_2^* (second lowest unoccupied MO) of abpy. The sharp intra-ligand (abpy^-) band disappears and a shoulder at 350 nm appears due to intra-ligand transitions (Fig 4.5.3).

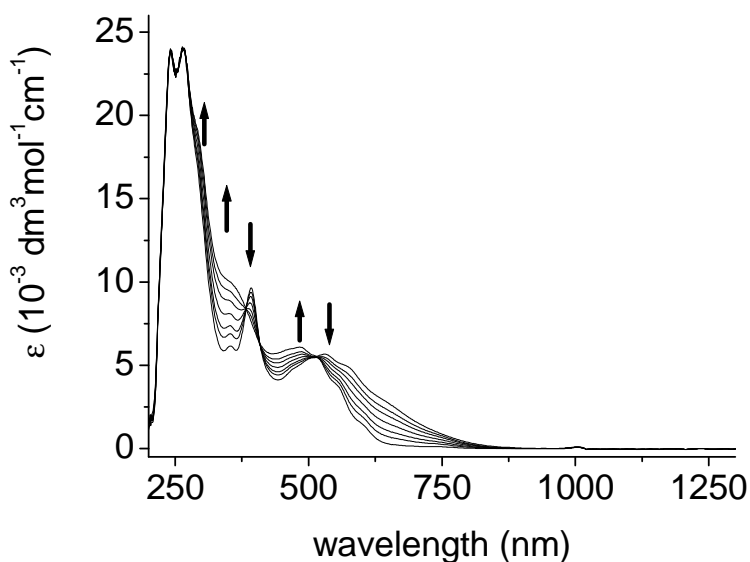


Fig. 4.5.3: Spectroelectrochemical reduction of $\{(\mu\text{-abpy})[\text{Cu}(\text{dppf})_2]\}^{\cdot+}$ to $\{(\mu\text{-abpy})[\text{Cu}(\text{dppf})_2]\}^0$ in $\text{CH}_2\text{Cl}_2 / 0.1$ M Bu_4NPF_6

Upon one electron oxidation at -0.38 V, the MLCT band at 530 nm is bathochromically shifted to 757 nm because of enhanced back donation from d_π Cu to the now completely empty π_1^* level of abpy (Fig. 4.5.4). This is comparable to the shift in charge transfer band from 700 nm to 930 nm for the abcp complex $\{(\mu\text{-abcp})[\text{Cu}(\text{PPh}_3)_2]_2\}^{2+}$ ^[85] and from 510 nm to 680 nm for di-nuclear copper(I) complex of abpy, $\{(\mu\text{-abpy})[\text{Cu}(\text{PPh}_3)_2]_2\}^{2+}$ ^[83]. The in situ generated $\{(\mu\text{-abpy})[\text{Cu}(\text{dppf})_2]\}^{2+}$ having an empty π_1^* level of the azo ligand also justifies the disappearance of the abpy^- intra-ligand band at 390 nm.^[81(b)]

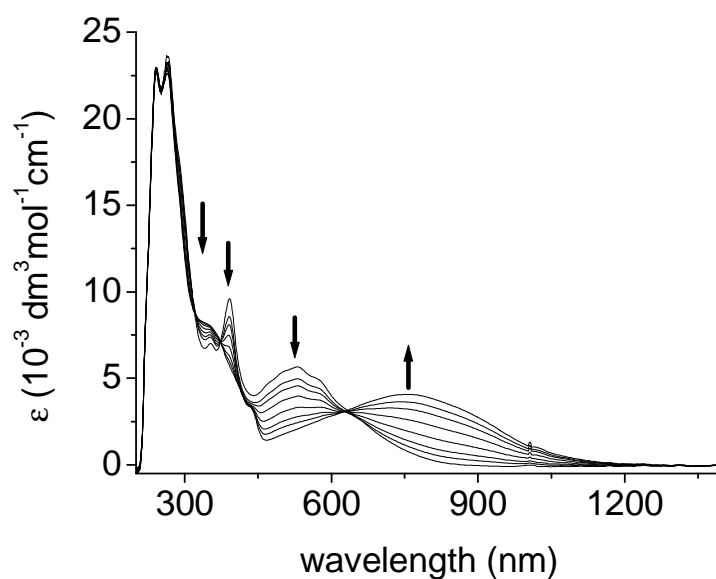


Fig. 4.5.4: Spectroelectrochemical oxidation of $\{(\mu\text{-abpy})[\text{Cu}(\text{dppf})]_2\}^+$ to $\{(\mu\text{-abpy})[\text{Cu}(\text{dppf})]_2\}^{2+}$ in $\text{CH}_2\text{Cl}_2 / 0.1 \text{ M Bu}_4\text{NPF}_6$

Further oxidation of ferrocenyl ancillaries at 0.45 V (vs $\text{Fc}^{0/+}$) results in the decrease of intensity of the MLCT band at 757 nm (Fig 4.5.5). The absorption data for all compounds are tabulated in Tab. 4.5.1.

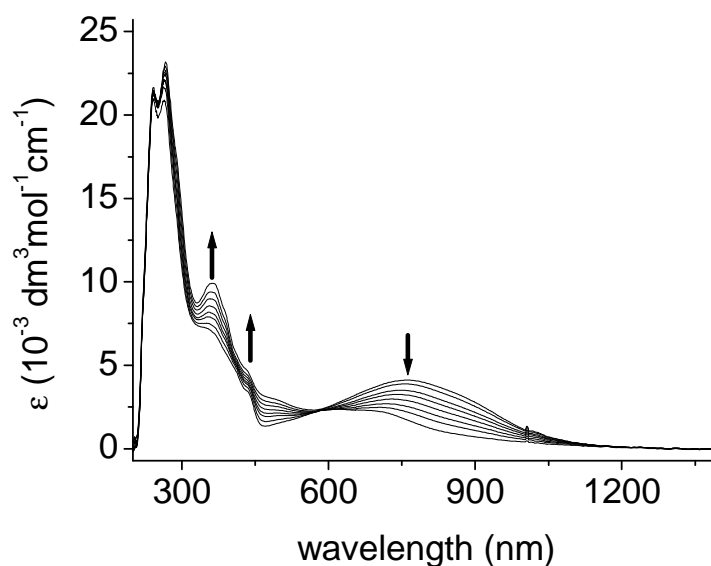


Fig. 4.5.5: Spectroelectrochemical oxidation of $\{(\mu\text{-abpy})[\text{Cu}(\text{dppf})]_2\}^{2+}$ to $\{(\mu\text{-abpy})[\text{Cu}(\text{dppf})]_2\}^{4+}$ in $\text{CH}_2\text{Cl}_2 / 0.1 \text{ M Bu}_4\text{NPF}_6$.

Tab. 4.5.1: Absorption data obtained from spectroelectrochemistry in CH₂Cl₂ / 0.1 M Bu₄NPF₆.

| Compound | λ_{\max} / nm (ϵ / 10 ⁻³ M ⁻¹ cm ⁻¹) |
|--|--|
| abpy ^{a)} [81(b)] | 312(8.7), 470(0.9) |
| abpy ^{-a)} [81(b)] | 286(sh), 360(sh), 408(26.5), 548(2.6) |
| abpy ^{2-a)} [81(b)] | 275(sh), 342(sh), 358(14.2), 380(sh), 450(sh) |
| [(abpy)Cu(dppf)] ^{2+b)} | 862(sh), 479(2.9) |
| [(abpy)Cu(dppf)] ^{+b)} | 630(sh), 530(2.6), 350(8.8) |
| [(abpy ⁻)Cu(dppf)] ^{b)} | 530(3.3), 389(6.9) |
| [(abpy ²⁻)Cu(dppf)] ^{-b)} | 579(sh) |
| {(μ-abpy)[Cu(PPh ₃) ₂] ₂ } ^{2+[83]} | 357, 680 |
| {(μ-abpy ⁻)[Cu(PPh ₃) ₂] ₂ } ^{+[83]} | 350, 510 |
| {(μ-abpy)[Cu(dppf)] ₂ } ^{4+b)} | 700(sh), 435(sh), 361(9.8) |
| {(μ-abpy)[Cu(dppf)] ₂ } ^{2+b)} | 757(4.1), 339(sh) |
| {(μ-abpy ⁻)[Cu(dppf)] ₂ } ^{·+b)} | 533(5.6), 390(9.6) |
| {(μ-abpy ²⁻)[Cu(dppf)] ₂ } ^{b)} | 484(6.1), 348(sh), 302(sh) |
| abcp ^{b)} | 455 (0.37), 286 (26.0) |
| abcp ^{-b)} | 555 (sh), 477 (sh), 404 (44), 350 (sh) |
| abcp ^{2-b)} | 457 (sh), 352 (45) |
| {(μ-abcp)[Cu(PPh ₃) ₂] ₂ } ^{2+b)[85]} | 930 (1.1), 870 (0.8), 365 (1.54) |
| {(μ-abcp)[Cu(PPh ₃) ₂] ₂ } ^{·+b)[85]} | 700 (0.63), 560 (0.9), 403 (2.6), 373 (2.6) |
| {(μ-abcp)[Cu(PPh ₃) ₂] ₂ } ^{b)[85]} | 515 (sh), 363 (2.8) |

a) in DMF / 0.1 M Bu₄NPF₆; b) in CH₂Cl₂ / 0.1 M Bu₄NPF₆

4.6 EPR spectroscopy

The heterodinuclear complex [(abpy)Cu(dppf)](BF₄) is diamagnetic. It is reduced in situ to generate the one-electron reduced neutral radical species [(abpy⁻)Cu(dppf)]. However, on extended reduction the compound shows an EPR spectrum identical to that of the heterotetranuclear complex ion {(μ-abpy)[Cu(dppf)]₂}⁻. This indicates the in situ formation of the tetranuclear species on one-electron reduction of [(abpy)Cu(dppf)](BF₄) because of lability of coordination of Cu^I and less negative reduction potential for dicopper system

(electron transfer assisted polymerization). The simulation parameters fit with one set of azo ^{14}N ($I = 1$), two pyridine ^{14}N ($I = 1$), four ^{31}P ($I = 3/2$) and two $^{63/65}\text{Cu}$ ($I = 3/2$) isotopes.

The heterotetranuclear complex $\{(\mu\text{-abpy})[\text{Cu}(\text{dppf})]_2\}(\text{BF}_4)$ is paramagnetic and hence EPR spectroscopy is directly applicable to determine the nature of the orbital where the electron is situated. The most important parameters are the isotropic g values and the splitting into g -components (g anisotropy), particularly at high field. At X-band (9.5 GHz) in CH_2Cl_2 solution the complex shows a well resolved line-rich EPR signal with $g_{\text{iso}} = 2.0069$. Two experimentally measured EPR spectra together with the simulated spectrum of $\{(\mu\text{-abpy})[\text{Cu}(\text{dppf})]_2\}(\text{BF}_4)$ are shown in Fig 4.6.2.

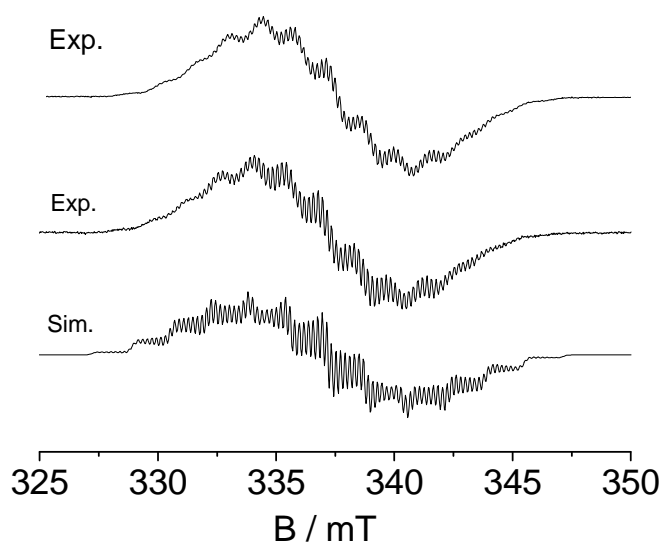


Fig. 4.6.2: X-band EPR spectra of electrochemically generated $\{(\mu\text{-abpy})^-\text{[Cu}(\text{dppf})]_2\}^+$ (top) obtained by insitu reduction of $[(\text{abpy})\text{Cu}(\text{dppf})]^+$ (in CH_2Cl_2 / 0.1 M Bu_4NPF_6 at RT) and (center) for $\{(\mu\text{-abpy})[\text{Cu}(\text{dppf})]_2\}(\text{BF}_4)$ as dissolved in CH_2Cl_2 at RT; (bottom): simulated spectrum with the data from the Tab 4.6.1 and a line-width of 0.23 mT .

The simulated spectrum was obtained by considering the coupling from $^{63/65}\text{Cu}$, ^{31}P , and ^{14}N isotopes. The isotopic hyperfine coupling constants are 0.565 mT (one set of azo ($\text{N}=\text{N}$)), 0.22 mT (two pyridine ^{14}N), 1.55 mT (two ^{63}Cu), 1.65 mT (two ^{65}Cu) and 1.79 mT (four ^{31}P), respectively (Fig 4.6.2 and Tab 4.6.1). The replacement of the ancillary phosphines in the complexes $\{(\mu\text{-abpy})[\text{Cu}(\text{PPh}_3)_2]_2\}^+^{[89]}$, $\{(\mu\text{-abpy})[\text{Cu}(\text{diPhos})]_2\}^+^{[89]}$ and $\{(\mu\text{-abpy})[\text{Cu}(\text{hexaPhos})]_2\}^+^{[57]}$ with dppf causes a significant improvement in EPR spectrum

resolution, resolving the hyperfine coupling from azo and pyridine ^{14}N because of the rigidity of the $[\text{Cu}(\text{dppf})]^+$, which in turn restricts line broadening by extensive rotation (Tab 4.6.1).

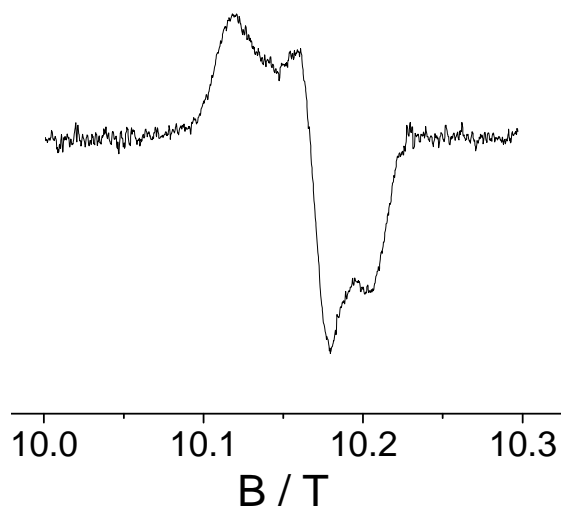


Fig. 4.6.3: 285 GHz EPR spectrum of $\{(\mu\text{-abpy})[\text{Cu}(\text{dppf})]_2\}(\text{BF}_4)$ at 5 K in CH_2Cl_2 / toluene (4:1).

To gain more information on the electronic structure through the g anisotropy in comparison to copper(II) and mixed-valent dicopper species, the stable paramagnetic complex $\{(\mu\text{-abpy})[\text{Cu}(\text{dppf})]_2\}(\text{BF}_4)$ was subjected to high frequency EPR measurements. At 285 GHz at 5 K, the complex shows a rhombic g component pattern as seen from the g values 2.0124, 2.0022 and 1.9957 (Fig. 4.6.3 and Tab 4.6.2). The identical splitting pattern of g components was observed for other mono-reduced azo-based ligand abpy^- and abcp^- bridged dicopper complexes. The fairly small g anisotropy ($\Delta g = g_1 - g_3$) of 0.0167 indicates predominantly ligand centered spin. The g anisotropies ($\Delta g = g_1 - g_3$) for tetrazine-centered radical complexes, which show axial splitting of g components, are much smaller than those of the azo bridged radical complexes indicating better π -acceptor ability of the azo function.^[82,85,87] The complex $\{(\mu\text{-abcp})[\text{Cu}(\text{PPh}_3)_2]_2\}^+$ shows an unresolved EPR spectrum in X-band with $g_{\text{iso}} = 2.0077$.^[82,85,86] Both the g anisotropy data from the high frequency measurement and the hyperfine coupling data from the X-band studies suggest a rather small amount of metal participation at the SOMO (singly occupied molecular orbital) of the azo radical complex, confirming the spin localization on the bridging ligand abpy . The X-band EPR spectra of azo-radical based dicopper(I) complexes reveal how the replacement of phosphines by

ferrocenylphosphine results in better EPR resolution so that the ^{14}N coupling from both the azo and the pyridine N nuclei can be determined.

Tab. 4.6.1: Hyperfine coupling constants from simulated EPR spectra.

| Compound | g_{iso} | $a(^{65/63}\text{Cu}, I = 3/2)^{\text{c}}$ | $a(^{31}\text{P}, I = 1/2)^{\text{c}}$ | $a(^{14}\text{N}, I = 1)^{\text{c}}$ |
|---|------------------|--|--|--------------------------------------|
| $\text{abpy}^{-\text{[85]}}$ | 2.0044 | - | - | - |
| $[(\text{abpy})^{-}\text{Cu}(\text{dppf})]$ | a) | a) | a) | a) |
| $\{(\mu\text{-abpy})[\text{Cu}(\text{dppf})]_2\}^{\cdot+}$ | 2.0069 | 1.55, 1.65 | 1.79 | 0.56, 0.22 |
| $\{(\mu\text{-abpy}^{-})[\text{Cu}(\text{PPh}_3)_2]_2\}^{\cdot+}$ | 2.0053 | 1.30 | 1.30 | - |
| $\{(\mu\text{-abpy}^{-})[\text{Cu}(\text{diPhos})]_2\}^{\cdot+}$ | 2.0046 | - | - | - |
| $\{(\mu\text{-abpy})[\text{Cu}(\text{hexaPhos})]_2\}^{\text{[57]}}$ | 2.0051 | 1.300, 1.393 | 1.48 | - |
| $\text{abcp}^{-\text{b)[88]}}$ | 2.0041 | - | - | - |
| $\{(\mu\text{-abcp})[\text{Cu}(\text{PPh}_3)_2]_2\}^{\cdot+\text{[82,88]}}$ | 2.0077 | 1.7 | 1.7 | - |

a) not obtained, formed heterotetranuclear species $\{(\mu\text{-abpy})[\text{Cu}(\text{dppf})]_2\}^{\cdot+}$ on in situ reduction.
 b) from reduction with K in THF solution at 298 K, insufficient hyperfine resolution; c) hyperfine coupling constants in mT.

Tab. 4.6.2: X-band and high frequency EPR data.

| Compound | $g_{\text{iso}}^{\text{b)}$ | $g_1^{\text{c)}$ | $g_2^{\text{c)}$ | $g_3^{\text{c)}$ | $g_{\text{av}}^{\text{d)}$ | $\Delta g^{\text{e)}$ |
|---|-----------------------------|------------------|------------------|------------------|----------------------------|-----------------------|
| $\text{abpy}^{-\text{a)}$ | 2.0044 | - | - | - | - | - |
| $[(\text{abpy})^{-}\{\text{Cu}(\text{dppf})\}]^{\text{a)}$ | f) | f) | f) | f) | f) | f) |
| $\{(\mu\text{-abpy})[\text{Cu}(\text{dppf})]_2\}^{\cdot+}$ | 2.0069 | 2.0124 | 2.0022 | 1.9957 | 2.0034 | 0.0167 |
| $\{(\mu\text{-abpy}^{-})[\text{Cu}(\text{PPh}_3)_2]_2\}^{\cdot+}$ | 2.0053 | - | - | - | - | - |
| $\{(\mu\text{-abpy}^{-})[\text{Cu}(\text{diPhos})]_2\}^{\cdot+}$ | 2.0046 | - | - | - | - | - |
| $\{(\mu\text{-abpy})[\text{Cu}(\text{hexaPhos})]_2\}^{\text{[57]}}$ | 2.0051 | 2.0134 | 2.0047 | 1.9968 | 2.0050 | 0.0166 |
| $\text{abcp}^{-\text{a)[88]}}$ | 2.0041 | - | - | - | - | - |
| $\{(\mu\text{-abcp})[\text{Cu}(\text{PPh}_3)_2]_2\}^{\cdot+\text{[82,88]}}$ | 2.0077 | 2.016 | 2.007 | 1.998 | 2.0077 | 0.018 |
| $\{(\mu\text{-bptz})[\text{Cu}(\text{PPh}_3)_2]_2\}^{\cdot+}$ | 2.0055 | 2.0067 | 2.0067 | 2.0026 | 2.0053 | 0.0041 |
| $\{(\mu\text{-bptz})[\text{Cu}(\text{hexaPhos})]_2\}^{\cdot+\text{[57]}}$ | 2.0054 | 2.007 | 2.007 | 2.0024 | 2.0055 | 0.0046 |

a) from electrochemically generated species; b) X-band EPR data at RT; c) from high frequency EPR measurements at 5 K; d) $g_{\text{av}} = \sqrt{(g_1^2 + g_2^2 + g_3^2)}/3$; e) $\Delta g = g_1 - g_3$; f) not obtained, forms heterotetranuclear species $\{(\mu\text{-abpy})[\text{Cu}(\text{dppf})]_2\}^{\cdot+}$ on in situ reduction.

4.7 Conclusion

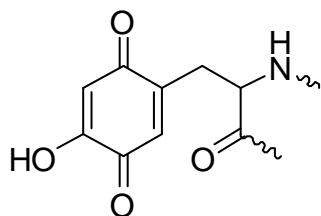
Using the special ferrocenylbis(diphenylphosphine)copper(I) fragment $[\text{Cu}^{\text{I}}(\text{dppf})]^+$, the first examples of a structurally characterized heterodinuclear complex $[(\text{abpy})\{\text{Cu}(\text{dppf})\}](\text{BF}_4)$ and radical bridged heterotetranuclear complex $\{(\mu\text{-abpy})[\text{Cu}(\text{dppf})]_2\}(\text{BF}_4)$ could be obtained. By applying a different synthetic route, the non-radical heterotetranuclear complex $\{(\mu\text{-abpy})[\text{Cu}(\text{dppf})]_2\}(\text{BF}_4)_2$ was also isolated and characterized in the diamagnetic form. The extra stabilizing power of dppf over other phosphines possibly plays a key role in isolation of the complexes in different oxidation states of the ligand abpy. From the X-ray crystal structures of $[(\text{abpy})\{\text{Cu}(\text{dppf})\}](\text{BF}_4)$ and $\{(\mu\text{-abpy})[\text{Cu}(\text{dppf})]_2\}(\text{BF}_4)$, the distinct change in azo bond length could be compared. The EPR signal of the in situ generated radical species from the heterodinuclear complex shows an identical pattern with the EPR signal from the radical bridged heterotetranuclear complex which indicates the formation of radical bridged species $\{(\mu\text{-abpy})[\text{Cu}(\text{dppf})]_2\}^{\cdot+}$ following one electron reduction of $[(\text{abpy})\text{Cu}(\text{dppf})]^+$. The replacement of normal phosphine ligands by rigid dppf in the present work also results in better resolution of the hyperfine couplings from two types of ^{14}N ($I = 1$) of the abpy-bridge apart from ^{31}P and $^{63/65}\text{Cu}$ isotopes. The detailed spectroelectrochemical studies show characteristic changes in the MLCT and ILCT bands on oxidation / reduction of the complexes.

Chapter 5

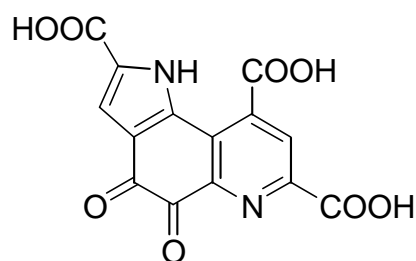
Stabilizing the elusive ortho-quinone/copper(I) oxidation state combination through π - π interaction in an isolated complex

5.1 Introduction.

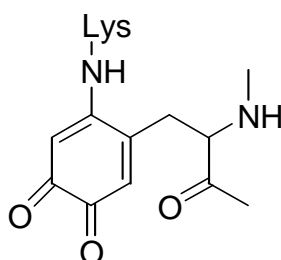
The *o*-quinone cofactors derived from tyrosine and tryptophan are involved in novel biological reactions that range from oxidative deaminations to free-radical redox reactions.^[90] Pyrroloquinoline quinone (PQQ) was the first of the *o*-quinone cofactors identified in many prokaryotic organism's alcohol and glucose dehydrogenase.^[11] Following the discovery of PQQ, other cofactors in *o*-quinone family, e.g., tryptophan tryptophylquinone (TTQ),^[91] topaquinone (TPQ),^[92] lysine tyrosylquinone (LTQ)^[93] were identified as the essential cofactors of different redox enzymes in various living organisms. Copper has been known as an essential bio-element for such quino-enzymes like tyrosinase,^[94,95] catechol oxidase,^[96] galactose oxidase,^[97] amine oxidase^[98-100]



Topaquinone (TPQ)



Pyrroloquinoline quinone (PQQ)



Lysine tyrosylquinone (LTQ)

Hence the copper/quinone interaction is relevant for research areas as diverse as biochemical systems (neurotransmitter and melanin metabolism, tyrosinase, polyphenol oxidase, and quinoproteins oxidase function), molecular devices (valence tautomerism),^[29,102,103,104(a)]

biodegradation (catechol-enhanced Fenton reaction),^[105] organic and industrial synthesis (copper catalyst for catechol or phenol synthesis)^[106] and photochemical charge transfer.^[107] Stable *o*-quinonemonoimine and *o*-quinonediimine complexes of copper(I) and copper(II) were reported, and the one electron and two electron reduced forms of O,O'-coordinating *o*-quinones, the semiquinones, and catecholates have long been known to form chelate complexes with Cu^I and Cu^{II}. So far there were many examples in the literature of the chelate complexes formed by ortho-semiquinones (Sq) and catecholates (Cat) with Cu(I) and Cu(II).^[104] Moreover the temperature controlled equilibrium between Cu^I-Sq and Cu^{II}-Cat is also known from literature.^[104(a)] In contrast, there has been no report of an isolated *o*-quinone copper(I) species with quinone-O coordinated metal possibly because of the lability of copper(I) vs. oxygen and low basicity of unreduced quinone ligands.

Using the organometallic coligand for copper(I), viz, dppf = 1,1'-bis(diphenylphosphino)-ferrocene, and a well established *o*-quinone in the form of PhenQ = 9,10-phenanthrenequinone, the first structural, theoretical and spectroscopic evidence for the O,O'-chelate coordination to electron rich copper(I) by unreduced quinone π acceptor is demonstrated in this chapter.

5.2 Synthesis and characterization

The heterodinuclear complex [(PhenQ)Cu(dppf)](BF₄) was synthesized by refluxing a 1:1 mixture of 9,10-phenanthroquinone (PhenQ) and [Cu(dppf)(CH₃CN)₂](BF₄)^[74] in dry dichloroethane for 12 h under argon atmosphere. After removal of the solvent under low pressure the deep green solid was washed several times with dry hexane and was recrystallized from dry dichloromethane/hexane (2:1). The complex was initially characterized by ¹H, ³¹P NMR, IR spectroscopy, elemental analysis and mass spectroscopy. ¹H, ³¹P NMR (Tab 5.2.1), IR spectrum and mass spectrum are discussed below and elemental analysis result is reported in the experimental section.

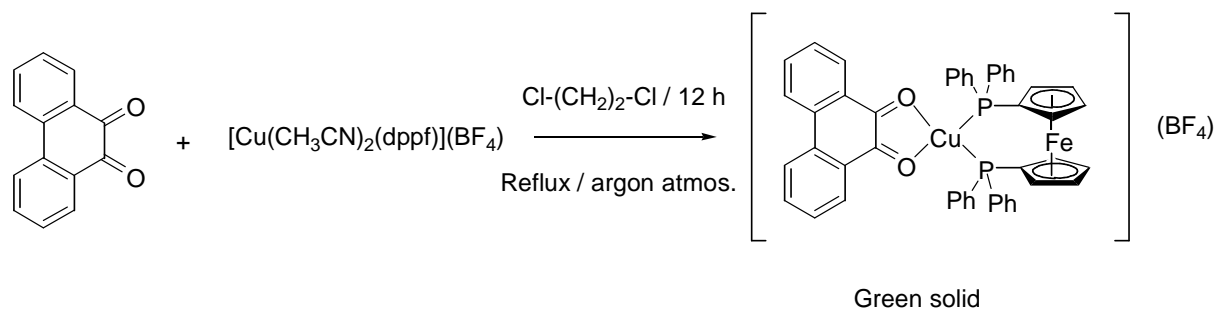
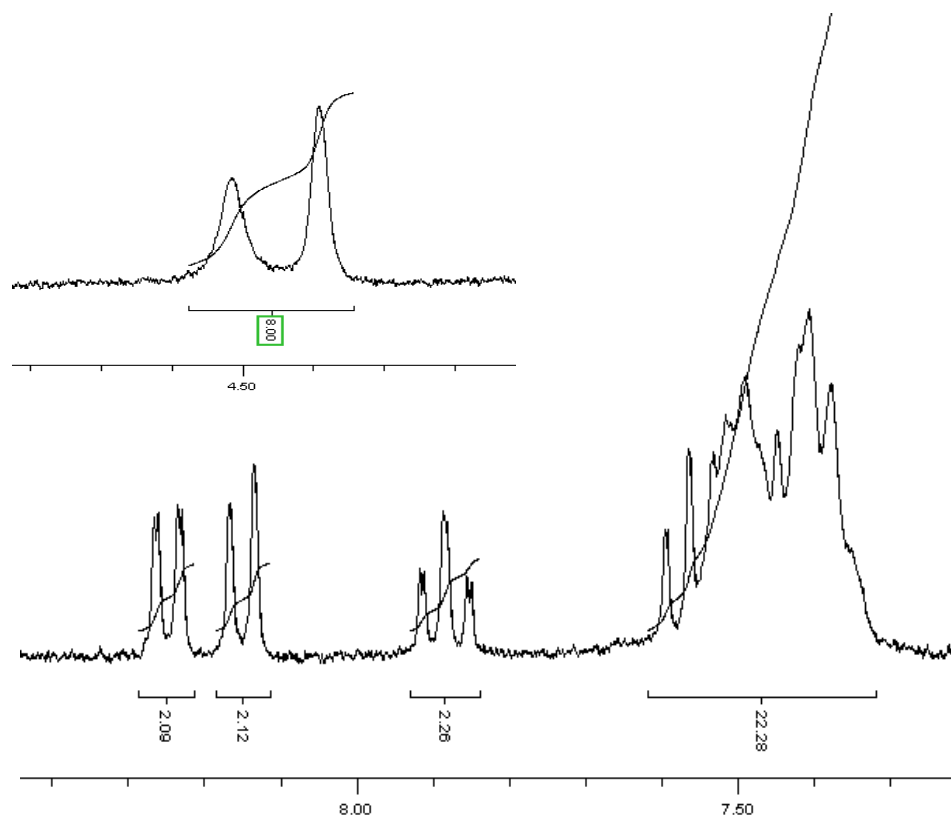


Fig 5.2.1: Synthesis of [(PhenQ)Cu(dppf)](BF₄).Fig 5.2.2: ¹H NMR of [(PhenQ)Cu(dppf)](BF₄) in CD₂Cl₂. Inset shows high field part of the spectrum.Tab 5.2.1: ¹H and ³¹P NMR data^{a)}.

| Compound | δ / ppm for ¹ H | δ / ppm for ³¹ P |
|--|---|------------------------------------|
| PhenQ | 7.45 (td, 2H, J = 7.4 Hz, 1, H ²); 7.70 (td, 2H, J = 8.2, 1.5 Hz, H ³); 7.99 (d, 2H, J = 8 Hz, H ¹); 8.17 (dd, 2H, J = 1.4, 7.8 Hz, H ⁴) | - |
| [Cu(dppf)(CH ₃ CN) ₂](BF ₄) | 2.07 (s, 6H, CH ₃ CN); 4.10 (s, 4H, Cp); 4.32 (s, 4H, Cp); 7.35-7.55 (m, 20H, Ph) | -13.21 |
| [(PhenQ)Cu(dppf)](BF ₄) | 4.39 (s, 4H, Cp); 4.51 (s, 4H, Cp); 7.35-7.55 (m, 20H, Ph), 7.56-7.59 (m, 2H, H ²), 7.88 (td, 2H, J = 7.5, 1.3 Hz, H ³); 8.15 (d, 2H, J = 8 Hz, H ¹); 8.24 (dd, 2H, J = 1.5, 7.8 Hz, H ⁴) | -10.40 |

^{a)} in CD₂Cl₂

Since in the complex PhenQ is expected to bind Cu(I) via non-reduced carbonyl (C=O) chelate, the IR spectrum of the complex should be quite informative. The $\nu_{\text{C=O}}$ for the free ligand appears at 1671 cm⁻¹ whereas in the complex the $\nu_{\text{C=O}}$ is at 1673 cm⁻¹. Negligible shift in $\nu_{\text{C=O}}$ indicates very weak back-bonding from Cu^I to quinone in the complex. Mass spectrum shows molecular ion peak at 825.08 Da corresponding to [(PhenQ)Cu(dppf)]⁺ and another intense peak at 617.03 Da for [Cu(dppf)]⁺ fragments.

Elemental analysis together with all spectroscopic data justify the formation and isolation of the first Cu^I-quinone complex [(PhenQ)Cu(dppf)](BF₄).

5.3 Crystal structure

The dark green block shaped crystals of [(PhenQ)Cu(dppf)](BF₄) were grown by slow diffusion of hexane in dichloromethane solution of the complex at 4 °C under argon atmosphere. It was crystallized in monoclinic *P2₁/n* space group. Two molecules of CH₂Cl₂ were found as a solvent of crystallization. The structural analysis confirms the O,O'-chelation to Cu(I) in [(PhenQ)Cu(dppf)](BF₄) and substantiated the unreduced quinone character of PhenQ via the C=O bond lengths of 1.257(11) and 1.244(10) Å (semiquinones have ≥ 1.27 Å) and the (O)C-C(O) single bond length of 1.499(13) Å (semiquinones have ≤ 1.46 Å). Free PhenQ has C=O bond length 1.22 Å and (O)C-C(O) bond length 1.52 Å.^[108] The elongation of the C=O bond lengths were due to π -back donation from d¹⁰(Cu) to π^* of PhenQ. The Cu-O bonds are remarkably different (Cu-O1 2.053(7) Å; Cu-O2 2.159(6) Å) as are the two Cu-P bonds at Cu-P1 2.208(3) Å and Cu-P2 2.254(3) Å; the stronger Cu-O1 and Cu-P1 bonds form a much larger angle at 132.3(2)° than the two longer such bonds at 99.55(19)°. Such strong distortions are not completely unknown in copper(I) chemistry.

Moreover, the crystal structure shows intramolecular and inter molecular π/π interactions. The intramolecular π/π interaction with shortest C-C distance 3.155 Å between one phenyl of dppf and PhenQ is seen clearly in the crystal structure (Fig 5.3.1). The molecular structure of the cation in the crystal is shown in fig 5.3.1.

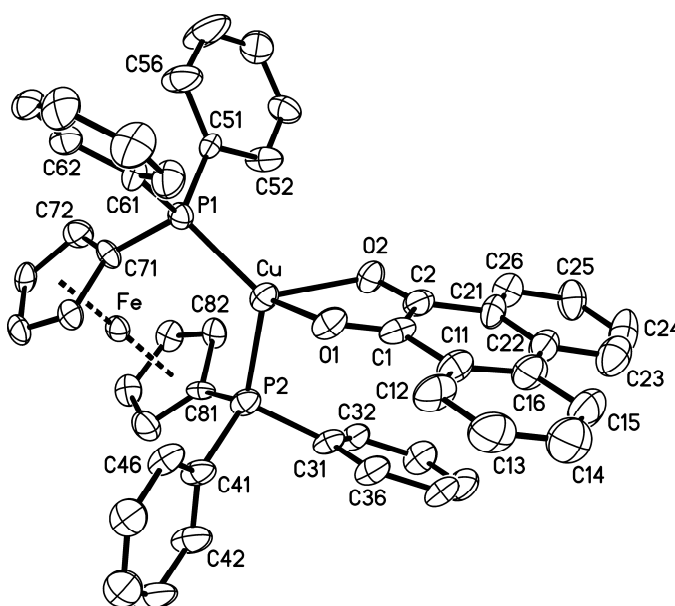


Fig 5.3.1: Molecular structure of the cation in the crystal structure of $[(\text{PhenQ})\text{Cu}(\text{dppf})](\text{BF}_4) \times 2 \text{CH}_2\text{Cl}_2$

The important bond lengths and bond angles are tabulated in tab 5.3.1.

Tab: 5.3.1: Important bond lengths (\AA) and bond angles ($^\circ$).

| Bond lengths (\AA) | | Bond angles ($^\circ$) and dihedral angles | |
|-------------------------------|-----------|--|----------|
| Cu-O1 | 2.053(7) | P1-Cu-P2 | 116.1(1) |
| Cu-O2 | 2.159(6) | P1-Cu-O2 | 119.2(2) |
| Cu-P1 | 2.208(3) | P1-Cu-O1 | 132.3(2) |
| Cu-P2 | 2.254(3) | P2-Cu-O1 | 103.1(2) |
| C1-O1 | 1.257(10) | P2-Cu-O2 | 99.56(2) |
| C2-O2 | 1.244(10) | O2-Cu-O1 | 76.8(3) |
| C1-C2 | 1.499(13) | O1-C1-C2-O2 | -0.66 |
| C1-C11 | 1.465(13) | | |
| C11-C16 | 1.417(14) | | |
| C16-C22 | 1.456(14) | | |
| C21-C22 | 1.379(13) | | |
| C2-C21 | 1.481(13) | | |

5.4 UV-vis spectroscopy

The complex $[(\text{PhenQ})\text{Cu}(\text{dppf})](\text{BF}_4)$ exhibits one long wavelength maximum at 693 nm ($\epsilon = 3390 \text{ M}^{-1}\text{cm}^{-1}$) and another band 420 nm ($\epsilon = 6540 \text{ M}^{-1}\text{cm}^{-1}$) which is similar to that reported for a reaction mixture between PhenQ and $(\text{Ph}_3\text{P})_2\text{Cu}(\text{BH}_4)$ in CH_2Cl_2 ($\lambda_{\text{max}} = 707, 418 \text{ nm}$).^[107] The band at 693 nm ($\epsilon = 3390 \text{ M}^{-1}\text{cm}^{-1}$) is attributed to the metal to ligand charge transfer (MLCT) from $(\text{d}^{10})\text{Cu}(\text{I})$ to π^* of PhenQ leading to an excited state formulation $(\text{d}^9)\text{Cu}(\text{II})/\text{PhenSQ}$. The 420 nm ($\epsilon = 6540 \text{ M}^{-1}\text{cm}^{-1}$) band can primarily be assumed to PhenQ based intra-ligand $\pi\text{-}\pi^*$ electronic transition which is comparable to free PhenQ (418 nm) which is further justified by TD-DFT calculations. The UV-vis spectra of $[(\text{PhenQ})\text{Cu}(\text{dppf})](\text{BF}_4)$ in shown in fig 5.4.1. The complex does not show any emission or photo-reactive properties.

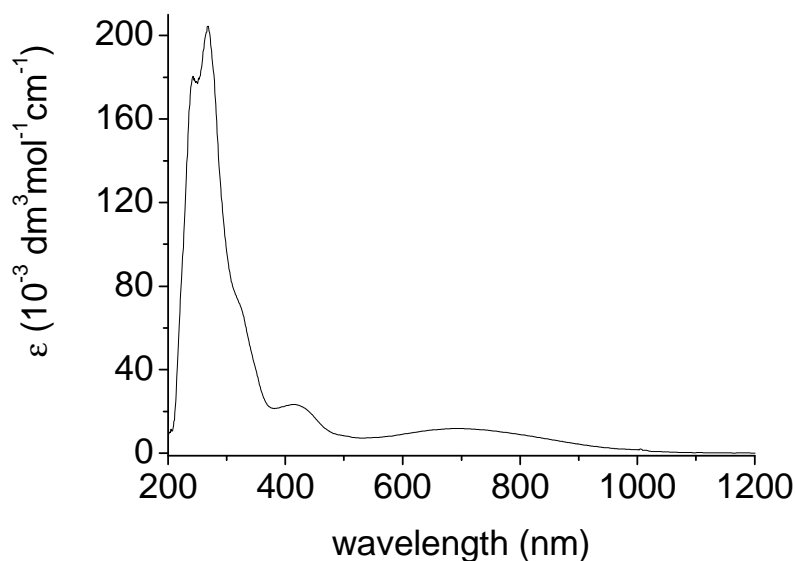


Fig 5.4.1: UV-vis spectra of $[(\text{PhenQ})\text{Cu}(\text{dppf})](\text{BF}_4)$ in CH_2Cl_2 .

5.5 Cyclic voltammetry

Cyclic voltammetry for the complex $[(\text{PhenQ})\text{Cu}(\text{dppf})](\text{BF}_4)$ was measured at -50°C to achieve reversibility in reduction. The complex has one reversible PhenQ ligand based reduction at -0.78 V ($\text{PhenQ} \rightarrow (\text{PhenQ})^-$) and one quasi-reversible reduction at -1.70 V ($(\text{PhenQ})^- \rightarrow (\text{PhenQ})^{2-}$) vs. ferrocene. After 1st reduction a small peak at -1.36 V was seen

due free ligand reduction from the dissociated complex. The complex shows one reversible one electron oxidation at 0.14 V vs. ferrocene. The oxidation is centered at the ferrocenyl co-ligand as copper oxidation in such a system can not be seen at such low potentials with reversibility. Low temperature cyclic voltammogram along with differential pulse voltammetry (DPV) is shown in fig 5.5.1 and 5.5.2 and the potentials are tabulated in tab 5.5.1.

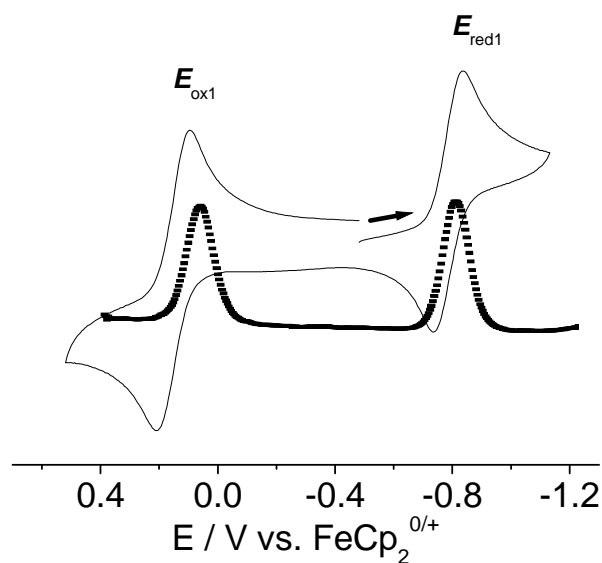


Fig 5.5.1 Cyclic voltammogram and differential pulse voltammogram for 1st oxidation and 1st reduction of [(PhenQ)Cu(dppf)](BF₄) at - 50° C in CH₂Cl₂ / 0.1 M Bu₄NPF₆ (scan rate 100 mV / s)

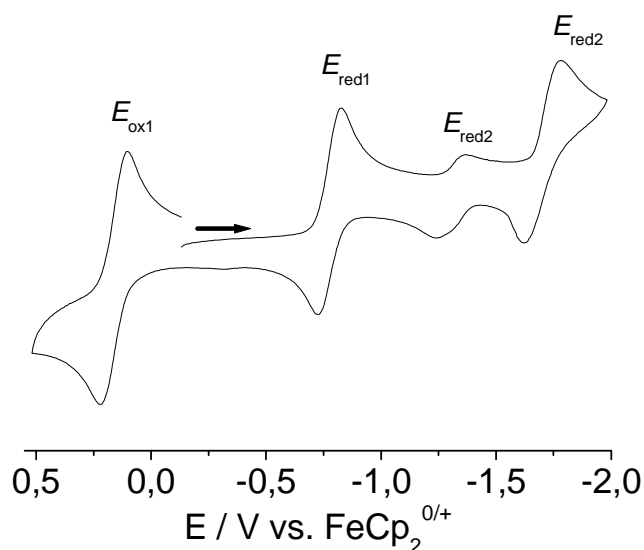


Fig 5.5.2: Cyclic voltammogram (full range) of [(PhenQ)Cu(dppf)](BF₄) at – 50° C in CH₂Cl₂ / 0.1 M Bu₄NPF₆ (scan rate 100 mV / s)

Tab 5.5.1: Electrochemical potential^{a)} from cyclic voltammetry at – 50° C.

| Compound | $E_{\text{ox1}}^{\text{c)}$ | $E_{\text{red1}}^{\text{c)}$ | $E_{\text{red2}}^{\text{c)}$ | $E_{\text{red3}}^{\text{c)}$ |
|-------------------------------------|-----------------------------|--------------------------------------|--------------------------------------|------------------------------|
| PhenQ | - | -1.34 ($E_{\text{pc}}^{\text{b)}$) | - | - |
| [(PhenQ)Cu(dppf)](BF ₄) | 0.14 | -0.78 | -1.36 ($E_{\text{pc}}^{\text{b)}$) | -1.70 |

^{a)} Potentials E in V vs. FeCp₂^{0/+} in CH₂Cl₂ / 0.1 M Bu₄NPF₆ (scan rate 100 mV / s); ^{b)} cathodic peak potentials corresponding to irreversible peak; ^{c)} half-wave potential corresponding to reversible step.

5.6 EPR spectroscopy

It was possible to measure the EPR spectrum of the in situ generated paramagnetic species [(PhenSQ)Cu(dppf)]^{•-}. The spectrum was recorded at 220 K due to the reversibility in cyclic voltammogram of the complex.

The complex [(PhenQ)Cu(dppf)](BF₄) on reduction gives a strong X-band EPR signal resulting from the formation of semiquinone (PhenSQ) radical species [(PhenSQ)Cu(dppf)]^{•-} with $g_{\text{iso}} = 2.0055$. The hyperfine for ^{63,65}Cu ($I = 3/2$), ³¹P ($I = 1/2$) and ¹H ($I = 1/2$) isotopes at 1.0 mT (1Cu), 1.4 mT (2P), and 0.15 mT (4H), respectively, agree with the phenanthrenesemiquinone data (0.165, 0.137, 0.042, 0.022 mT, 2H each)^[109] and with typical values for copper(I) radical complexes. The experimental X-band EPR spectra along with simulation are shown in Fig 5.6.1 and the hyperfine coupling constant values obtained from simulation are tabulated in Tab 5.6.1.

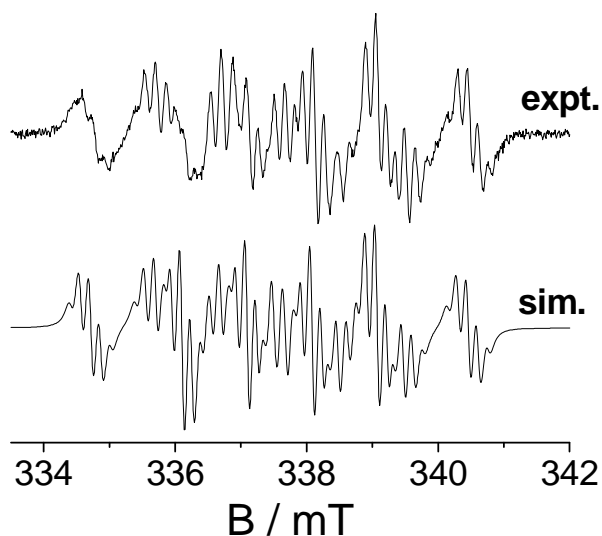


Figure 5.6.1: X-band EPR of electrochemically generated $[(\text{PhenSQ})\text{Cu}(\text{dppf})]^-$ at 220 K in $\text{CH}_2\text{Cl}_2 / 0.1 \text{ M Bu}_4\text{NPF}_6$ (top) and simulation (bottom).

Table 5.6.1: EPR data^{a)}

| Compound | g_{iso} | a_1 ($^{63/65}\text{Cu}$) ^{c)} | a_2 (^{31}P) ^{c)} | a_3 (^1H) ^{c)} |
|---|----------------------|---|---|--------------------------------------|
| $(\text{PhenSQ})^{-[109]}$ | - | - | - | 0.165, 0.137, 0.042, 0.022 |
| $[(\text{PhenSQ})\text{Cu}(\text{dppf})]^-$ | 2.0055 ^{b)} | 1.00 | 1.40 | 0.15 |

^{a)} X-band EPR data obtained from electrochemically generated radical species in $\text{CH}_2\text{Cl}_2 / 0.1 \text{ M Bu}_4\text{NPF}_6$ ^{b)} from X-band EPR measurements at 220 K in CH_2Cl_2 ; ^{c)} hyperfine coupling constants in mT.

5.7 DFT and TD DFT calculation

DFT calculations have been carried out by Dr. S. Zálíš from J. Heyrovský Institute of Physical Chemistry in Prague. These calculations were performed on $[(\text{PhenQ})\text{Cu}(\text{dppf})](\text{BF}_4)$ and $[(\text{PhenQ})\text{Cu}(\text{dmpf})](\text{BF}_4)$ where dmpf is 1,1'-bis(dimethylphosphino)ferrocene i.e. all the phenyls of dppf were replaced by methyl.

DFT studies shows that bond lengths are comparable and the distortion in structure is justified due to intra-molecular π/π stacking between phenyl rings of dppf and PhenQ because when the phenyls at P are replaced by methyls the distortion is absent. DFT optimized structures are shown in fig 5.7.1 and the bond lengths (Å) and bond angles (°) obtained from DFT calculation are tabulated in Tab 5.7.1.

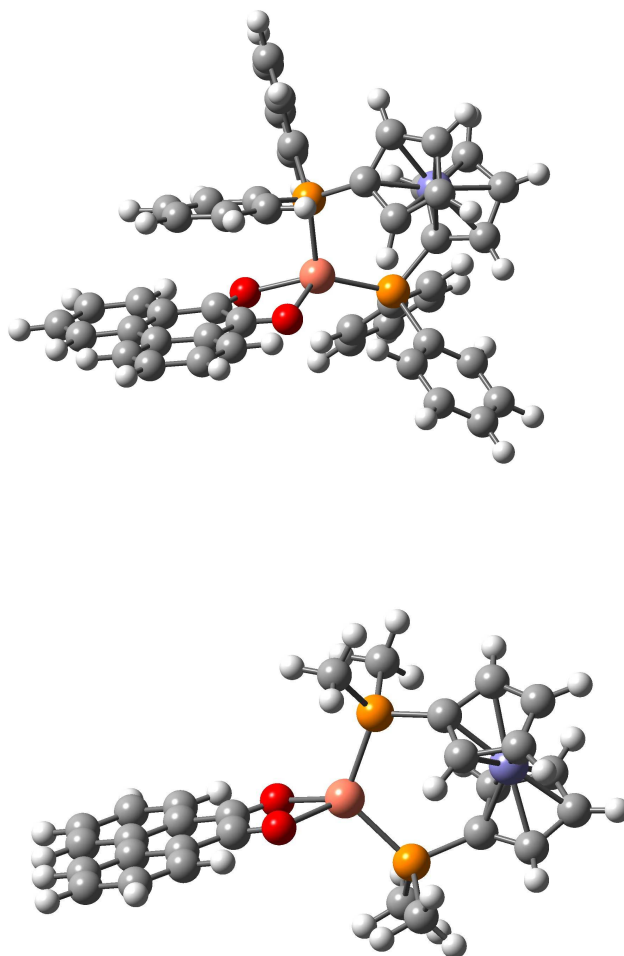


Fig 5.7.1: DFT optimized structures of $[(\text{PhenQ})\text{Cu}(\text{dppf})]^+$ (top) and a model with P-phenyl substituents replaced by P-methyl (bottom).

Tab 5.7.1: Comparison of selected bond lengths (\AA) and angles (deg) of $[(\text{PhenQ})\text{Cu}(\text{dppf})]^+$ with DFT calculation result.

| Bond lengths | Experimental | Calculated |
|--------------|--------------|------------|
| Cu-O1 | 2.053(7) | 2.058 |
| Cu-O2 | 2.159(6) | 2.126 |
| Cu-P1 | 2.208(3) | 2.237 |
| Cu-P2 | 2.254(3) | 2.249 |
| C1-O1 | 1.257(11) | 1.233 |
| C2-O2 | 1.244(10) | 1.232 |

| | | |
|-------------|------------|-------|
| C1-C2 | 1.499(13) | 1.517 |
| Bond angles | | |
| O1-Cu-O2 | 76.8(3) | 77.3 |
| O1-Cu-P1 | 132.3(2) | 131.0 |
| O2-Cu-P1 | 119.20(19) | 124.0 |
| O2-Cu-P2 | 99.55(19) | 95.6 |
| P1-Cu-P2 | 116.07(11) | 113.9 |
| P2-Cu-O1 | 102.95(16) | 105.8 |

TD DFT calculation was performed to confirm the specificity of electronic transitions. The TD DFT shows a MLCT band at 741 nm attributed to the $d(\text{Cu/Fe}) \rightarrow \pi^*$ of PhenQ transition leading to the excited state $\text{Cu}^{\text{II}}\text{-PhenSQ}$. The 418 nm band is comprised of MLCT and LLCT to π^* of PhenQ according to TD DFT.

5.8 Conclusion

It has been shown in this chapter that by using a special copper(I) complex fragment $[\text{Cu}(\text{dppf})]^+$ and a polycyclic quinone ligand (PhenQ) we could characterize structurally and spectroscopically the first Cu(I)/quinone complex. By electrochemistry and EPR spectroelectrochemistry we have successfully characterized insitu generated Cu(I)-PhenSQ species. DFT calculation proved that the distortion in geometry was because of intramolecular π/π interaction between phenyls of dppf and PhenQ which was absent on replacing phenyls by methyls. Considering the broad relevance of copper/quinone interactions and role of π -interactions in the proteins it will be tempting to study its potential for electron transfer reactivity and to elucidate the role of π/π interactions in stabilizing such species.

Chapter 6

Heterohexanuclear (Cu₃Fe₃) Complexes of Substituted Hexaazatrinaphthylene (HATN) Ligands: Twofold BF₄⁻ Association in the Solid and Stepwise Oxidation or Reduction to Spectroelectrochemically Characterized Species

6.1 Introduction

Inorganic supramolecules with redox active units are of interest for their wide application as sensors, machines, electronic devices^[112-114] and their relation to enzymatic systems^[115]. Over the last decades, several groups have been working with the highly symmetric (D_{3h}) 1,4,5,8,9,12-hexaazatriphenylene (HAT) (Fig. 6.1.1) ligand as a platform to build homo and hetero-nuclear polymetallic compounds. Three bidentate chelating sites to the metal ions, electron deficient π -systems to exhibit metal to ligand charge transfer, C₃ symmetry axis to have degenerate π^* orbitals make it so attractive to the chemists.^[117] The Different derivatives of Diquinoxalino[2,3-a:2',3'-c]phenazine (dqp), also known as hexaazatrinaphthylene (HATN) (Fig. 6.1.1), which is a homologue of HAT, are now also being used widely in supramolecular coordination compounds,^[118] coordination polymers,^[119] and organometallics^[120] as well as in photophysical studies,^[121] their conversion to liquid crystalline acceptor materials.^[122,123] It has created the option to use such ligands in conjunction with coordinated donors which might serve as charge-separating molecular devices.^[122,123] The main advantage of dqp over HAT is the synthesis which is a simple condensation of two commercially available reagents, hexaketocyclohexane and phenylenediamine.^[124-126] These tris-bidentate ligands have been used recently in various contexts: Gray et al. have reported on mono- and heterodinuclear palladium and rhenium complexes of the hexamethyl derivative,^[126] while studies on triruthenium(II,III) complexes have shown the capability of dqp ligands to mediate three-way valence exchange.^[127] One such robust donor coming to mind would be the widely used ferrocene group,^[70,73,128,129] or, in a more detailed structure, a ferrocenylcopper(I) moiety such as [(Cu(dppf))⁺]^[70,73,129]

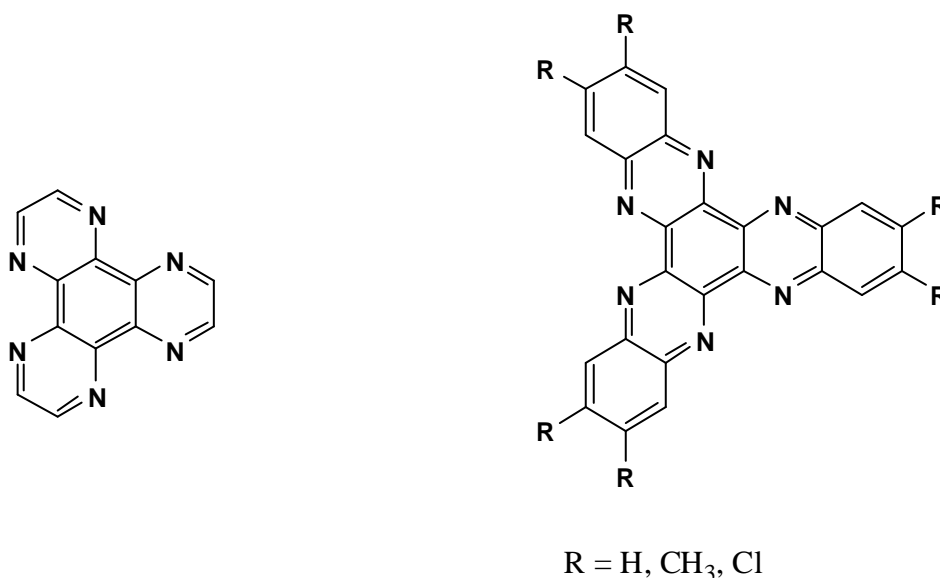


Fig 6.1.1: 1,4,5,8,9,12-hexaazatriphenylene (HAT) and different derivatives of diquinoxalino[2,3-a:2',3'-c]phenazine (dqp)

This chapter describes the synthesis of hetero-hexanuclear Cu^I(dppf) complexes with tris-bidentate dqp ligands, and their electrochemical and spectroelectrochemical characterization. One of the compounds could be crystallized for X-ray structure determination. Both X-band and high frequency EPR are employed here to study the mono-reduced intermediate.

6.2 Synthesis and characterization

The set of complexes $[(\mu_3\text{-dqp})\{\text{Cu}(\text{dppf})\}_3](\text{BF}_4)_3$, $[(\mu_3\text{-Me}_6\text{-dqp})\{\text{Cu}(\text{dppf})\}_3](\text{BF}_4)_3$, $[(\mu_3\text{-Cl}_6\text{-dqp})\{\text{Cu}(\text{dppf})\}_3](\text{BF}_4)_3$ and $[(\mu_3\text{-dqp})\{\text{Cu}(\text{dppf})\}_3](\text{PF}_6)_3$, $[(\mu_3\text{-Me}_6\text{-dqp})\{\text{Cu}(\text{dppf})\}_3](\text{PF}_6)_3$, $[(\mu_3\text{-Cl}_6\text{-dqp})\{\text{Cu}(\text{dppf})\}_3](\text{PF}_6)_3$ were obtained in a straightforward way using 1 equivalent corresponding dqp derivative and 3 equivalents of $[\text{Cu}(\text{dppf})(\text{CH}_3\text{CN})_2]\text{BF}_4$ or $[\text{Cu}(\text{dppf})(\text{CH}_3\text{CN})_2](\text{PF}_6)$ in dry CH_2Cl_2 at RT. The green color solid was collected by removing the solvent under reduced pressure and washed properly with hexane. The complexes were characterized by ¹H, ³¹P, ¹⁹F NMR and elemental analysis. Due to fragmentation, mass spectroscopy was not informative. The detailed experimental procedure is given in experimental section (Chapter 7).

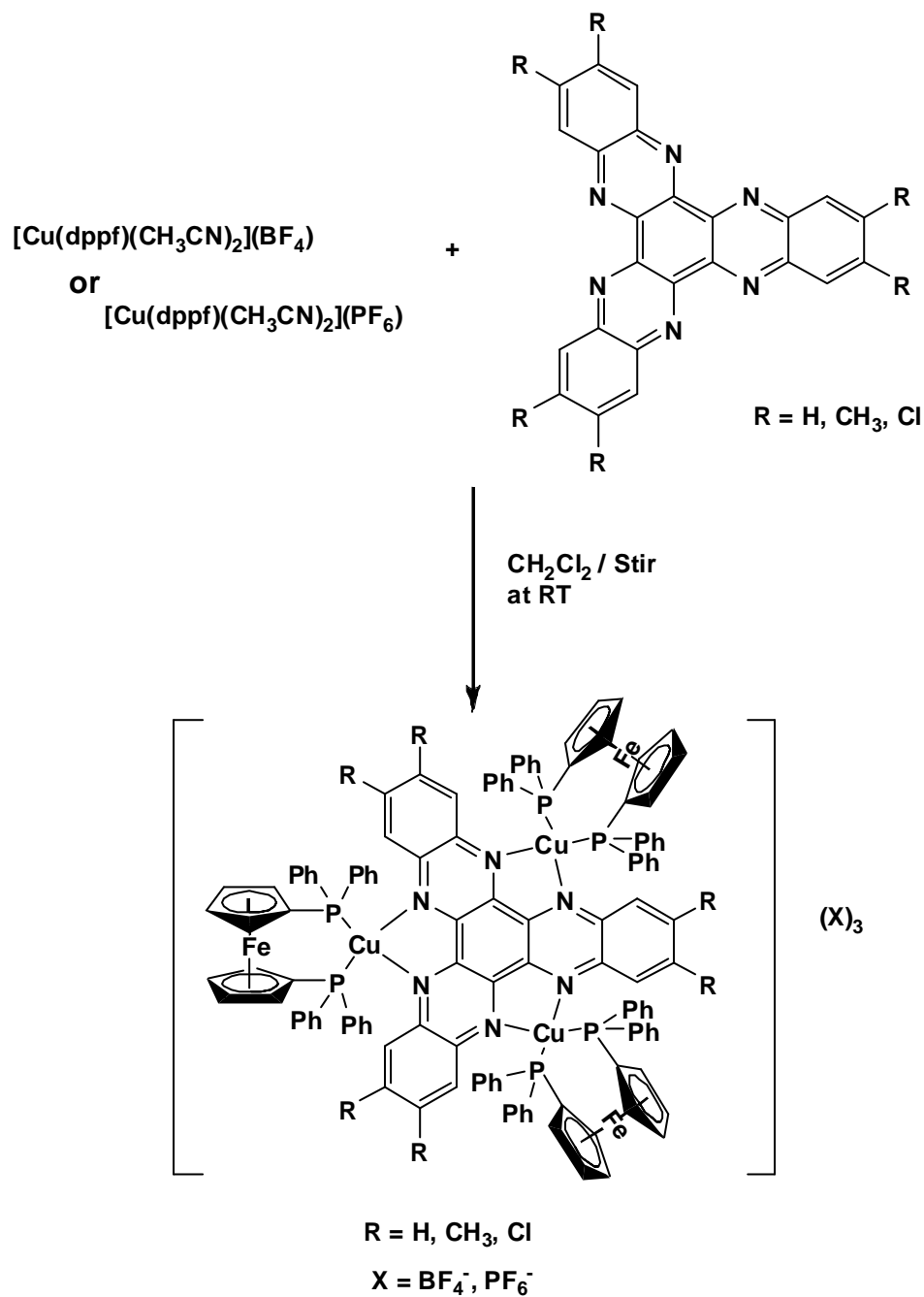


Fig. 6.2.1 Reaction scheme for the synthesis of hetero hexa-nuclear $[(\mu_3\text{-Rdqp})\{\text{Cu}(\text{dppf})\}_3](\text{BF}_4)_3$ (R = H, CH₃, Cl).

Tab. 6.2.1: NMR data^{a)}.

| Compound | ¹ H NMR (δ / ppm) | ³¹ P NMR (δ / ppm) |
|----------|--------------------------------------|---------------------------------------|
| dqp | 8.03 (m, 6H), 8.68 (m, 6H) | - |

| | | |
|---|--|-------|
| $[(\mu_3\text{-dqp})\{\text{Cu}(\text{dppf})\}_3](\text{BF}_4)_3$ | 4.71(s, 12H, Cp), 4.78 (s, 12H, Cp), 6.88-7.04 (m, 30H, Ph), 7.3-7.35 (m, 30H, Ph), 7.41(m, 6H, L ¹), 8.18 (m, 6H, L ¹). | -7.25 |
| Me ₆ -dqp | 2.62 (s, 18H), 8.40 (s, 6H) | - |
| $[(\mu_3\text{-Me}_6\text{-dqp})\{\text{Cu}(\text{dppf})\}_3](\text{BF}_4)_3$ | 2.24 (s, 6H, Me), 4.72(s, 12H, Cp), 4.75 (s, 12H, Cp), 6.86-7.35 (m, 60H, Ph), 7.98(s, 6H, L ²). | -6.25 |
| Cl ₆ -dqp | 8.78 (s, 6H) | - |
| $[(\mu_3\text{-Cl}_6\text{-dqp})\{\text{Cu}(\text{dppf})\}_3](\text{BF}_4)_3$ | 4.67(s, 12H, Cp), 4.82 (s, 12H, Cp), 6.91-7.33 (m, 60H, Ph), 8.26(s, 6H, L ³). | -5.95 |

^{a)} in CD₂Cl₂ at RT

To study the possible anion binding in solution, the ³¹P and ¹⁹F NMR experiments were carried out at room temperature as well as at low temperature (223 K) on both the set of compounds $[(\mu_3\text{-dqp})\{\text{Cu}(\text{dppf})\}_3](\text{BF}_4)_3$, $[(\mu_3\text{-Me}_6\text{-dqp})\{\text{Cu}(\text{dppf})\}_3](\text{BF}_4)_3$, $[(\mu_3\text{-Cl}_6\text{-dqp})\{\text{Cu}(\text{dppf})\}_3](\text{BF}_4)_3$ and $[(\mu_3\text{-dqp})\{\text{Cu}(\text{dppf})\}_3](\text{PF}_6)_3$, $[(\mu_3\text{-Me}_6\text{-dqp})\{\text{Cu}(\text{dppf})\}_3](\text{PF}_6)_3$, $[(\mu_3\text{-Cl}_6\text{-dqp})\{\text{Cu}(\text{dppf})\}_3](\text{PF}_6)_3$. In ³¹P NMR, one singlet from the dppf ligands is observed for all the complexes in addition to one septet at about -145 ppm for the complexes with PF₆⁻ counter anion which is attributed to the ³¹P from the PF₆⁻ counter anions. In ¹⁹F NMR experiment, the complexes with PF₆⁻ show a doublet at around -73 ppm for the PF₆⁻ anions and a singlet around -152 ppm for the complexes with BF₄⁻ anion. The NMR results thus confirm weak binding (fast exchange) or dissociation of the counter anions, BF₄⁻ or PF₆⁻, on the NMR time scale in solution.

6.3 Crystal structures

The dark-green crystals of $[(\mu_3\text{-dqp})\{\text{Cu}(\text{dppf})\}_3](\text{BF}_4)_3$ were grown by slow diffusion of Hexane in the solution of $[(\mu_3\text{-dqp})\{\text{Cu}(\text{dppf})\}_3](\text{BF}_4)_3$ in CH₂Cl₂ at 4° C. It is crystallized in orthorhombic *P*_{bca} space group. Due to coordination of three [Cu(dppf)]⁺ units to dqp ligand, two diastereomeric conformers, the chiral propeller (C₃) and C₁ are possible.

The crystallized $[(\mu_3\text{-dqp})\{\text{Cu}(\text{dppf})\}_3](\text{BF}_4)_3$ (Figures 6.3.1) exhibits a C₁ conformation for $[(\mu_3\text{-dqp})\{\text{Cu}(\text{dppf})\}_3]^{3+}$ with characteristic distortion: The Cu-N bonds Cu2-N4 and Cu3-N5

at the quasi-mirror plane (bottom picture of Fig 6.3.1) are relatively long in comparison to the other four Cu-N bonds (Table 6.3.1).

In addition to this symmetry-breaking there is a distinct association visible between the hexanuclear complex trication and two tetrafluoroborate anions (Fig 6.3.1): BF_4^- ions are positioned above and below the quasi-trigonal center of $\{(\mu_3\text{-dqp})[\text{Cu}(\text{dppf})]_3\}^{3+}$ where the 1,1'-bis(diphosphinoferrocenyl) entities leave cavities open for approach (Figure 6.3.2). One triangular faces of each BF_4^- is directed to the dqp ligand to cover the central six-membered ring in an approximately symmetrical fashion (Fig 6.3.3). One tetrafluoroborate ion per complex trication remains unattached (Fig 6.3.2), creating an effective formula $\{(\mu_3\text{-dqp})[\text{Cu}(\text{dppf})]_3(\eta^3\text{-BF}_4)_2\}(\text{BF}_4)$.

A related kind of association was reported previously by Kitagawa et al. with one-electron reduced hexaazatriphenylene hexacarbonitrile in system $\{(\mu_3\text{-CN}_6\text{-HAT})[\text{Cu}(\text{dppf})]_3\}^{2+}$ (Fig 6.3.1) and PF_6^- or CF_3SO_3^- anions.^[33(b)] Due to the lowered charge these paramagnetic species contain no free anions. The distances between boron atoms of the two the associated anions and the central plane of the complex cation are 3.47 Å (B2) and 3.44 Å (B3), respectively, indicating a fairly close approach.

While the dqp ligand is largely planar with only small distortion from planarity (cf. below), the geometry at the copper(I) centers shows the typical distorted tetrahedral configuration with small N-Cu-N chelate bite angles of ca. 80° and dppf-determined P-Cu-P angles of about 112°. While the central C=N bonds show only little variation between 1.32 and 1.33 Å, there is a distinct lengthening by about 0.07 Å for two of the six Cu-N bonds, viz., for Cu2-N4 and Cu3-N5 (Tab 6.3.1). This distortion removes the trigonal symmetry and, accordingly, the Cu2--Cu3 distance is almost 0.1 Å longer than the two other Cu--Cu distances. The difference is even more pronounced for the ca. 14 Å separated ferrocene iron atoms (Tab 6.3.1) the distance of which is of significance for the splitting of oxidation potentials (cf. below). The distortion on the Cu2/Cu3 side is also evident from the relatively large deviation (9.7° dihedral angle) of the corresponding benzene ring (C17-C22) from planarity with the central six-membered ring.

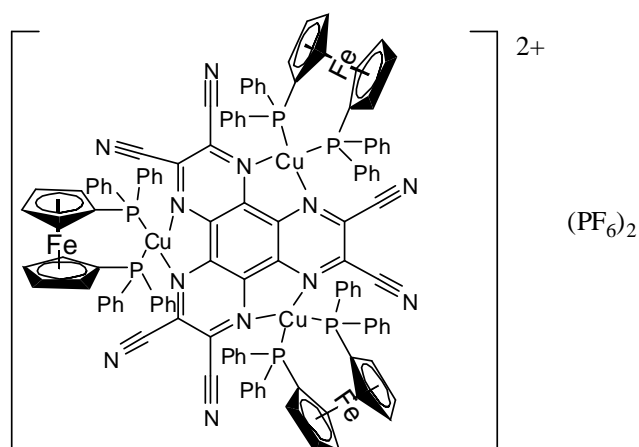


Fig 6.3.1: Chemical structure of $\{(\mu_3\text{-CN}_6\text{HAT})[\text{Cu}(\text{dppf})]_3\}^{2+}$ [15].

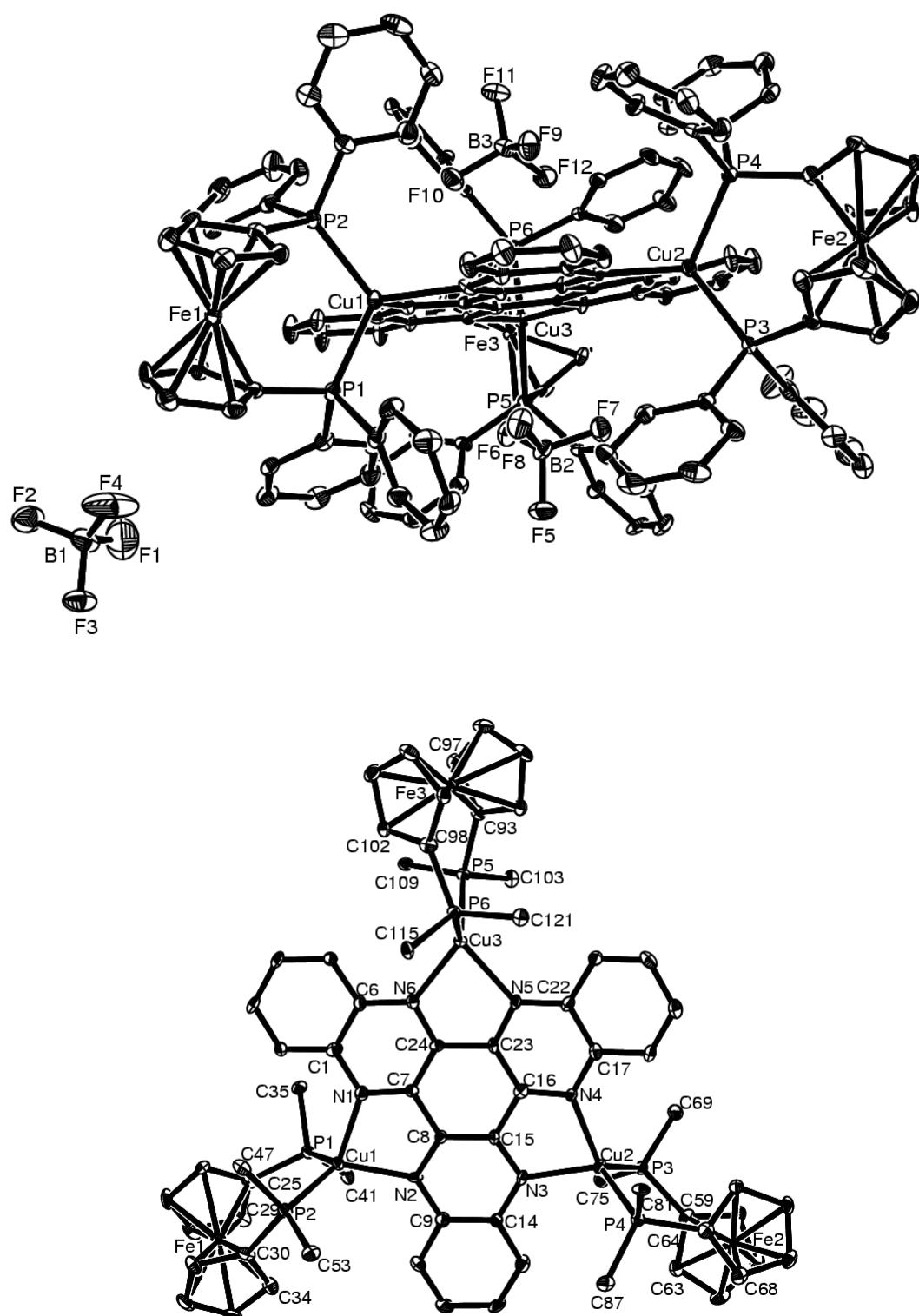


Fig. 6.3.2: Molecular structure of $[(\mu_3\text{-dbq})\{\text{Cu}(\text{dppf})\}_3](\text{BF}_4)_3$ (top); top view of the cation $[(\mu_3\text{-dbq})\{\text{Cu}(\text{dppf})\}_3]^{3+}$ (bottom).

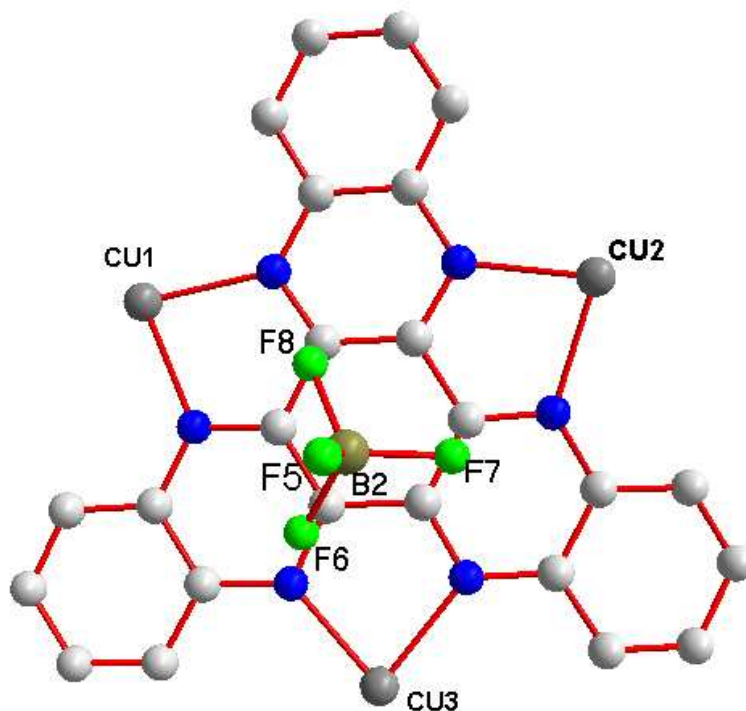


Fig. 6.3.3: Structure of the cation $[(\mu_3\text{-dbq})\{\text{Cu}(\text{dppf})\}_3(\text{BF}_4)_2]^+$ in the crystal of $[(\mu_3\text{-dbq})\{\text{Cu}(\text{dppf})\}_3](\text{BF}_4)_3$ (top view) showing the orientation of associated tetrafluoroborate anions.

Tab. 6.3.1: Important bond lengths (Å) and bond angles (°).

| Bond lengths (Å) | | Bond angles (°) | |
|------------------|----------|-----------------|------------|
| Cu(1)-N(2) | 2.080(6) | N2-Cu1-N1 | 80.4(2) |
| Cu(1)-N(1) | 2.081(6) | N2-Cu1-P2 | 116.41(16) |
| Cu(1)-P(2) | 2.246(2) | N1-Cu1-P2 | 116.64(16) |
| Cu(1)-P(1) | 2.265(2) | N2-Cu1-P1 | 117.83(16) |
| Cu(2)-N(3) | 2.073(5) | N1-Cu1-P1 | 108.73(16) |
| Cu(2)-N(4) | 2.142(5) | P2-Cu1-P1 | 112.83(7) |
| Cu(2)-P(4) | 2.264(1) | N3-Cu2-N4 | 79.2(2) |

| | | | |
|--------------|----------|-----------|------------|
| Cu(2)-P(3) | 2.278(2) | N3-Cu2-P4 | 112.74(15) |
| Cu(3)-N(6) | 2.066(5) | N4-Cu2-P4 | 114.66(15) |
| Cu(3)-N(5) | 2.132(5) | N3-Cu2-P3 | 114.57(16) |
| Cu(3)-P(5) | 2.276(2) | N4-Cu2-P3 | 119.98(15) |
| Cu(3)-P(6) | 2.282(1) | P4-Cu2-P3 | 111.83(7) |
| Cu(1)..Cu(2) | 6.926 | N6-Cu3-N5 | 79.3(2) |
| Cu(1)..Cu(3) | 6.927 | N6-Cu3-P5 | 116.15(16) |
| Cu(2)..Cu(3) | 7.022 | N5-Cu3-P5 | 118.48(16) |
| Fe(1)..Fe(2) | 13.804 | N6-Cu3-P6 | 115.05(16) |
| Fe(1)..Fe(3) | 14.061 | N5-Cu3-P6 | 111.62(16) |
| Fe(2)..Fe(3) | 14.198 | P5-Cu3-P6 | 112.46(7) |

6.4 Cyclic voltammetry

The expected oxidation of ferrocene groups and the reduction of dq_p acceptor ligands with up to three electrons occur as reversible process according to cyclic voltammetric measurements in CH₂Cl₂ / 0.1 M Bu₄NPF₆ (Fig 6.4.1). Oxidation of Cu(I) center and organophosphine groups are not observed below 1.6 V vs. Fc^{0/+} and would be expected to proceed irreversibly.^[70,73,129]

The iron oxidation process of three separated dppf moieties seem to coincide at one potential in a three electron wave, as was similarly reported for the closer spaced dppf groups in a hexacyanotriphenylene bridged system. The oxidation potential of 0.3 to 0.6 V vs. Fc^{0/+} is typical for ferrocenylcopper(I) species.^[70,73,129]

Two ($[(\mu_3\text{-dq}_p)\{\text{Cu}(\text{dppf})\}_3]^{3+}$, $[(\mu_3\text{-Me}_6\text{-dq}_p)\{\text{Cu}(\text{dppf})\}_3]^{3+}$) or three ($[(\mu_3\text{-Cl}_6\text{-dq}_p)\{\text{Cu}(\text{dppf})\}_3]^{3+}$) well separated one electron reduction waves with surprisingly variable spacing can be observed for the compounds (Fig 6.4.1, Tab 6.4.1). Whereas the hexacyanotriphenylene bridged system by Kitagawa et al. (Fig 6.3.1) shows three rather evenly spaced potentials for ligand based electron transfers,^[15] the present compounds exhibit a smaller potential difference between the first and second reduction than between second and third electron uptake (Fig 6.4.1, Tab 6.4.1). This variation which has similarly been observed for some triruthenium(II) compounds,^[127,130] can be tentatively associated with weak interaction between the first and second added electron. In fact, the result that lowest unoccupied MO (LUMO, becoming the SOMO in the radical complex) and the doubly

degenerate SLUMO (second lowest unoccupied MO) are calculated to be very close suggest the possibility of a triplet state for the two-electron reduced form.^[116] However, EPR studies have not provided positive evidence for this explanation because no half-field signal was detected, however, the reduction potential pattern for sequential ligand-based electron addition suggests formation of first a radical and then a triplet species, reflected by close lying potentials for electron addition to different MOs. In contrast, the third reduction, detectable for hexachloro-substituted $[(\mu_3\text{-Cl}_6\text{-dqp})\{\text{Cu}(\text{dppf})\}_3]^{3+}$, occurs at a significantly more negative potential, in agreement with electron pairing in one of the low-lying π^* MOs.

The additional cyano acceptor substitution in system $[(\mu_3\text{-CN}_6\text{HAT})\{\text{Cu}(\text{dppf})\}_3](\text{PF}_6)_2$ (Fig 6.3.1) shifts the redox potentials to higher values compared to present set of compounds (Table 6.4.1). Accordingly, the one-electron reduced form was isolated and structurally characterized by Kitagawa et al.^[33(b)] whereas the ferrocene-based oxidation was not reversible. Within the series of compounds ($[(\mu_3\text{-dqp})\{\text{Cu}(\text{dppf})\}_3]^{3+}$, $[(\mu_3\text{-Me}_6\text{-dqp})\{\text{Cu}(\text{dppf})\}_3]^{3+}$) or three ($[(\mu_3\text{-Cl}_6\text{-dqp})\{\text{Cu}(\text{dppf})\}_3]^{3+}$) the expected substituent effects, i.e. donor influence from six methyl groups and acceptor effect from six chloro substituents manifests itself in the redox potentials (Table 6.4.1), the latter allows to detect a third one-electron reduction (Figure 6.4.1).

The result that both the BF_4^- and the PF_6^- salts of trication $[(\mu_3\text{-dqp})\{\text{Cu}(\text{dppf})\}_3]^{3+}$, $[(\mu_3\text{-Me}_6\text{-dqp})\{\text{Cu}(\text{dppf})\}_3]^{3+}$) or three ($[(\mu_3\text{-Cl}_6\text{-dqp})\{\text{Cu}(\text{dppf})\}_3]^{3+}$) display virtually identical cyclic voltammetric as well as spectroelectrochemical response (cf. below) in $\text{CH}_2\text{Cl}_2/0.1 \text{ M Bu}_4\text{NPF}_6$ (Table 3) suggests that the association found for the solid $\{(\mu_3\text{-dqp})[\text{Cu}(\text{dppf})]_3(\square^3\text{-BF}_4)_2\}(\text{BF}_4)$ is not retained to the same extent in solution.

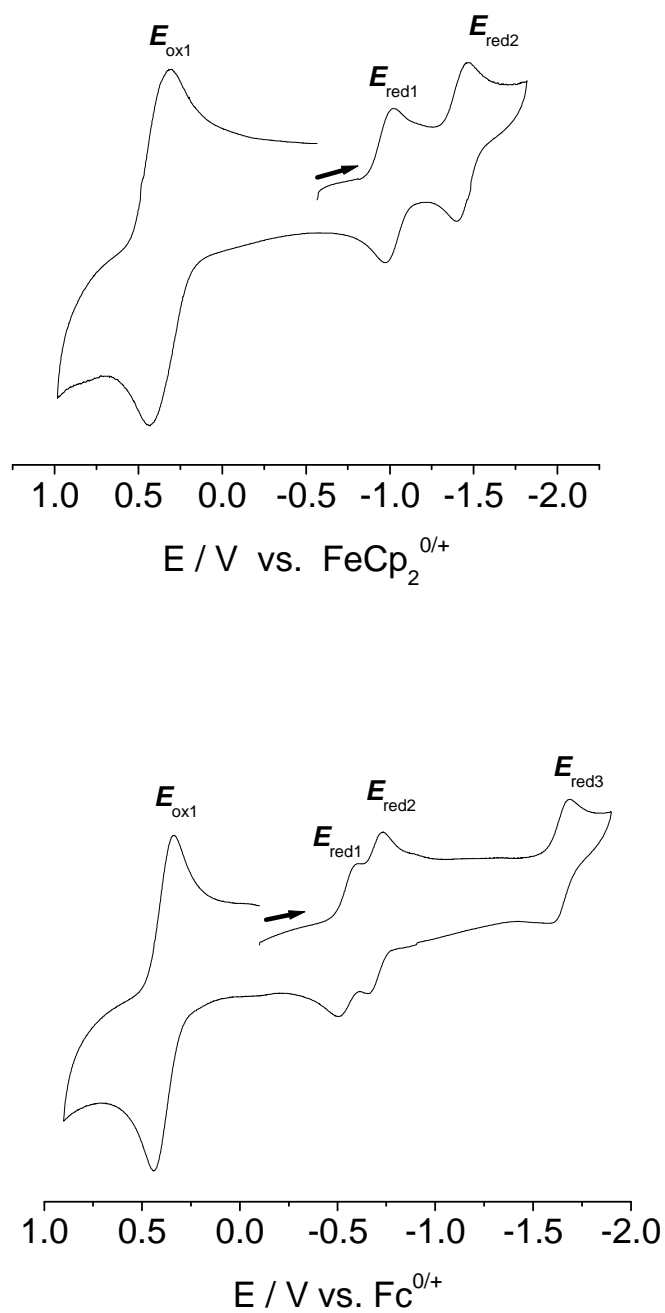


Fig. 6.4.1: Cyclic voltammogram of $[(\mu_3\text{-Me}_6\text{-dqp})\{\text{Cu}(\text{dppf})\}_3](\text{BF}_4)_3$ (top) and $[(\mu_3\text{-Cl}_6\text{-dqp})\{\text{Cu}(\text{dppf})\}_3](\text{BF}_4)_3$ (bottom) in CH_2Cl_2 / 0.1 M Bu_4NPF_6 at 100 mV / S scan rate at RT

Tab. 6.4.1: Electrochemical potential^{a)} from cyclic voltammetry.

| Complex | E_{298}°/V ($\Delta E_p/\text{mV}$) ^{a)} | | | |
|---|---|-------------------|-------------------|-------------------|
| | E_{ox1} | E_{red1} | E_{red2} | E_{red3} |
| $[(\mu_3\text{-dqp})\{\text{Cu}(\text{dppf})\}_3](\text{BF}_4)_3$ | 0.364 (103) | -0.612 (120) | -0.899 (93) | ^{b)} |

| | | | | |
|--|--------------------|--------------|-------------|-------------|
| $[(\mu_3\text{-dqp})\{\text{Cu}(\text{dppf})\}_3](\text{PF}_6)_3$ | 0.41(110) | -0.56(120) | -0.84(90) | b) |
| $[(\mu_3\text{-Me}_6\text{-dqp})\{\text{Cu}(\text{dppf})\}_3](\text{BF}_4)_3$ | 0.372 (123) | -0.99 (40) | -1.43 (60) | b) |
| $[(\mu_3\text{-Me}_6\text{-dqp})\{\text{Cu}(\text{dppf})\}_3](\text{PF}_6)_3$ | 0.51(100) | -0.90(75) | -1.27(70) | b) |
| $[(\mu_3\text{-Cl}_6\text{-dqp})\{\text{Cu}(\text{dppf})\}_3](\text{BF}_4)_3$ | 0.388 (101) | -0.549 (93) | -0.696 (73) | -1.63 (90) |
| $[(\mu_3\text{-Cl}_6\text{-dqp})\{\text{Cu}(\text{dppf})\}_3](\text{PF}_6)_3$ | 0.565 (122) | -0.526 (100) | -0.698 (80) | -1.75 (100) |
| $[(\mu_3\text{-CN}_6\text{HAT})\{\text{Cu}(\text{dppf})\}_3](\text{BF}_4)_3^{\text{c)}}$ | 0.63 ^{d)} | 0.30 | -0.09 | -0.50 |

^{a)} $\text{CH}_2\text{Cl}_2/0.1 \text{ M Bu}_4\text{NPF}_6$ at 100 mV/s scan rate, potentials are measured against $\text{FeCp}_2^{0/+}$, ΔE_p : difference in peak potentials; ^{b)} not obtained; ^{c)} w.r.t. Ag/Ag^+ ; ^{d)} E_{pa} corresponding to irreversible oxidation

6.5 UV-vis-NIR spectroelectrochemistry

UV-Vis-NIR spectroelectrochemical experiments for $[(\mu_3\text{-dbq})\{\text{Cu}(\text{dppf})\}_3](\text{BF}_4)_3$, $[(\mu_3\text{-Me}_6\text{-dbq})\{\text{Cu}(\text{dppf})\}_3](\text{BF}_4)_3$, $[(\mu_3\text{-Cl}_6\text{-dbq})\{\text{Cu}(\text{dppf})\}_3](\text{BF}_4)_3$ and $[(\mu_3\text{-Cl}_6\text{-dbq})\{\text{Cu}(\text{dppf})\}_3](\text{PF}_6)_3$ were performed in $\text{CH}_2\text{Cl}_2 / 0.1 \text{ M Bu}_4\text{NPF}_6$ at 298 K using a OTTLE cell. The spectroelectrochemical monitoring of multielectron processes is an excellent way to detect weak interactions which are not always apparent from direct cyclic voltammetric or differential pulse voltammetric techniques.^[131] The presence of clean isobestic points during each conversion and complete electrochemical generation of oxidized and reduced species with out any appreciable degradation established the reversibility of the redox processes under spectroelectrochemical condition.

In particular, the stepwise potential variation for the oxidation of the compound $[(\mu_3\text{-dbq})\{\text{Cu}(\text{dppf})\}_3](\text{BF}_4)_3$ gave a series of spectral changes which could be associated with various intermediates (Fig 6.5.1 and 6.5.3, Tab 6.5.1). Unfortunately the most characteristic but typically weak ferrocenium band for the MLCT (${}^2E_{1u}$) transition around 600 nm^[132,133] is obscured here by much more intense $d^{10}(\text{Cu}^I)$ to π^* of dqp metal to ligand charge transfer absorption, however overall spectral changes are still obvious.

Stepwise one-electron reduction (Fig 6.5.1) produces for the first dicationic intermediates which shows a broad near-infrared band with the maximum at about 2000 nm (Fig 6.5.4, Tab 6.5.1) attributed to a transition between close lying SOMO and LUMO (Fig 6.5.2). On 2nd reduction to monocationic two electron reduced intermediate, 2000 nm band disappears with the appearance of several new bands at lower wave length region (1000 to 2000 nm) in agreement with a tentative triplet state (Fig 6.5.4, Tab 6.5.1). For the hexachloro substituted

complexes $[(\mu_3\text{-Cl}_6\text{-dbq})\{\text{Cu}(\text{dppf})\}_3](\text{BF}_4)_3$ and $[(\mu_3\text{-Cl}_6\text{-dbq})\{\text{Cu}(\text{dppf})\}_3](\text{PF}_6)_3$, 3rd reduction is observed which diminishes the bands generated from 2nd reduction and grows new band at about 1170 nm (Fig 6.5.4, Tab 6.5.1).

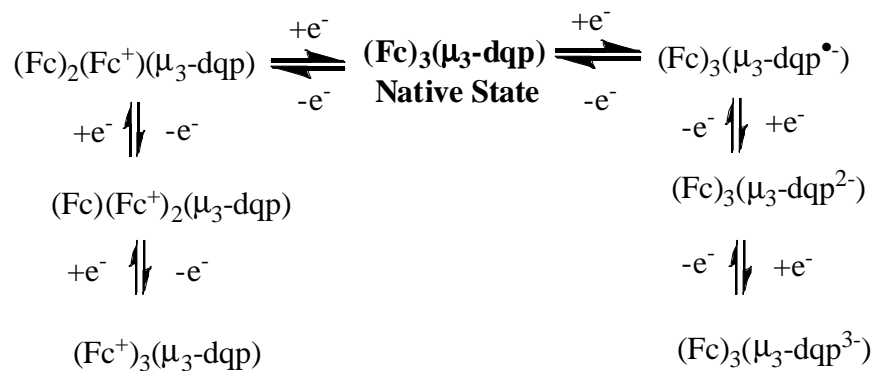


Fig 6.5.1: Scheme for stepwise electrochemical processes.

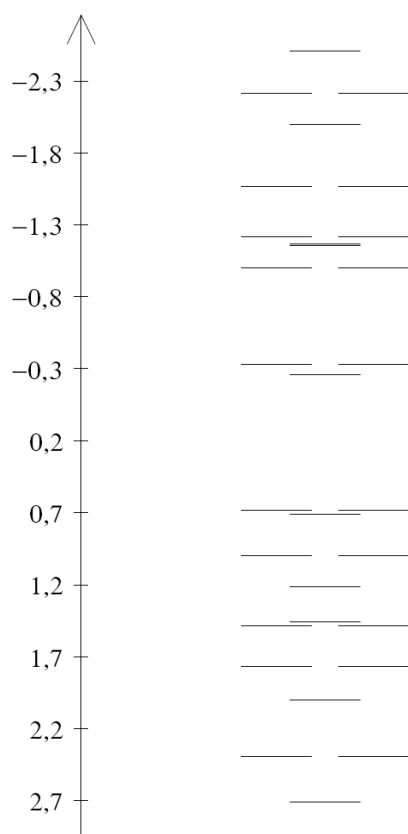


Fig 6.5.2: Orbital energy diagram for dqp from DFT calculation.

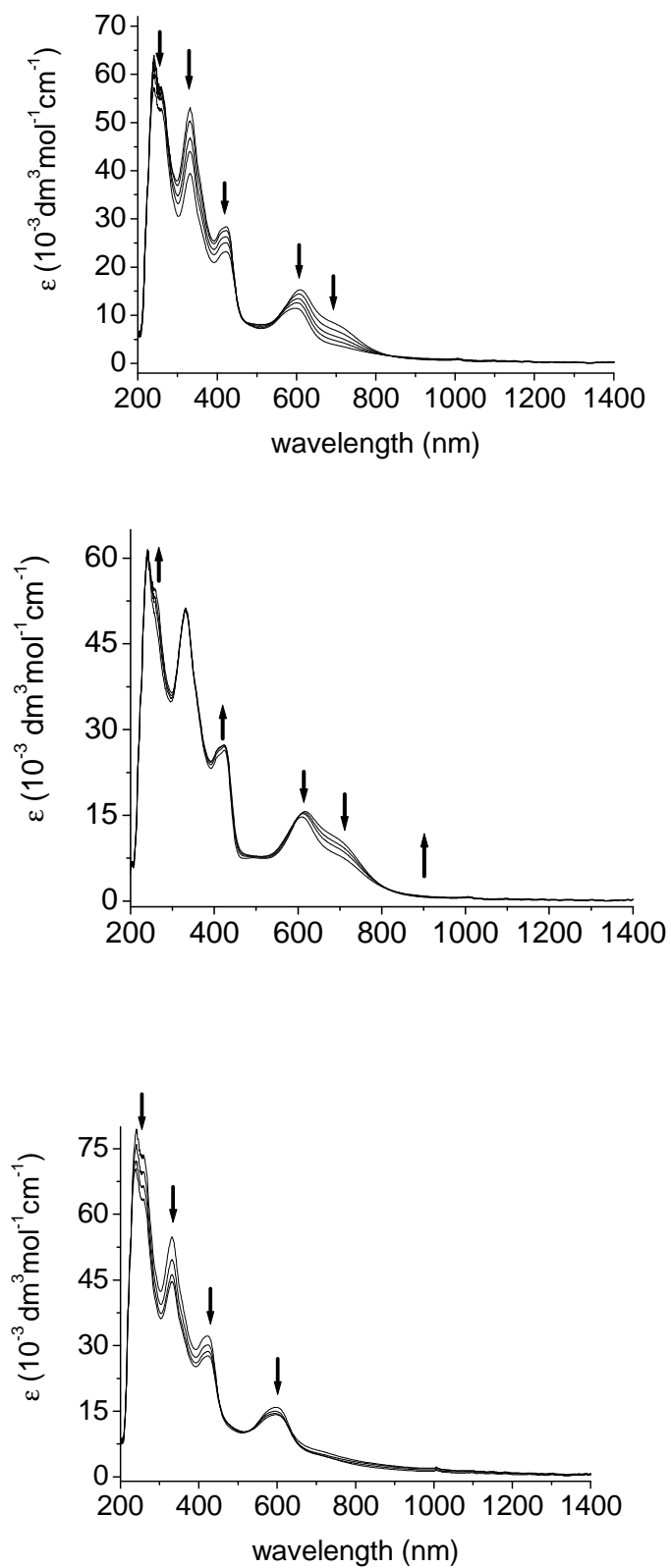


Figure 6.5.3: Stepwise spectroelectrochemical oxidation of $[(\mu_3\text{-dbq})\{\text{Cu}(\text{dppf})\}_3]^{3+} \rightarrow [(\mu_3\text{-dbq})\{\text{Cu}(\text{dppf})\}_3]^{4+}$ (top), $[(\mu_3\text{-dbq})\{\text{Cu}(\text{dppf})\}_3]^{4+} \rightarrow [(\mu_3\text{-dbq})\{\text{Cu}(\text{dppf})\}_3]^{5+}$ (middle), and $[(\mu_3\text{-dbq})\{\text{Cu}(\text{dppf})\}_3]^{5+} \rightarrow [(\mu_3\text{-dbq})\{\text{Cu}(\text{dppf})\}_3]^{6+}$ (bottom) in $\text{CH}_2\text{Cl}_2/0.1 \text{ M Bu}_4\text{NPF}_6$.

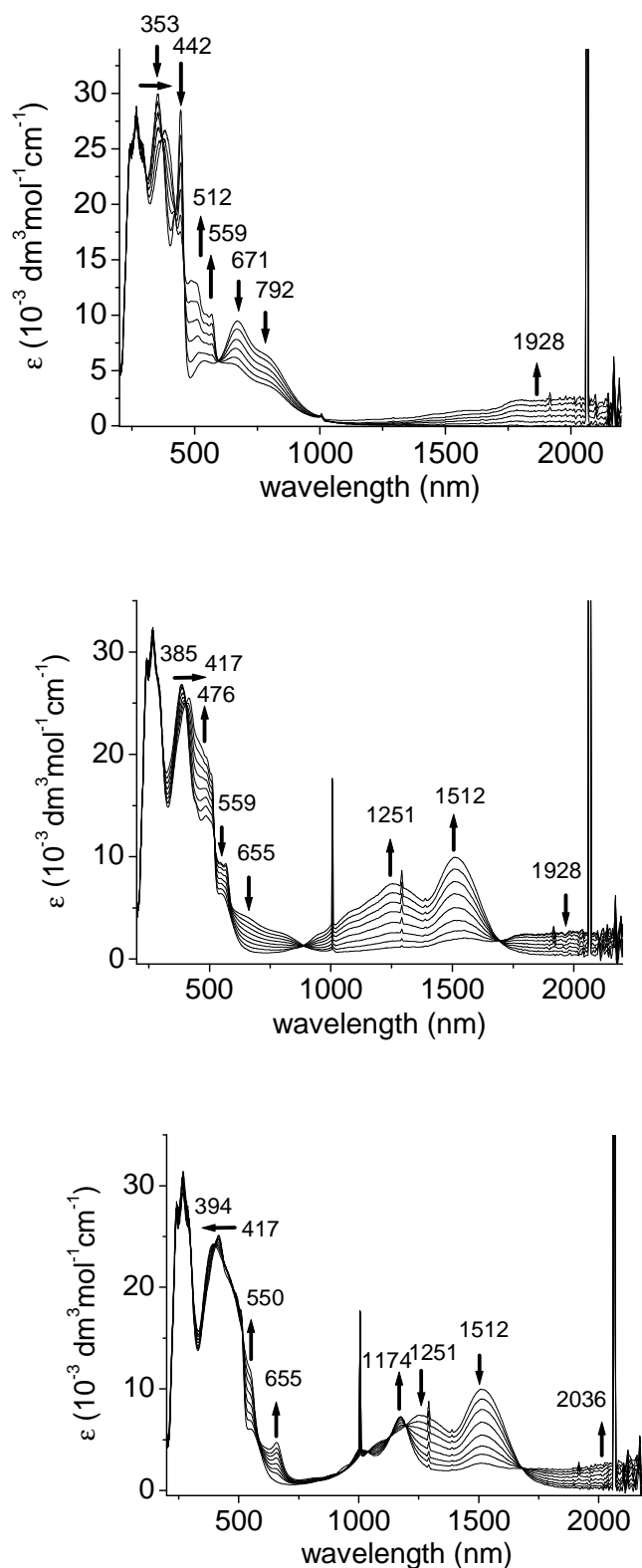


Figure 6.5.4: Stepwise spectroelectrochemical reduction of $[(\mu_3\text{-Cl}_6\text{-dbq})\{\text{Cu}(\text{dppf})\}_3]^{3+} \rightarrow [(\mu_3\text{-Cl}_6\text{-dbq})^-\{\text{Cu}(\text{dppf})\}_3]^{2+}$ (top); $[(\mu_3\text{-Cl}_6\text{-dbq})^-\{\text{Cu}(\text{dppf})\}_3]^{2+} \rightarrow [(\mu_3\text{-Cl}_6\text{-dbq})^{2-}\{\text{Cu}(\text{dppf})\}_3]^+$ (middle), and $[(\mu_3\text{-Cl}_6\text{-dbq})^{2-}\{\text{Cu}(\text{dppf})\}_3]^+ \rightarrow [(\mu_3\text{-Cl}_6\text{-dbq})^3\{\text{Cu}(\text{dppf})\}_3]$ (bottom) in $\text{CH}_2\text{Cl}_2/0.1 \text{ M Bu}_4\text{NPF}_6$.

The absorption data from UV-vis-NIR spectroelectrochemistry for all the three complexes are tabulated in Tab. 6.5.1.

Tab. 6.5.1: Absorption data obtained from spectroelectrochemistry in CH_2Cl_2 / 0.1 M Bu_4NPF_6 for $[(\mu_3\text{-dbq})\{\text{Cu}(\text{dppf})\}_3]^{3+}$, $[(\mu_3\text{-Me}_6\text{-dbq})\{\text{Cu}(\text{dppf})\}_3]^{3+}$ and $[(\mu_3\text{-Cl}_6\text{-dbq})\{\text{Cu}(\text{dppf})\}_3]^{3+}$.

| Compound | $\lambda_{\text{max}}/\text{nm}$ ($\epsilon/\text{M}^{-1}\text{cm}^{-1}$) ^a |
|---|--|
| $[(\mu_3\text{-dbq})\{\text{Cu}(\text{dppf})\}_3]^+$ | 1438(10230), 1211(8530), 448(sh) |
| $[(\mu_3\text{-dbq})\{\text{Cu}(\text{dppf})\}_3]^{2+}$ | 1938(sh), 543(sh), 490(sh), 364(37010) |
| $[(\mu_3\text{-dbq})\{\text{Cu}(\text{dppf})\}_3]^{3+}$ | 696(sh), 616(15330), 423(26220), 331(50820) |
| $[(\mu_3\text{-dbq})\{\text{Cu}(\text{dppf})\}_3]^{4+}$ | 900(sh), 696(sh), 616(14620), 423 (27300), 331(53140) |
| $[(\mu_3\text{-dbq})\{\text{Cu}(\text{dppf})\}_3]^{5+}$ | 900(sh), 725(sh), 597(11440), 420(23160), 331(39400), |
| $[(\mu_3\text{-dbq})\{\text{Cu}(\text{dppf})\}_3]^{6+}$ | 900(sh), 725(sh), 423(27530), 331(44450), 257(sh), 239(70310) |
| $[(\mu_3\text{-Me}_6\text{-dbq})\{\text{Cu}(\text{dppf})\}_3]^+$ | 1464(11630), 1225(9100), 481(sh), 419(35100) |
| $[(\mu_3\text{-Me}_6\text{-dbq})\{\text{Cu}(\text{dppf})\}_3]^{2+}$ | 1982(sh), 550(sh), 496(sh), 385(35400) |
| $[(\mu_3\text{-Me}_6\text{-dbq})\{\text{Cu}(\text{dppf})\}_3]^{3+}$ | 626(9170), 435(33340), 346(43400) |
| $[(\mu_3\text{-Me}_6\text{-dbq})\{\text{Cu}(\text{dppf})\}_3]^{6+}$ | 802(sh), 557(9930) |
| $[(\mu_3\text{-Cl}_6\text{-dbq})\{\text{Cu}(\text{dppf})\}_3]^0$ | 2036(sh), 1174(7200), 655(4650), 550(sh), 394(24200) |
| $[(\mu_3\text{-Cl}_6\text{-dbq})\{\text{Cu}(\text{dppf})\}_3]^+$ | 1512(9920), 1251(7280), 476(sh), 417(25300) |
| $[(\mu_3\text{-Cl}_6\text{-dbq})\{\text{Cu}(\text{dppf})\}_3]^{2+}$ | 1966(sh), 559(sh), 512(sh), 378(26660) |
| $[(\mu_3\text{-Cl}_6\text{-dbq})\{\text{Cu}(\text{dppf})\}_3]^{3+}$ | 792(sh), 671(9430), 442(28500), 353(29900) |
| $[(\mu_3\text{-Cl}_6\text{-dbq})\{\text{Cu}(\text{dppf})\}_3]^{5+}$ | 1100(sh), 790(sh), 661(7220) |
| $[(\mu_3\text{-Cl}_6\text{-dbq})\{\text{Cu}(\text{dppf})\}_3]^{6+}$ | 1100(sh), 790(sh), 624(6260), 440(27040) |

^awavelengths in nm.(molar extinction coefficient in $\text{M}^{-1}\text{cm}^{-1}$)

6.6 EPR spectroscopy

While ferrocenium centers in $(\text{dppf})^+$ exhibit typically broad EPR features, even at very low temperatures,^[132,133] the reduction of HAT-type π acceptor molecules leads to radical anion complexes^[127,130,17] and beyond. EPR spectroscopy is particularly suited to analyze the nature of half filled orbitals (singly occupied molecular orbitals, SOMOs) in connection with calculation results.

The one electron reduced forms, generated by *intra muros* electrolysis in $\text{CH}_2\text{Cl}_2/0.1$ M Bu_4NPF_6 in the EPR cavity of an X-band spectrometer (9.5 GHz) display intense but poorly resolved resonances at room temperature. Calculations at the Hückel MO and DFT levels suggest a spin density distribution for unsubstituted dpq^- (HATN radical anion) with 68.4 %

cumulated spin density at the N atoms and 21.2 and 10.4 % at the two kinds of peripheral CH centers (Figure 6.6.1). Together with the expected^[70,73,129] small, but non-negligible hyperfine coupling from ^{31}P ($I = 1/2$) and $^{63,65}\text{Cu}$ ($I = 3/2$) nuclei the resulting large number of $13 \times 7 \times 7 \times 7 \times 10 = 44590$ theoretical lines for coupling with six ^{14}N , two times six ^1H , six ^{31}P and three $^{63,65}\text{Cu}$ nuclei in the range of 0-1.0 mT renders the observed EPR resonance poorly resolved (Fig 6.6.1); hyperfine splitting of about 0.9 mT was deduced for $[(\mu_3\text{-dbq})^- \{\text{Cu}(\text{dppf})\}_3]^{2+}$ and $[(\mu_3\text{-Me}_6\text{-dbq})^- \{\text{Cu}(\text{dppf})\}_3]^{2+}$, involving three copper and six P nuclei, in agreement with similar values for related species.^[70,73,129] The DFT calculated LUMO of the dqp π system shows moderate contributions from the N and CH π centres (Figure 6.6.1)^[116] which, however, are not sufficiently large as to cause detectable hyperfine splitting. The isotropic g factors vary to some extent, with the donor substitution (CH_3) in $[(\mu_3\text{-Me}_6\text{-dbq})^- \{\text{Cu}(\text{dppf})\}_3]^{2+}$ diminishing the g_{iso} and the chloride acceptor substituents in $[(\mu_3\text{-Cl}_6\text{-dbq})^- \{\text{Cu}(\text{dppf})\}_3]^{2+}$ resulting in an increase of g_{iso} . These effects reflect subtle differences in the orbital energies of highest occupied, singly occupied, and lowest unoccupied MOs.^[17] Apparently, the influence of six chloride acceptors is indeed to stabilize the SOMO (see anodically shifted reduction of the precursor), thus diminishing the HOMO–SOMO difference relative to the SOMO-LUMO distance.^[17]

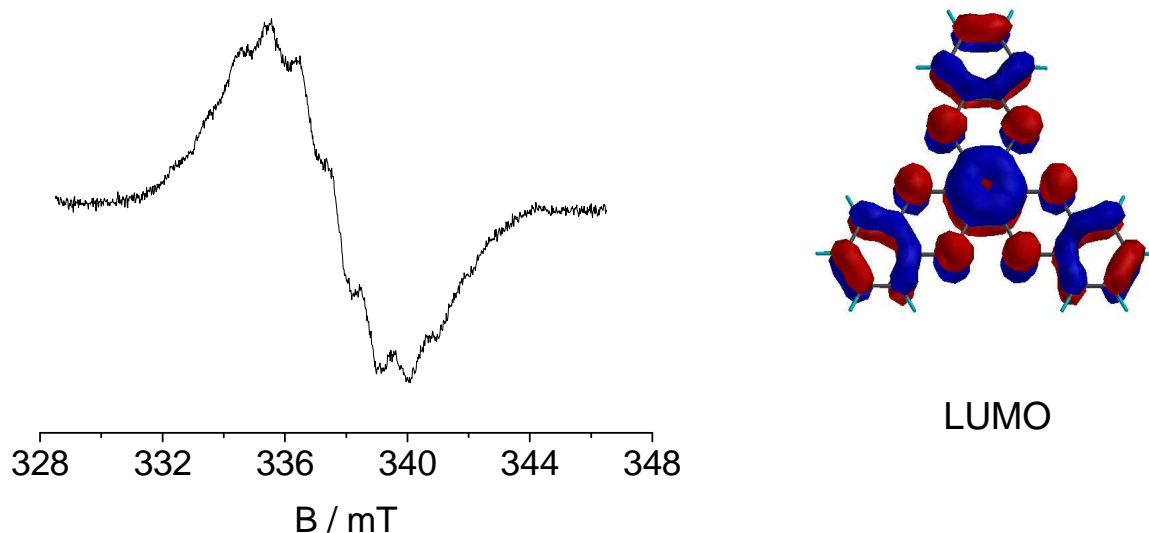


Fig 6.6.1: X-band (9.5 GHz) EPR spectrum of $[(\mu_3\text{-dbq})^- \{\text{Cu}(\text{dppf})\}_3]^{2+}$ in CH_2Cl_2 / 0.1 M Bu_4NPF_6 at RT (right), and LUMO (-2.6311 eV) Characteristics of dqp from DFT calculation.

The relatively high stability of the one-electron reduced complexes allowed us to study these species by high-frequency EPR at 95 or 115 GHz in the glassy frozen solution state (Fig 6.6.2, Tab 6.6.1). This technique yielded results for the g factor anisotropy which has become a useful information for metal complexes of radical ligands.^[30] The Fig 6.6.2 and the data from Tab 6.6.1 show that the symmetry of the system is reflected by the axial g component splitting which, however, is not uniform throughout the series: For $[(\mu_3\text{-dbq})^- \{\text{Cu}(\text{dppf})\}_3]^{2+}$ and $[(\mu_3\text{-Me}_6\text{-dbq})^- \{\text{Cu}(\text{dppf})\}_3]^{2+}$ the $g_{\perp} > g_{\parallel}$ whereas the reverse holds for $[(\mu_3\text{-Cl}_6\text{-dbq})^- \{\text{Cu}(\text{dppf})\}_3]^{2+}$. The altered frontier orbital pattern as indicated above may be invoked to rationalize this reversal of g components. In general, the $g_1 - g_3 = \Delta g$ and the g_{iso} values conform with those of copper(I) coordinated anion radicals of N heterocyclic ligands.^[21]

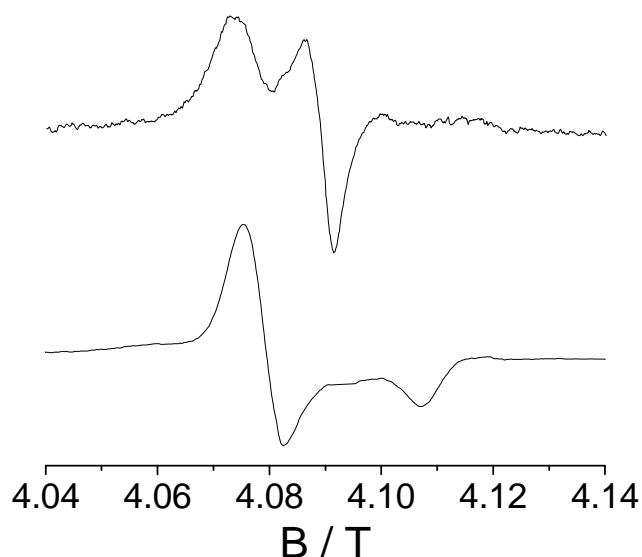


Fig 6.6.2: 115 GHz EPR spectra in toluene/ CH_2Cl_2 (1/4) at 5 K of complex dications $[(\mu_3\text{-Cl}_6\text{-dbq})^- \{\text{Cu}(\text{dppf})\}_3]^{2+}$ (top) and $[(\mu_3\text{-dbq})^- \{\text{Cu}(\text{dppf})\}_3]^{2+}$ (bottom) from Zn reduction of the tris(tetrafluoroborates).

Tab 6.6.1: EPR data.

| Compound | g_{iso} ^{a)} | g_{\perp} | g_{\parallel} | Δg |
|--|-------------------------|----------------------|----------------------|------------|
| $[(\mu_3\text{-dbq})^- \{\text{Cu}(\text{dppf})\}_3]^{2+}$ | 2.0050 | 2.0143 ^{b)} | 2.0005 ^{b)} | 0.0138 |
| $[(\mu_3\text{-Me}_6\text{-dbq})^- \{\text{Cu}(\text{dppf})\}_3]^{2+}$ | 2.0039 | 2.006 ^{c)} | 1.993 ^{c)} | 0.013 |
| $[(\mu_3\text{-Cl}_6\text{-dbq})^- \{\text{Cu}(\text{dppf})\}_3]^{2+}$ | 2.0062 | 2.0095 ^{b)} | 2.0168 ^{b)} | 0.0073 |

^{a)}From X-band EPR in CH_2Cl_2 / 0.1 M Bu_4NPF_6 , ^{b)} from high field (115 GHz) at 5 K in CH_2Cl_2 / toluene (4:1); ^{c)} high-field EPR (95 GHz) at 5 K in CH_2Cl_2 /toluene (4/1).

6.7 Conclusion

In earlier chapters, the ferrocenylcopper(I) $[\text{Cu}^{\text{I}}(\text{dppf})]^+$ moiety has been shown to coordinate weakly basic π acceptors such as *o*-quinones^[129] or α -azodicarbonyl chelators.^[73] A double association (“inverse sandwich”) between the tricationic complex of unsubstituted HATN and two of the three BF_4^- counter-anions in the quasi-trigonal axis is observed in the solid state where as the NMR experiments proves to have fast exchange or dissociation in solution. Electrochemical, UV/VIS/NIR spectroelectrochemical, and EPR studies reveal small but in some cases detectable splitting of the three ferrocene-based oxidations. Three reversible one-electron reduction waves are observed for the hexachloro-substituted complex. The EPR measurements at 9.5, 95 or 115 GHz for the one-electron reduced forms show subtle differences and substituents effects while UV/VIS/NIR spectroelectrochemistry reveals not only intense MLCT bands but also strong near IR absorptions for the one- and two-electron reduced states due to several closely spaced low-lying unoccupied π^* molecular orbitals of the bridging ligands.

Chapter 7

Experimental section.

7.1 Instrumentation:

EPR spectroscopy

X-band EPR spectra at 9.5 GHz were obtained from Bruker system ESP 300 equipped with a Hewlett-Packard Frequency counter 5350B, a Bruker ER035M gaussmeter for g values determination as a Bruker system EMX and a continuous flow cryostat ESR 900 of Oxford instruments for measurements at liquid helium temperature (4 K). For measurements between 110-300K, same instrumental configuration was used with liquid nitrogen cryostat. The measurements were carried out by Dr. Biprajit Sarkar at Institut für Anorganische Chemie, Universität Stuttgart. Spectra at high frequency were taken on a laboratory made spectrometer at the Grenoble High Magnetic Laboratory in frozen solution at 5 K by Dr. Biprajit Sarkar and Dr. Carole Duboc. The accuracy of g values is estimated at ± 0.0003 .

A two-electrode capillary^[134] served to electrogenerate intermediates for X-band EPR while Zn was used as reductant in the high-frequency EPR study.

Simulations of the spectra were done by using Bruker WINEPR / Simfonia programs.

NMR spectroscopy

¹H and ³¹P NMR spectroscopy at a frequency of 250 MHz were carried out by Mrs. Török on a Bruker AC 250 spectrometer. Tetramethylsilane (TMS) was used as the external standard.

IR spectroscopy

IR spectra were obtained using Nicolet 6700 FT-IR spectrometer. Solution measurements were done by using CaF₂ windows and solid state measurements were performed by using high performance diamond ATR unit called Smart Orbit.

UV-vis-NIR spectroscopy

Absorption spectra were recorded on Shimadzu UV-160 spectrometer (200-3200 nm). For measurements Quartz cuvettes of 1 cm path length were used.

UV-vis-NIR and IR spectroelectrochemistry

UV-vis-NIR and IR spectroelectrochemistry measurements were done by Mr. Jan Fiedler. The measurements were performed under argon atmosphere using an Optically Transparent Thin Layer Electrochemical (OTTLE) cell developed by Mr. Krejčík.^[69] The windows of the cell consists of CaF₂ plates. Between the cell working (platinum mesh), auxiliary (platinum mesh) and reference electrodes (silver wire as pseudo reference) are melt-sealed.

Cyclic voltammetry

Cyclic and Differential Pulse voltammetry measurements were performed on an EG&G PAR 273 potentiostat. The measurements were carried out under argon atmosphere in 0.1 M tetrabutylammonium hexafluorophosphate solutions using a three electrode configuration (glassy carbon as working electrode, platinum as counter electrode and silver as pseudoreference electrode). The ferrocene / ferrocenium couple served as the internal reference.

Elemental analysis

Elemental analysis was performed on Perkin Elmer Analyzer 240 by Mrs. B. Förtsch.

7.2 Solvents and Working conditions

All metal complexes were synthesized under argon atmosphere using conventional Schlenk techniques. The ligands were synthesized in air.

Solvents were dried by refluxing under argon over calcium hydride (dichloromethane, dichloroethane, acetonitrile, and hexane), magnesium oxide (ethanol), sodium (toluene) or lithium aluminium hydride (diethyl ether). They were degassed by freeze-pump-thaw method.

7.3 Syntheses

Following compounds were commercially available:

- Ditertiarybutylazodicarboxylate, diisopropylazodicarboxylate, 2,2'-dipyridyl, sodium hypochlorite from Acros,
- Azodicarboxylic dipiperidide, N,N,N',N'-tetramethylazodicarboxymide from Fluka
- 9,10-Phenanthroquinone, 4,5-dichloro-1,2-phenylenediamine, 4,5-dimethyl-1,2-phenylenediamine, hexaketocyclohexane octahydrate, o-phenylenediamine, 2-cyanopyridine from Aldrich.

The ligands abpy^[75], Diquinoxalino-[2,3-a:2',3'-c]phenazine^[135] 2,3,8,9,14,15-hexamethyldiquinoxalino-[2,3-a:2',3'-c]phenazine^[136], and 2,3,8,9,14,15-hexachlorodiquinoxalino-[2,3-a:2',3'-c]phenazine^[137] were synthesized according to literature procedure.

7.3.1 Synthesis of Copper precursors:

Synthesis of [Cu(CH₃CN)₄]BF₄

A mixture of activated Cu powder (190 mg, 3 mmol) and Cu(BF₄)₂·H₂O (1 gm, 3 mmol) were heated to reflux in dry acetonitrile under argon for 4 h. The color of the solution gradually changed from blue to colorless. Copper powder was filtered out under argon and the acetonitrile was removed under vacuum to get a white crystalline solid.

(Very very moisture sensitive both in solid and solution)

Elemental analysis: C₈H₁₂N₄B₁F₄Cu₁ (314.5 g / mol)

Calculated: C 30.55 %, H 3.85 %, N 17.81 %

Experimental: C 30.10 %, H 3.15 %, N 16.65 %

¹H NMR (CDCl₃): δ / ppm = 2.02

Synthesis of [Cu(dppf)(CH₃CN)₂]BF₄

[Cu(CH₃CN)₄]BF₄ (300 mg, 0.95 mmol) and 1,1'-diphenylphosphinoferrocene (dppf) (500 mg, 0.95 mmol) were stirred at room temperature in dry acetonitrile for 8 h. Acetonitrile was removed from the yellow solution under reduced pressure to get the yellow color solid.

Yield: 500 mg (75 %)

Elemental analysis: C₃₈H₃₄N₂B₁F₄P₂Cu₁Fe₁ (786.8 g / mol)

Calculated: C 58.01 %, H 4.36 %, N 3.56 %

Experimental: C 57.57 %, H 4.55 %, N 2.98 %

¹H NMR (CD₂Cl₂): δ / ppm = 2.18 (s, 6H, CH₃CN), 4.09 (s, 4H, Cp), 4.27 (s, 4H, Cp), 7.28-7.62 (m, 20H, Ph); ³¹P NMR (CD₂Cl₂): δ / ppm = -13.8

UV / Vis (CH₂Cl₂): λ_{max} / nm (ε / M⁻¹cm⁻¹) 427 (260)

7.3.2 Synthesis of dinuclear Cu complex with adcOR ligands:

Synthesis of {(μ-adcO^tBu)[Cu(dppf)]₂}(PF₆)

A mixture of di-*tert.*-butylazodicarboxylic ester (54 mg, 0.236 mmol), 1,1'-bis-(diphenylphosphino)ferrocene (26 mg, 0.472 mmol) and activated Cu powder (30 mg, 0.472 mmol) were first refluxed in methanol (2% water, 25 ml) for 20 minutes and then stirred vigorously under air at room temperature for 30 hours. During this time a deep blue solution developed. The solution was filtered and the product precipitated by adding 100 mg of tetrabutylammonium hexafluorophosphate in 7 ml methanol. The precipitate was filtered and washed with methanol (3 × 10 ml) and diethyl ether (2 × 7 ml) and was dissolved in 10 ml dichloromethane. Removal of the solvent gave a blue powder which was crystallized from dichloromethane/diethyl ether (5/1) at 4° C.

Yield: 211 mg (55 %).

Elemental analysis: C₇₈H₇₄N₂F₆P₅O₄Cu₂Fe₂ (1611.1 g / mol)

Calculated.: C 58.15 %, H 4.63 %, N 1.74%

Experimental: C 57.55 %, H 4.37 %, N 1.61 %

IR (CH₂Cl₂): 1597 cm⁻¹

UV / Vis (CH₂Cl₂): λ_{max} / nm (ε / M⁻¹cm⁻¹) 798 (4040)

Synthesis of $\{(\mu\text{-adcO}^i\text{Pr})[\text{Cu}(\text{dppf})]_2\}(\text{PF}_6)$

A mixture of di-isopropyl azodiformate (50 mg, 0.247 mmol), 1,1'-bis-(diphenylphospheno)ferrocene (27 mg, 0.494 mmol) and activated Cu powder (31 mg, 0.494 mmol) were first refluxed in methanol (2% water) (25 ml) for 20 minutes and then stirred vigorously under air at room temperature for 15 hours. During this time a deep blue color solution developed. The solution was filtered off and the filtrate was precipitated by adding 100 mg of tetrabutylammonium hexafluorophosphate in 7 ml methanol. The precipitate was filtered off and washed with methanol (3× 10 ml) and diethyl ether (2× 7 ml) and was dissolved in 10 ml dichloromethane. Removal of the solvent gave the blue powdered solid. The solid was recrystallised from dichloromethane/diethyl ether (5/1) at 4° C.

Yield: 189 mg (48 %)

Elemental analysis: $\text{C}_{76}\text{H}_{70}\text{N}_2\text{F}_6\text{P}_5\text{O}_4\text{Cu}_2\text{Fe}_2$ (1583.06 g / mol)

Calculated: C 57.66 %, H 4.46 %, N 1.77 %

Experimental: C 56.87 %, H 4.36 %, N 1.68 %

IR (CH_2Cl_2): 1579 cm^{-1}

UV / Vis (CH_2Cl_2): $\lambda_{\text{max}} / \text{nm}$ ($\epsilon / \text{M}^{-1}\text{cm}^{-1}$) 824 (3220).

7.3.3 Synthesis of mono-nuclear Cu complexes with *adc-NR*₂ ligands

Synthesis of $\{(\text{adc}^i\text{pip})[\text{Cu}(\text{dppf})]\}(\text{BF}_4)$:

$[\text{Cu}(\text{dppf})(\text{CH}_3\text{CN})_2]\text{BF}_4$ (50 mg, 0.714 mmol) and azodicarboxylic dipiperidide (20 mg, 0.792 mmol) in 20 ml of dry dichloromethane were stirred at room temperature for 8 hours under Argon. During this time the solution turned violet. After removal of the solvent the solid was washed with hexane and crystallized from dichloromethane/hexane (1/5).

Yield: 41 mg (55 %)

Elemental Analysis: $\text{C}_{46}\text{H}_{48}\text{N}_4\text{Cu}_1\text{Fe}_1\text{B}_1\text{F}_4\text{P}_2\text{O}_2, \text{CH}_2\text{Cl}_2$ (1041.9 g / mol)

Calculated: C 54.18 %, H 4.84 %, N 5.38 %

Experimental: C 55.62 %, H 5.10 %, N 5.49 %

IR (CH_2Cl_2): 1672 cm^{-1} (coordinated C=O), 1703 cm^{-1} (free C=O)

$^1\text{H NMR}(\text{CD}_2\text{Cl}_2)$: $\delta / \text{ppm} = 1.61\text{-}1.82$ (m, pip), 3.42 (m, pip), 3.75 (m, pip), 4.32 (s, 4H, Cp), 4.52 (s, 4H, Cp), 7.35 (m, 20H, Ph); $^{31}\text{P NMR}(\text{CD}_2\text{Cl}_2)$: -6.87 ppm

UV / Vis (CH_2Cl_2): $\lambda_{\text{max}} / \text{nm}$ ($\epsilon / \text{M}^{-1}\text{cm}^{-1}$) 261 (12650), 520 (2550)

Synthesis of {(adcNMe₂)[Cu(dppf)]}BF₄:

[Cu(dppf)(CH₃CN)₂]BF₄ (50 mg, 0.714 mmol) and N,N,N',N'- tetramethylazodicarboxamide (12 mg, 0.714 mmol) in 20 ml of dry dichloromethane were stirred at room temperature for 4 hours under Argon. The solution turned violet. After removal of the solvent the solid was washed with hexane and crystallized from dichloromethane/hexane (1/3).

Yield: 45 mg (65 %)

Elemental Analysis: C₄₀H₄₀N₄Cu₁Fe₁B₁F₄P₂O₂.CH₂Cl₂ (961.8 g / mol)

Calculated: C 51.20 %, H 4.40 %, N 5.82 %

Experimental: C 50.77 %, H 4.46 %, N 5.87 %

IR (CH₂Cl₂): 1680 cm⁻¹ (coordinated C=O), 1713 cm⁻¹ (free C=O)

¹H NMR (CD₂Cl₂): δ/ppm = 2.98 (s, 6H, CH₃), 3.16 (s, 6H, CH₃), 4.32 (s, 4H, Cp), 4.40 (s, 4H, Cp), 7.42 ppm (m, 20H, Ph); ³¹P NMR (CD₂Cl₂): -7.58 ppm

UV / Vis (CH₂Cl₂): λ_{max} / nm (ε / M⁻¹cm⁻¹) 269 (4470), 522 (1220)

7.3.4 Synthesis of Cu complexes with abpy

Synthesis of {(abpy)[Cu(dppf)]}BF₄:

[Cu(dppf)(CH₃CN)₂]BF₄ (56 mg, 0.714 mmol) and 2,2'-azobispyridine (13 mg, 0.714 mmol) in 20 ml of dry dichloromethane were stirred at room temperature for 8 hours under Argon. During this time the solution turned violet. After removal of the solvent the solid was washed with hexane and crystallized from dichloromethane/hexane (1/3).

Yield: 43 mg (68 %)

Elemental analysis: C₄₄H₃₆N₄Cu₁Fe₁B₁F₄P₂.CH₂Cl₂ (973.8 g / mol)

Calculated: C 55.50 %, H 3.93%, N 5.75 %

Experimental: C 55.77 %, H 3.96 %, N 6.11 %

¹H NMR(CD₂Cl₂)(223 K): δ / ppm = 4.26-4.69 (8H, Cp); 6.96-7.45 (m, 20H, (Ph-H));

7.42(d, 1H, J = 6.6 Hz); 7.62 (t, 1H, J = 6.7 Hz); 7.82 (m, 2H); 8.17 (d, 1H, J = 4.1 Hz); 8.35 (t, 1H, J = 7.6 Hz); 8.55 (d, 2H, J = 7.1 Hz); ³¹P NMR(CD₂Cl₂): δ/ppm= -3.76

UV / Vis (CH₂Cl₂): λ_{max} / nm (ε / M⁻¹cm⁻¹) 354 (8890), 529 (2570), 638 (sh)

Synthesis of $\{(\mu\text{-abpy})[\text{Cu}(\text{dppf})]_2\}(\text{BF}_4)_2$:

A mixture of $\{(\text{abpy})[\text{Cu}(\text{dppf})]\text{BF}_4\}$ (20 mg, 0.224 mmol) and $[\text{Cu}(\text{dppf})(\text{CH}_3\text{CN})_2]\text{BF}_4$ (17 mg, 0.224 mmol) in 20 ml of dry dichloromethane was stirred at room temperature for 6 hours under Argon. During this time the solution turned greenish blue. After removal of the solvent the solid was washed with hexane and crystallized from dichloromethane/hexane (1/5).

Yield: 22 mg (63 %)

Elemental analysis: $\text{C}_{78}\text{H}_{64}\text{N}_4\text{Cu}_2\text{B}_2\text{Fe}_2\text{F}_8\text{P}_4$ (1593.7 g / mol)

Calculated: C 58.79 %, H 4.05 %, N 3.52 %

Experimental: C 57.70 %, H 4.01 %, N 3.67 %

^1H NMR(CD_2Cl_2): $\delta/\text{ppm} = 4.46\text{-}4.78$ (16H, Cp); 6.96-7.45 (m, 40H, (Ph-H)); 7.58(t, 2H); 8.00 (t, 2H); 8.39 (d, 2H, J = 8.0 Hz); 8.51 (d, 2H, J = 5.0 Hz); ^{31}P NMR(CD_2Cl_2): $\delta/\text{ppm} = -0.82$

UV / Vis (CH_2Cl_2): $\lambda_{\text{max}} / \text{nm}$ ($\epsilon / \text{M}^{-1}\text{cm}^{-1}$) 757 (4100)

Synthesis of $\{(\mu\text{-abpy})[\text{Cu}(\text{dppf})]_2\}(\text{BF}_4)_2$:

12 mg(0.19 mmol) of activated Cu powder, 22 mg (0.062 mmol) of $\text{Cu}(\text{BF}_4)_2 \cdot x \text{H}_2\text{O}$, 25 mg (0.135 mmol) of abpy and 150 mg (0.270 mmol) of 1,1'-bis-diphenylphosphino ferrocene in 20 ml of dry dichloromethane were stirred at room temperature for 4 hours under Argon. During this time the solution turned wine red. Solution was filtered off from the Cu powder and the solvent was removed in vacuum. The solid was washed with hexane and was crystallized from dichloromethane/hexane (1/3).

Yield: 110 mg (54 %)

Elemental analysis: $\text{C}_{78}\text{H}_{64}\text{N}_4\text{Cu}_2\text{B}_1\text{Fe}_2\text{F}_4\text{P}_4, \text{CH}_2\text{Cl}_2$ (1506.8 g / mol)

Calculated: C 59.61 %, H 4.18 %, N 3.52 %

Experimental: C 59.75 %, H 4.37 %, N 3.99%

UV / Vis (CH_2Cl_2): $\lambda_{\text{max}} / \text{nm}$ ($\epsilon / \text{M}^{-1}\text{cm}^{-1}$) 533 (5680), 392(9680)

7.3.5 Synthesis of Cu complex with 9,10-phenanthroquinone

Synthesis of $\{(\text{PhnQ})[\text{Cu}(\text{dppf})]\}\text{BF}_4$:

A mixture of 9,10-phenanthrenequinone (L) (44 mg, 0.214 mmol) and $[\text{Cu}(\text{dppf})(\text{CH}_3\text{CN})_2](\text{BF}_4)$ (168 mg, 0.214 mmol) in 30 mL dry dichloroethane were heated to reflux under argon atmosphere for 12 h. The bluish green solution was removed under reduced pressure and the solid was washed several times with dry hexane. The blue solid was recrystallised with dry dichloromethane/hexane (2/1) at 4° C.

Yield: 43 mg (68%)

Elemental analysis: $\text{C}_{48}\text{H}_{36}\text{Cu}_1\text{Fe}_1\text{B}_1\text{O}_2\text{P}_2\text{F}_4, 2.\text{CH}_2\text{Cl}_2$ (1082.8 g / mol)

Calculated C 55.46 %, H 3.72 %

Experimental: C 55.34 %, H 3.75 %

^1H NMR (CD_2Cl_2): δ / ppm = 4.39(s, 4H, Cp), 4.51 (s, 4H, Cp), 7.35-7.55 (m, 20H, Ph), 7.56-7.59(m, 2H, H^2), 7.88 (td, 2H, $J = 7.5, 1.3$ Hz, H^3), 8.15 (d, 2H, $J = 8$ Hz, H^1), 8.24 (dd, 2H, $J = 1.5, 7.8$ Hz, H^4). ^{31}P NMR(CD_2Cl_2): $\delta/\text{ppm} = -10.40$.

IR/ cm^{-1} (solid): 1673 ($\nu_{\text{C=O}}$); 1591 (Cp).

Mass spectrum: molecular ion peak centered at $m/z = 825.08$, corresponding to $[(\text{PhnQ})\{\text{Cu}(\text{dppf})\}]^+$

UV / Vis (CH_2Cl_2): $\lambda_{\text{max}} / \text{nm}$ ($\epsilon / \text{M}^{-1}\text{cm}^{-1}$) 323 (sh), 420 (6540), 697 (3390)

7.3.6 Synthesis of tri-nuclear Cu complexes with different substituted diquinoxalino-[2,3-a:2',3'-c]phenazine (dqp) ligands

Synthesis of $[(\mu_3\text{-dqp})\{\text{Cu}(\text{dppf})\}_3](\text{BF}_4)_3$ and $[(\mu_3\text{-dqp})\{\text{Cu}(\text{dppf})\}_3](\text{PF}_6)_3$:

A mixture of $[\text{Cu}(\text{dppf})(\text{CH}_3\text{CN})_2]\text{BF}_4$ or $[\text{Cu}(\text{dppf})(\text{CH}_3\text{CN})_2]\text{PF}_6$ (100 mg, 1.28 mmol) and diquinoxalino-[2,3-a:2',3'-c]phenazine (16 mg, 0.428 mmol) in 20 mL dry dichloromethane were stirred at room temperature for 8 h under argon atmosphere. During the course of the reaction the solution turned to green. After removal of the solvent under reduced pressure the solid thus obtained was washed thoroughly with hexane and the dried product was recrystallized from dichloromethane/hexane (1/3).

Yield of $[(\mu_3\text{-dqp})\{\text{Cu}(\text{dppf})\}_3](\text{BF}_4)_3$: 43 mg (68 %)

Elemental analysis: $\text{C}_{126}\text{H}_{96}\text{N}_6\text{B}_3\text{F}_{12}\text{P}_6\text{Cu}_3\text{Fe}_3$ (2498.6 g / mol)

Calculated: C, 60.57 %, H 3.87 %, N 3.36 %

Experimental: C 59.98 %, H 4.11 %, N 3.48 %

^1H NMR (CDCl_3): δ / ppm = 4.71(s, 12H, Cp), 4.78 (s, 12H, Cp), 6.88-7.04 (m, 30H, Ph), 7.3-7.35 (m, 30H, Ph), 7.41(m, 6H, L^1), 8.18 (m, 6H, L^1); ^{31}P NMR(CDCl_3): δ / ppm = -7.25.

UV / Vis (CH_2Cl_2): λ_{max} / nm (ϵ / $\text{M}^{-1}\text{cm}^{-1}$) 696(sh), 616(15330), 423(26220), 331(50820)

Yield of $[(\mu_3\text{-dqp})\{\text{Cu}(\text{dppf})\}_3](\text{PF}_6)_3$: Yield: 39 mg (35%);

Elemental analysis: $\text{C}_{126}\text{H}_{96}\text{N}_6\text{F}_{18}\text{P}_9\text{Cu}_3\text{Fe}_3$ (2673.1 g / mol)

Calculated: C, 56.61 %, H 3.62 %, N 3.14 %

Experimental: C 57.75 %, H 3.68 %, N 3.33 %

^1H NMR[CDCl_3 , δ (ppm)] 4.71(s, 12H, Cp), 4.78 (s, 12H, Cp), 6.88-7.04 (m, 30H, Ph), 7.3-7.35 (m, 30H, Ph), 7.41(m, 6H, L^1), 8.18 (m, 6H, L^1). ^{31}P NMR[CDCl_3 , δ (ppm)]: -7.25, -145.5 (sp, $J_{\text{PF}} = 713$ Hz, PF_6); ^{19}F NMR[CDCl_3 , δ (ppm)]: -73.1 (d, $J_{\text{FP}} = 713$ Hz, PF_6);

Synthesis of $[(\mu_3\text{-Me}_6\text{-dqp})\{\text{Cu}(\text{dppf})\}_3](\text{BF}_4)_3$ and $[(\mu_3\text{-Me}_6\text{-dqp})\{\text{Cu}(\text{dppf})\}_3](\text{PF}_6)_3$:

$[\text{Cu}(\text{dppf})(\text{CH}_3\text{CN})_2]\text{BF}_4$ or $[\text{Cu}(\text{dppf})(\text{CH}_3\text{CN})_2]\text{PF}_6$ (100 mg, 1.28 mmol) and 2,3,8,9,14,15-hexamethyldiquinoxalino-[2,3-a:2',3'-c]phenazine (20 mg, 0.426 mmol) in 25 mL dry dichloromethane were stirred at room temperature for 8 h under argon atmosphere. After removal of the solvent under reduced pressure the solid thus obtained was washed thoroughly with hexane and the dried product was recrystallized from dichloromethane/hexane (1/5).

Yield of $[(\mu_3\text{-Me}_6\text{-dqp})\{\text{Cu}(\text{dppf})\}_3](\text{BF}_4)_3$: 65 mg(58 %)

Elemental analysis: $\text{C}_{132}\text{H}_{108}\text{N}_6\text{B}_3\text{F}_{12}\text{P}_6\text{Cu}_3\text{Fe}_3$ (2582.81 g / mol)

Calculated: C, 61.38 %, H 4.27 %, N 3.25 %

Experimental: C 60.77 %, H 4.17 %, N 3.21 %

^1H NMR (CDCl_3): δ / ppm = 2.24 (s, 6H, Me), 4.72(s, 12H, Cp), 4.75 (s, 12H, Cp), 6.86-7.35 (m, 60H, Ph), 7.98(s, 6H, L^2); ^{31}P NMR(CDCl_3): δ / ppm = -6.25

UV / Vis (CH_2Cl_2): λ_{max} / nm (ϵ / $\text{M}^{-1}\text{cm}^{-1}$) 626(9170), 435(33340), 346(43400)

Yield of $[(\mu_3\text{-Me}_6\text{-dqp})\{\text{Cu}(\text{dppf})\}_3](\text{PF}_6)_3$: 54 mg (58%);

Elemental analysis: $\text{C}_{132}\text{H}_{108}\text{N}_6\text{F}_{18}\text{P}_9\text{Cu}_3\text{Fe}_3$ (2757.3 g / mol)

Calculated: C, 57.50 %, H 3.95 %, N 3.05 %

Experimental: C 58.26 %, H 4.35 %, N 3.38 %

^1H NMR[CDCl_3 , $\delta(\text{ppm})$]: 2.25 (s, 6H, Me), 4.75(s, 12H, Cp), 4.82 (s, 12H, Cp), 6.92-7.35 (m, 60H, Ph), 8.04 (s, 6H, L^2). ^{31}P NMR[CDCl_3 , $\delta(\text{ppm})$]: -6.66 (s, dppf), -145.3 (sp, $J_{\text{PF}} = 712$ Hz, PF_6); ^{19}F NMR[CDCl_3 , $\delta(\text{ppm})$]: -73.4 (d, $J_{\text{FP}} = 712$ Hz, PF_6);

Synthesis of $[(\mu_3\text{-Cl}_6\text{-dqp})\{\text{Cu}(\text{dppf})\}_3](\text{BF}_4)_3$ and $[(\mu_3\text{-Cl}_6\text{-dqp})\{\text{Cu}(\text{dppf})\}_3](\text{PF}_6)_3$:

$[\text{Cu}(\text{dppf})(\text{CH}_3\text{CN})_2]\text{BF}_4$ (100 mg, 1.28 mmol) or $[\text{Cu}(\text{dppf})(\text{CH}_3\text{CN})_2]\text{PF}_6$ and 2,3,8,9,14,15-hexachlorodiquinoxalino-[2,3-a:2',3'-c]phenazine (20 mg, 0.426 mmol) in 25 mL dry dichloromethane were stirred at room temperature for 8 h under argon atmosphere. After removal of the solvent under reduced pressure the solid thus obtained was washed thoroughly with hexane and the dried product was recrystallized from dichloromethane/hexane (1/5).

Yield of $[(\mu_3\text{-Cl}_6\text{-dqp})\{\text{Cu}(\text{dppf})\}_3](\text{BF}_4)_3$: 72 mg(62 %)

Elemental analysis: $\text{C}_{126}\text{H}_{90}\text{N}_6\text{B}_3\text{Cl}_6\text{F}_{12}\text{P}_6\text{Cu}_3\text{Fe}_3$ (2705.3 g / mol)

Calculated: C 55.94 %, H 3.35 %, N 3.11 %

Experimental: C 54.58 %, H 3.32 %, N 3.25 %

^1H NMR (CDCl_3): δ / ppm = 4.67(s, 12H, Cp), 4.82 (s, 12H, Cp), 6.91-7.33 (m, 60H, Ph), 8.26(s, 6H, L^3). ^{31}P NMR(CDCl_3): δ / ppm = -5.95.

UV / Vis (CH_2Cl_2): λ_{max} / nm (ϵ / $\text{M}^{-1}\text{cm}^{-1}$) 792(sh), 671(9430), 442(28500), 353(29900)

Yield of $[(\mu_3\text{-Cl}_6\text{-dqp})\{\text{Cu}(\text{dppf})\}_3](\text{PF}_6)_3$: 60 mg (68%);

Elemental analysis: $\text{C}_{126}\text{H}_{90}\text{N}_6\text{Cl}_6\text{F}_{18}\text{P}_9\text{Cu}_3\text{Fe}_3$ (2879.7 g / mol)

Calculated: C 52.55 %, H 3.15 %, N 2.92 %

Experimental: C 53.50 %, H 3.55 %, N 3.29 %

^1H NMR[CDCl_3 , $\delta(\text{ppm})$]: 4.73(s, 12H, Cp), 4.88 (s, 12H, Cp), 6.99-7.29 (m, 60H, Ph), 8.27(s, 6H, L^3). ^{31}P NMR[CDCl_3 , $\delta(\text{ppm})$]: -5.55 (s, dppf), -145.4 (sp, $J_{\text{PF}} = 713$ Hz, PF_6); ^{19}F NMR[CDCl_3 , $\delta(\text{ppm})$]: -73.5 (d, $J_{\text{FP}} = 713$ Hz, PF_6).

7.4 Crystallography

Crystallographic data collection was carried out by Dr. F. Lissner, Priv. Doz. Dr. M. Niemeyer, Mr. Denis Bubrin from University of Stuttgart and Mr. S. Mobin from Indian Institute of Technology, Bombay. Structure solving was done by Dr. F. Lissner, Priv. Doz. Dr. M. Niemeyer, Mr. Denis Bubrin and Mr. S. Mobin.

Data collection was performed on four circle diffractometer NONIUS Kappa-CCD or Siemens P4 with a Mo-K α radiation of 0.71073 Å (graphite-monocromatized) at 293 K or 173 K. The crystals were sealed in capillaries for the measurements.

The structure were solved via direct methods using the programme SHELXS-97.^[138] Refinement was carried out by the full matrix least squares method employing the programme SHELXL-97.^[139] All non-hydrogen atoms are refined anisotropically, hydrogen atoms were introduced in proper positions with coupled isotropic factors using the riding model. Absorption corrections were performed numerically using the programme HABITUS.^[140] The programme DIAMOND 2.1e^[141] was used for structure drawing.

Crystallographic parameters:

$$\text{GOF} = \left\{ \sum w(|F_o|^2 - |F_c|^2)^2 / (n - m) \right\}^{1/2} \quad \text{where } n = \text{number of data and } m = \text{number of variables}$$

$$R = (\sum | |F_o| - |F_c| |) / \sum |F_o|$$

$$\text{WR} = \left\{ \sum [w(|F_o|^2 - |F_c|^2)^2] / \sum [w(F_o^4)] \right\}^{1/2}$$

7.4.1: $\{(\mu\text{-adcO}^t\text{Bu})[\text{Cu}(\text{dppf})_2](\text{PF}_6)\}$

Deep blue colored prism shaped crystals were obtained from CH₂Cl₂ / Et₂O (5:1)

Crystallographic data and refinement parameters for $\{(\mu\text{-adcO}^t\text{Bu})[\text{Cu}(\text{dppf})_2](\text{PF}_6)\}$

| | |
|---------------------|---|
| Empirical formula | C ₇₈ H ₇₄ Cu ₂ F ₆ Fe ₂ N ₂ O ₄ P ₅ |
| Formula wt. | 1611.02 g mol ⁻¹ |
| Crystal size | 0.50 × 0.30 × 0.15 mm |
| Temperature | 173 K |
| Wavelength | 0.71073 Å |
| Crystal system | monoclinic |
| Space group | P2 ₁ /m |
| Unit cell dimension | a = 11.434(2) Å α = 90° b = 26.180(4) Å β = 106.687(17)° |

| | |
|-----------------------------------|--|
| | $c = 15.929(2) \text{ \AA}$ $\gamma = 90^\circ$ |
| Cell volume | $4567.6(14) \text{ \AA}^3$ |
| Calculated density | 1.171 g cm^{-3} |
| Absorption coefficient | 0.911 mm^{-1} |
| Max 2θ | 50° |
| Index ranges | $-13 \leq h \leq 13$ $0 \leq k \leq 31$ $0 \leq l \leq 18$ |
| Formula units per cell, Z | 2 |
| Reflection collected | 8650 |
| Unique reflections | 8184 |
| $R_{\text{int}} / R_\sigma$ | 0.0621 / 0.1614 |
| GOF / F^2 | 0.818 |
| Data / restraints / parameter | 8184 / 6 / 443 |
| R indices (for all data) | $R1 = 0.1293$, $wR2 = 0.1952$ |
| R indices (for $I > 2\sigma(I)$) | $R1 = 0.735$, $wR2 = 0.1768$ |
| Largest residual densities | $1.010 / - 1.091 \text{ e \AA}^3$ |

7.4.2: $[\text{Cu}^{\text{I}}(\text{adc-pip})(\text{dppf})](\text{BF}_4)$

Dark violet block shaped single crystals for X-ray diffraction were obtained from CH_2Cl_2 layered with hexane.

Crystallographic data and refinement parameters for $[\text{Cu}^{\text{I}}(\text{adc-pip})(\text{dppf})](\text{BF}_4)$

| | |
|---------------------|--|
| Empirical formula | $\text{C}_{46}\text{H}_{48}\text{B}_1\text{Cu}_1\text{F}_4\text{Fe}_1\text{N}_4\text{O}_3$ |
| Formula wt. | $937.02 \text{ g mol}^{-1}$ |
| Crystal size | $0.50 \times 0.30 \times 0.15 \text{ mm}$ |
| Temperature | 100 K |
| Wavelength | 0.71073 \AA |
| Crystal system | monoclinic |
| Space group | $P2_1/n$ |
| Unit cell dimension | $a = 18.9131(12) \text{ \AA}$ $\alpha = 90^\circ$ $b = 9.3832(6) \text{ \AA}$ $\beta = 106.199(4)^\circ$ $c = 26.1565(12) \text{ \AA}$ $\gamma = 90^\circ$ |

| | |
|-----------------------------------|--|
| Cell volume | 4457.6(5) Å ³ |
| Calculated density | 1.450 g cm ⁻³ |
| Absorption coefficient | 0.937 mm ⁻¹ |
| Max 2θ | 56.52° |
| Index ranges | -24 ≤ h ≤ 24 -12 ≤ k ≤ 11 -34 ≤ l ≤ 33 |
| Formula units per cell, Z | 4 |
| Reflection collected | 8692 |
| Unique reflections | 8184 |
| R _{int} / R _σ | 0.1172 / 0.0910 |
| GOF / F ² | 1.120 |
| Data / restraints / parameter | 8692 / 0 / 555 |
| R indices (for all data) | R1 = 0.1229, wR2 = 0.1784 |
| R indices (for I > 2σ(I)) | R1 = 0.084, wR2 = 0.1967 |
| Largest residual densities | 1.808, - 1.520 e Å ³ |

7.4.3: {(abpy)[Cu(dppf)]}BF₄

Dark purple needle shaped crystals were obtained from CH₂Cl₂ layered with hexane (1:3).

Crystallographic data and refinement parameters for {(abpy)[Cu(dppf)]}BF₄

| | |
|---------------------|---|
| Empirical formula | C ₄₄ H ₃₆ B ₁ Cu ₁ F ₄ Fe ₁ N ₄ P ₂ |
| Formula wt. | 888.91 g mol ⁻¹ |
| Crystal size | 1.00 × 0.80 × 0.20 mm |
| Temperature | 110 K |
| Wavelength | 0.71073 Å |
| Crystal system | triclinic |
| Space group | P $\bar{1}$ |
| Unit cell dimension | a = 11.804(3) Å α = 72.155(14)° b = 11.925(3) Å β = 89.095(13)° c = 15.680(4) Å γ = 68.464(10)° |
| Cell volume | 1942.7(9) Å ³ |
| Calculated density | |

| | |
|-----------------------------------|---|
| Absorption coefficient | 1.150 g cm ⁻³ |
| Max 2θ | 1.061 mm ⁻¹ |
| Index ranges | 25° -13 ≤ h ≤ 13 -12 ≤ k ≤ 13 |
| Formula units per cell, Z | -18 ≤ l ≤ 18 |
| Reflection collected | 2 |
| Unique reflections | 7105 |
| R _{int} / R _σ | 6747 |
| GOF / F ² | 0.0323 / 0.0367 |
| Data / restraints / parameter | 0.999 |
| R indices (for all data) | 6747 / 0 / 514 |
| R indices (for I > 2σ(I)) | R1 = 0.0557, wR2 = 0.1367 |
| Largest residual densities | R1 = 0.051, wR2 = 0.1341 0.958, - 1.444 e Å ³ |

7.4.4: {(μ-abpy)[Cu(dppf)]₂}(BF₄)

Dark red block shaped crystals were obtained from dry CH₂Cl₂ layered with dry hexane (1:3).

Crystallographic data and refinement parameters for {(μ-abpy)[Cu(dppf)]₂}(BF₄)

| | |
|------------------------|--|
| Empirical formula | C ₇₈ H ₆₈ B ₁ Cu ₂ F ₄ Fe ₂ N ₄ O ₂ P ₄ |
| Formula wt. | 1542.83 g mol ⁻¹ |
| Crystal size | 0.80 × 0.40 × 0.25 mm |
| Temperature | 293 K |
| Wavelength | 0.71073 Å |
| Crystal system | monoclinic |
| Space group | P2 ₁ /c |
| Unit cell dimension | a = 11.87170(10) Å α = 90° b = 19.8267(2) Å β = 93.7240(10)° c = 31.0639(3) Å γ = 90° |
| Cell volume | 7296.13(12) Å ³ |
| Calculated density | 1.405 g cm ⁻³ |
| Absorption coefficient | 1.112 mm ⁻¹ |

| | |
|-----------------------------------|--|
| Max 2 θ | 28.22° |
| Index ranges | -13 ≤ h ≤ 15 -26 ≤ k ≤ 25 -31 ≤ l ≤ 41 |
| Formula units per cell, Z | 4 |
| Reflection collected | 17639 |
| Unique reflections | 11858 |
| R _{int} / R _σ | 0.0953 / 0.0638 |
| GOF / F ² | 1.456 |
| Data / restraints / parameter | 17639 / 0 / 875 |
| R indices (for all data) | R1 = 0.1180, wR2 = 0.2377 |
| R indices (for I > 2σ(I)) | R1 = 0.0787 wR2 = 0.2155 |
| Largest residual densities | 2.337, - 1.148 e Å ³ |

7.4.5: {(PhenQ)[Cu(dppf)]}BF₄

Dark green block shaped crystals were obtained from dry CH₂Cl₂ layered with dry hexane (1:3).

Crystallographic data and refinement parameters for {(PhenQ)[Cu(dppf)]}BF₄

| | |
|------------------------|---|
| Empirical formula | C ₄₉ H ₃₈ B ₁ Cl ₂ Cu ₁ F ₄ Fe ₁ O ₂ P ₂ |
| Formula wt. | 997.83 g mol ⁻¹ |
| Crystal size | 0.80 × 0.40 × 0.25 mm |
| Temperature | 173 K |
| Wavelength | 0.71073 Å |
| Crystal system | monoclinic |
| Space group | P2 ₁ /c |
| Unit cell dimension | a = 12.268(3) Å α = 90° b = 27.661(6) Å β = 93.29(2)° c = 14.155(3) Å γ = 90° |
| Cell volume | 4795.7(18) Å ³ |
| Calculated density | 1.382 g cm ⁻³ |
| Absorption coefficient | 0.977 mm ⁻¹ |
| Max 2 θ | 26° |

| | |
|-----------------------------------|---|
| Index ranges | -4 ≤ h ≤ 15 -18 ≤ k ≤ 34 -17 ≤ l ≤ 17 |
| Formula units per cell, Z | 4 |
| Reflection collected | 9381 |
| Unique reflections | 2757 |
| R _{int} / R _σ | 0.1114 / 0.2700 |
| GOF / F ² | 0.763 |
| Data / restraints / parameter | 9381 / 6 / 576 |
| R indices (for all data) | R1 = 0.2309, wR2 = 0.2481 |
| R indices (for I > 2σ(I)) | R1 = 0.0820 wR2 = 0.1922 |
| Largest residual densities | 0.680, - 1.163 e Å ³ |

7.4.6: [(μ₃-dqp){Cu(dppf)}₃](BF₄)₃

Dark green block shaped crystals were obtained from CH₂Cl₂ layered with hexane (1:2).

Crystallographic data and refinement parameters for [(μ₃-dqp){Cu(dppf)}₃](BF₄)₃

| | |
|------------------------|---|
| Empirical formula | C ₁₂₈ H ₁₀₀ B ₃ Cl ₄ Cu ₃ F ₁₂ Fe ₃ N ₆ O ₆ P ₆ |
| Formula wt. | 2764.36 g mol ⁻¹ |
| Crystal size | 0.28 × 0.21 × 0.18 mm |
| Temperature | 150 K |
| Wavelength | 0.71073 Å |
| Crystal system | orthorhombic |
| Space group | Pbca |
| Unit cell dimension | a = 17.6119(3) Å α = 90° b = 33.9414(5) Å β = 90° c = 39.9397(7) Å γ = 90° |
| Cell volume | 23874.9(7) Å ³ |
| Calculated density | 1.538 g cm ⁻³ |
| Absorption coefficient | 1.128 mm ⁻¹ |
| Max 2θ | 26° |
| Index ranges | -20 ≤ h ≤ 18 -23 ≤ k ≤ 40 |

| | |
|-----------------------------------|---------------------------------|
| | $-47 \leq l \leq 47$ |
| Formula units per cell, Z | 8 |
| Reflection collected | 82199 |
| Unique reflections | 20414 |
| $R_{\text{int}} / R_{\sigma}$ | 0.1228 / 0.2700 |
| GOF / F^2 | 1.057 |
| Data / restraints / parameter | 20414 / 0 / 1540 |
| R indices (for all data) | R1 = 0.1083, wR2 = 0.2270 |
| R indices (for $I > 2\sigma(I)$) | R1 = 0.0722, wR2 = 0.1973 |
| Largest residual densities | 2.884, - 0.966 e \AA^3 |

Chapter 8

Summary.

Oligonuclear metal complexes with multiple redox processes are gaining in importance because of their wide relevance from molecular devices to enzymatic systems. In this doctoral work, the 1,1'-bis(diphenylphosphino)ferrocenylcopper(I) moiety $[\text{Cu}(\text{dppf})]^+$ has been used to form complexes with various non-innocent ligands like 2,2'-azobispyridine (abpy), esters and amides of azodicarboxylic acid, *o*-quinones and hexaazatrinaphthlene derivatives.

In chapter 2, the heterotetranuclear complexes of $[\text{Cu}(\text{dppf})]^+$ with the strong π -acceptor ligands di-*tert*-butyl- or di-*iso*-propyl- azodicarboxylate (adc-OR) are described: $[(\mu\text{-adcO}^t\text{Bu})\{\text{Cu}^{\text{I}}(\text{dppf})\}_2](\text{PF}_6)$ and $[(\mu\text{-adcO}^i\text{Pr})\{\text{Cu}^{\text{I}}(\text{dppf})\}_2](\text{PF}_6)$. The complexes were isolated in the stable radical bridged state. The complex $[(\mu\text{-adcO}^t\text{Bu})\{\text{Cu}^{\text{I}}(\text{dppf})\}_2](\text{PF}_6)$ was characterized structurally showing how two $[\text{Cu}(\text{dppf})]^+$ moieties are held together by the central di-*tert*-butylazodicarboxylate radical anion bridge (Fig 8.1). The presence of one PF_6^- as counter anion confirms the radical nature of the complex.

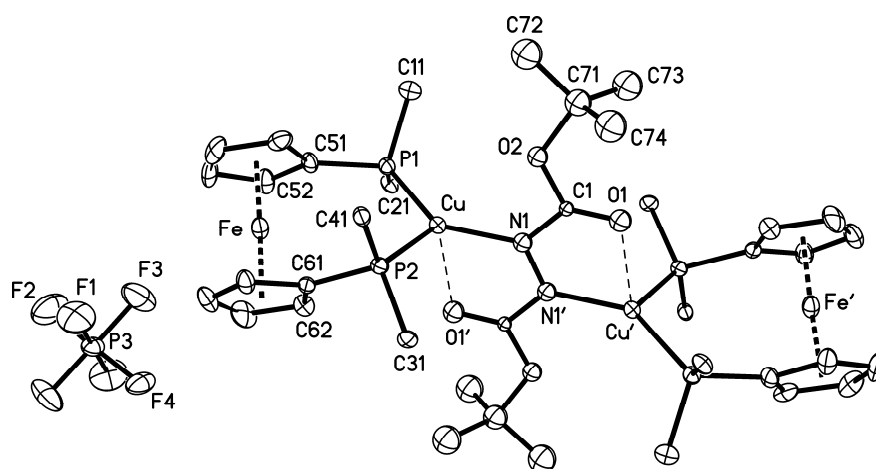


Fig 8.1: Molecular structure of $[(\mu\text{-adcO}^t\text{Bu})\{\text{Cu}^{\text{I}}(\text{dppf})\}_2](\text{PF}_6)$ in the crystal (P-phenyl groups omitted for clarity).

At 298 K the X-band EPR spectra of both complexes show fairly resolved line-rich EPR spectrum at $g_{\text{iso}} = 2.011$ and 2.012 respectively, which can be simulated using two $^{63/65}\text{Cu}$ ($I = 3/2$), four ^{31}P ($I = 1/2$) and two azo ^{14}N ($I = 1/2$) nuclei (Fig 8.2). At high frequency (285 GHz), the EPR spectra of the complexes show rhombic g splitting in the glassy frozen state with small g anisotropy, confirming predominantly ligand centered spin.

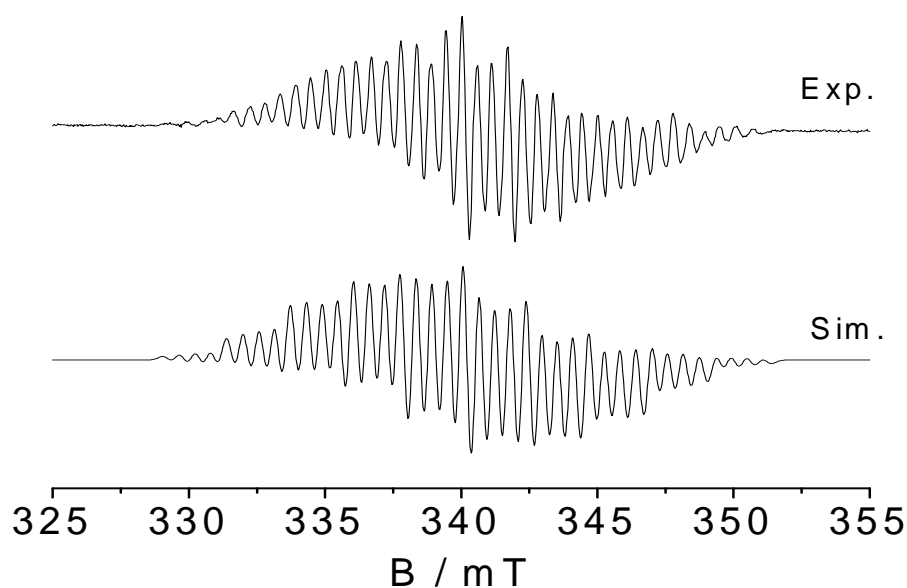


Fig 8.2: X-band EPR spectrum of $\{(\mu\text{-adcO}^t\text{Bu})[\text{Cu}(\text{dppf})]_2\}^+$ at 298 K in CH_2Cl_2 with simulation.

The blue radical complexes show long-wavelength bands at around 800 nm for the MLCT transition $d(\text{Cu}^{\text{I}}) \rightarrow \pi^*(\text{adcOR}^{\bullet-})$. Upon reversible one-electron oxidation the MLCT band shifts to higher wavelengths (1100 nm) due to formation of a partially empty π^* molecular orbital of (adcOR). The reversible one-electron reduction $\{(\mu\text{-adcOR})[\text{Cu}(\text{dppf})]_2\}^{(+)\rightarrow(0)}$ causes the disappearance of MLCT band due to complete electron filling of the π^* orbital of $\text{adcOR}^{\bullet-}$. The compounds can be further oxidized reversibly by two-electrons, the process occurring on the ferrocene termini. The large separation between the ferrocenyl phosphines prevents any electronic communication, resulting in a two-electron wave in the cyclic voltammograms.

Chapter 3 deals with heterodinuclear complexes of $[\text{Cu}(\text{dppf})]^+$ with amides of azodicarboxylic acids. The azodicarboximides have similar coordination sites and an identical redox nature as other azodicarbonyl ligands. The chapter presents the first examples of heterodinuclear complexes $[\text{Cu}^{\text{I}}(\text{adc-pip})(\text{dppf})](\text{BF}_4)$ and $[\text{Cu}^{\text{I}}(\text{adc-NMe}_2)(\text{dppf})](\text{BF}_4)$ with a non-reduced chelating $\text{N}=\text{N}-\text{C}=\text{O}$ group which is established from X-ray crystal structure determination (fig 8.3). The bond lengths ($d_{\text{N}=\text{N}} = 1.258(7)$ Å, $d_{\text{C}-\text{N}} = 1.466(8)$ Å, and $d_{\text{C}=\text{O}} = 1.234(7)$ Å) obtained from the structure analysis implies the binding of $[\text{Cu}(\text{dppf})]^+$ by the non-reduced $\text{N}=\text{N}-\text{C}=\text{O}$ group (Fig 8.3). Apparently there is non enough π -back donation from $d^{10}(\text{Cu})$ to $\pi^*(\text{adc-NR}_2)$ for full electron transfer.

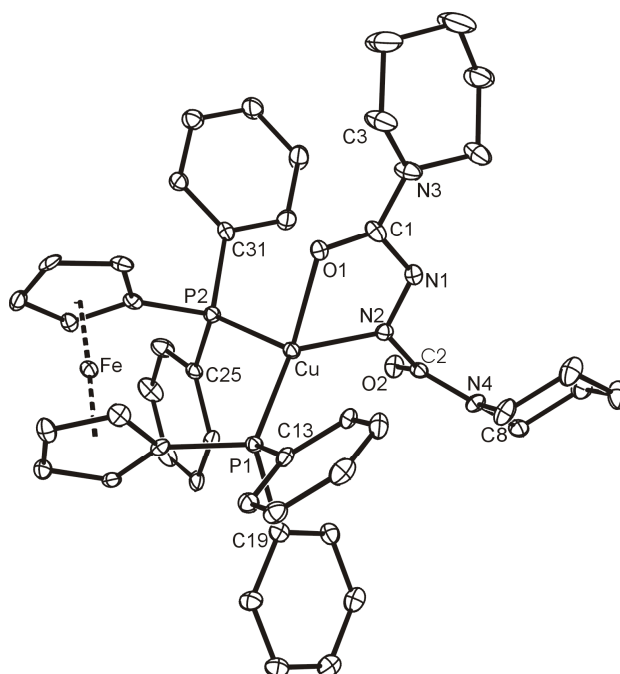


Fig 8.3: Molecular structure of $[\text{Cu}^{\text{I}}(\text{adc-pip})(\text{dppf})]^+$.

The compounds were further examined by IR spectroelectrochemistry. IR spectra shows two $\nu_{\text{C=O}}$ stretching bands for the metal-bonded and free carbonyl groups of the ligand adc-NR_2 . Upon 1st reversible reduction there is a shift in the metal-bonded carbonyl stretching bands, however, the free carbonyl stretching band remains unchanged. Even on 2nd reduction the free carbonyl stretching frequency does not change which indicates that the reduction of the chelate ring N=N-C=O-Cu keeps the non-bonded C=O undisturbed.

In chapter 4, another well known azo ligand, 2,2'-azobispyridine (abpy), was used as non-innocent ligand. This chapter demonstrates how abpy was used to make a heterodinuclear complex $[(\text{abpy})\text{Cu}(\text{dppf})](\text{BF}_4)$, a heterotetranuclear complex with neutral abpy bridge $\{(\mu\text{-abpy})[\text{Cu}(\text{dppf})_2](\text{BF}_4)_2$ and also a one-electron reduced radical form $\{(\mu\text{-abpy}^-)[\text{Cu}(\text{dppf})_2](\text{BF}_4)$. The dppf plays an important role in the isolation of such complexes. The compounds were characterized by X-ray crystal structure analysis and hence the azo bond lengths in non-reduced $[(\text{abpy})\text{Cu}(\text{dppf})](\text{BF}_4)$ ($d_{\text{N=N}} = 1.274(3) \text{ \AA}$) and one-electron reduced $\{(\mu\text{-abpy})[\text{Cu}(\text{dppf})_2](\text{BF}_4)$ ($d_{\text{N=N}} = 1.317(5) \text{ \AA}$) (Fig 8.4) could be compared.

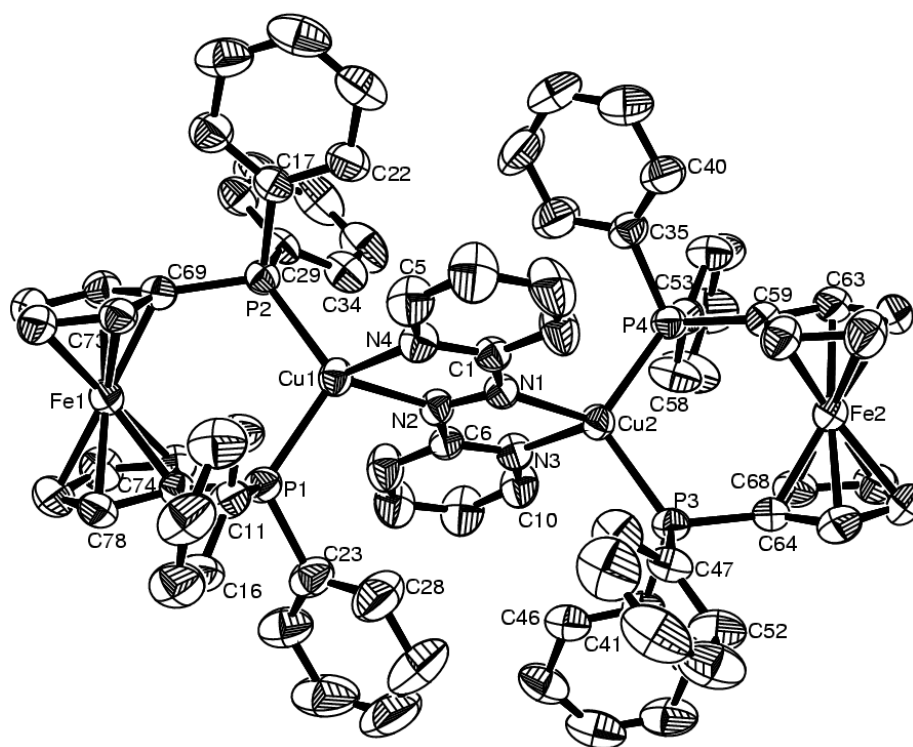


Fig 8.4: Molecular structure of $\{(\mu\text{-abpy}^-)[\text{Cu}^{\text{I}}(\text{dppf})]_2\}^+$.

The electronic property of the complexes was further studied by X-band (9.5 GHz) and high frequency (285 GHz) EPR. The paramagnetic complex $\{(\mu\text{-abpy})[\text{Cu}(\text{dppf})]_2\}^+$ shows a well resolved line-rich EPR spectrum at $g_{\text{iso}} = 2.0069$ in X-band which can be simulated by considering two azo ^{14}N , two pyridine ^{14}N , four ^{31}P and two $^{63/65}\text{Cu}$ nuclei (Fig 8.5). The in situ generated one-electron reduced species from $[(\text{abpy})\text{Cu}(\text{dppf})]^+$ gave an EPR spectrum identical to that of the heterotetranuclear complex $\{(\mu\text{-abpy})[\text{Cu}(\text{dppf})]_2\}^+$, suggesting the conversion on reduction (Fig 8.5). The high frequency EPR measurements of $\{(\mu\text{-abpy})[\text{Cu}(\text{dppf})]_2\}^+$ showed rhombic g splitting with little g anisotropy, implying mostly ligand centered spin (Fig 8.5).

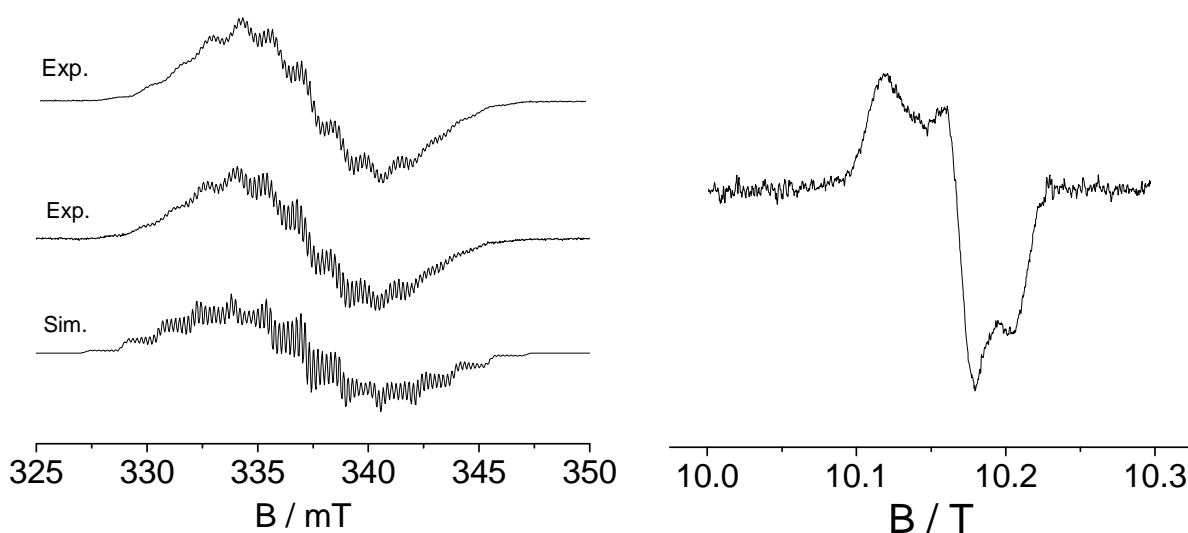


Fig 8.5: X-band EPR spectra of electrochemically generated $\{(\mu\text{-abpy})^{\text{--}}[\text{Cu}(\text{dppf})_2]^{\text{+}}\}$ (left-top) obtained by in situ reduction of $[(\text{abpy})\text{Cu}(\text{dppf})]^{\text{+}}$ (in CH_2Cl_2 / 0.1 M Bu_4NPF_6 at RT) and (left-center) for $\{(\mu\text{-abpy})[\text{Cu}(\text{dppf})_2]\}(\text{BF}_4)$ as dissolved in CH_2Cl_2 at RT; and simulated spectrum (bottom-left) and 285 GHz EPR spectrum of $\{(\mu\text{-abpy})[\text{Cu}(\text{dppf})_2]\}(\text{BF}_4)$ at 5 K in CH_2Cl_2 / toluene (4/1) in right.

In chapter 5, a Cu^{I} complex of 9,10-phenanthrenequinone = PhenQ is discussed. Though there are many reports on Cu^{I} -semiquinone, Cu^{II} -semiquinone and Cu^{II} -catecholate complexes, this is the first example of binding between Cu^{I} and *o*-quinone in chelate fashion. The *o/p*-quinones are redox non-innocent ligands and can be reduced in two steps to form catecholate. In this chapter, the heterodinuclear complex $[(\text{PhenQ})\text{Cu}^{\text{I}}(\text{dppf})](\text{BF}_4)$ has been characterized structurally and spectroscopically. The structural analysis (Fig 8.5) confirms the O,O'-chelation to Cu^{I} in $[(\text{PhenQ})\text{Cu}(\text{dppf})](\text{BF}_4)$ and substantiates the unreduced quinone character of PhenQ via the C=O bond lengths of 1.257(11) and 1.244(10) Å (semiquinones have ≥ 1.27 Å) and the (O)C-C(O) single bond length of 1.499(13) Å (semiquinones have ≤ 1.46 Å) (Fig 8.5). The geometry around Cu^{I} is distorted tetrahedral. The crystal structure also shows intra-molecular and intermolecular π - π stacking which is confirmed by DFT calculations.

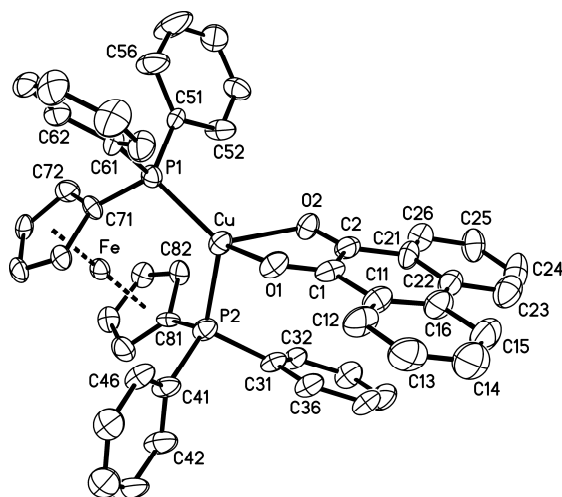


Fig 8.6: Molecular structure of $[(\text{PhenQ})\text{Cu}^{\text{I}}(\text{dppf})]^+$

In cyclic voltammetry, the complex shows reversible reduction $[(\text{PhenQ})\text{Cu}^{\text{I}}(\text{dppf})]^+ \rightarrow [(\text{PhenQ}^{\cdot-})\text{Cu}^{\text{I}}(\text{dppf})]$ and one-electron oxidation based on the ferrocene group. The electrochemically generated $[(\text{PhenQ}^{\cdot-})\text{Cu}^{\text{I}}(\text{dppf})]$ was studied by X-band EPR spectroscopy. Due to formation of the PhenSQ radical, it shows a typical signal with hyperfine couplings from $^{63,65}\text{Cu}$, ^{31}P and ^1H isotopes of 1.0 mT (1Cu), 1.4 mT (2P), and 0.15 mT (4H), respectively.

Chapter 6 deals with new compounds $\{(\mu_3\text{-dqp})[\text{Cu}(\text{dppf})]_3\}(\text{BF}_4)_3$, where dqp is hexamethyl, hexachloro- and un-substituted diquinoxalino[2,3-*a*:2',3'-*c*]phenazine, also known as hexaazatrinaphthylene (HATN). The complexes with BF_4^- and PF_6^- counter anions were characterized structurally, spectroscopically and electrochemically. The molecular structure of $\{(\mu_3\text{-dqp})[\text{Cu}(\text{dppf})]_3\}(\text{BF}_4)_3$ shows binding of three $[\text{Cu}^{\text{I}}(\text{dppf})]^+$ units to the central dqp bridge in C_1 conformation with distortions along Cu-N and Cu-P bonds (Fig 8.7). From the crystal structure the trapping of counter anions BF_4^- on both sides of the central dqp bridge can be seen (Fig 8.7).

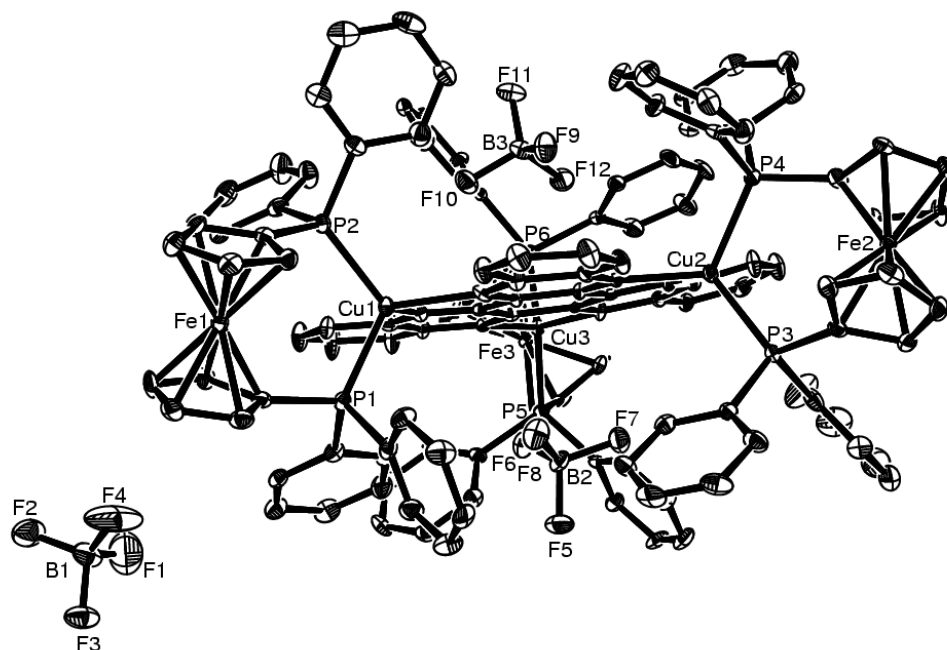


Fig 8.7: Molecular structure of $\{(\mu_3\text{-dqp})[\text{Cu}(\text{dppf})]_3\}(\text{BF}_4)_3$

The complexes show (Fig 8.8) two to three ligand-centered reversible reductions and one three-electron reversible oxidation (Fig 8.8). Like in all other cases, the oxidation wave is attributed to the iron oxidation of the dppf moieties. However, it was possible to monitor the step-wise oxidation of the ferrocene ancillaries by UV-vis-NIR spectroelectrochemistry. On successive reduction, bands in the near-IR region are generated due to intra-ligand transitions.

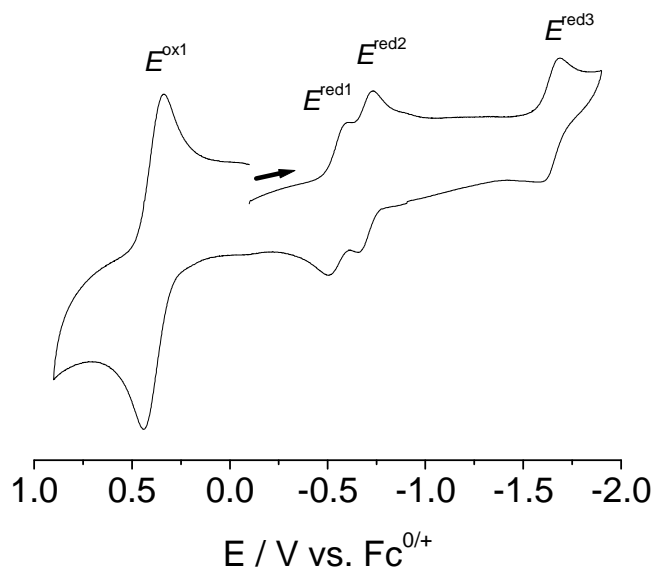


Fig 8.8: Cyclic voltammogram of $\{(\mu_3\text{-Cl}_6\text{-dqp})[\text{Cu}(\text{dppf})_3](\text{BF}_4)_3\}$ in CH_2Cl_2 / 0.1 M Bu_4NPF_6 at RT.

Due to the relatively high stability of the one-electron reduced species $\{(\mu_3\text{-dqp})^-[\text{Cu}(\text{dppf})_3]^{2+}\}$, high frequency EPR at 95 and 115 GHz could be carried out. The g components show axial splitting with small g anisotropy implying copper(I) coordinated anion radicals of N heterocyclic ligands.

Perspective.

The coordination chemistry of pteridine and iso(alloxazine) derivatives of oxido-reductase enzymes has been subject of interest for many years. These molecules are potential ligands for metal centers, which binds predominantly through O(4) and N(5) to form five-membered redox-active α -iminoketo chelate ring. Seeing the biological importance of flavin-metal interaction, it would be very interesting to study $[\text{Cu}(\text{dppf})]^+$ complexes of pteridine or iso(alloxazine) derivatives (Fig 8.9). This work is currently in progress.

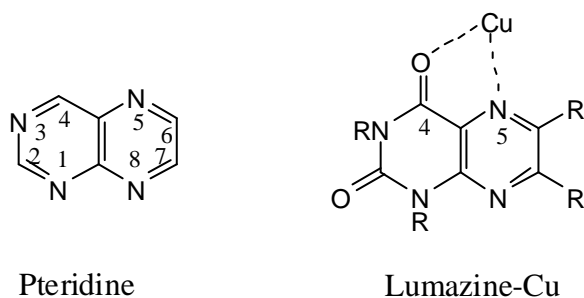


Fig 8.9: Pteridine ligand and interaction of Lumazine with Cu.

The use of esters and amides of azodicarboxylic acid to form metal complexes where these ligands are in the non-reduced (adc-R) and mono-reduced state (adc-R^-) has been illustrated in this doctoral work. The structural and spectroscopic properties of metal complexes with doubly reduced azodicarbonyl (adc-R^{2-}) will be of great interest to compare and contrast the properties of complexes with the same ligand in different oxidation state. The dinuclear ruthenium(III) complexes with the esters of azodicarboxylic acid (adc-OR) bridge have been synthesized and the structural and spectroscopic properties have been investigated. The X-ray crystal structure analysis shows binding of two $[\text{Ru}^{\text{III}}(\text{acac})_2]^+$ moieties with the edge sharing

unsaturated five-membered chelate rings by fully reduced azodicarbonyl, in hydrazido form (adc-OR^{2-}), with long N-N distance of 1.440(5) Å and short C-O of 1.263(4) Å and the rather short metal-metal distances of 4.764 Å (Fig 8.10).

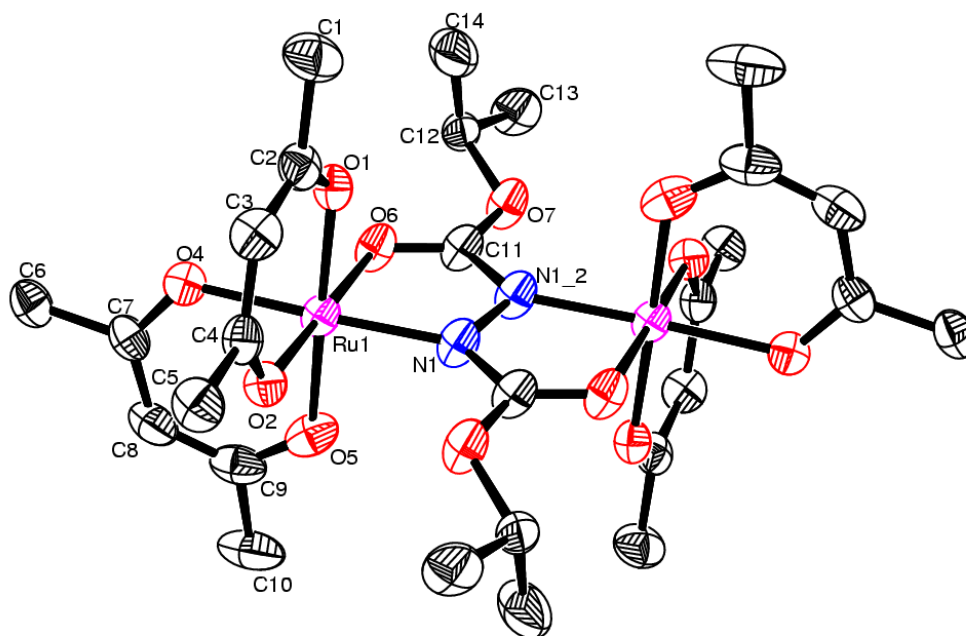


Fig 8.10: Molecular structure of $[(\mu\text{-adc-OR}^{2-})\{\text{Ru}(\text{acac})_2\}_2]$.

The appearance of the IVCT band on one-electron reduction in the NIR region around 2000 nm and the comproportionation constant $K_c > 10^8$, determined for that state points to a strong electronic communication between the ruthenium centers in the mixed-valent state. The magnetic measurements of the complexes are essential to get more insights into the magnetic coupling between the $\text{Ru}^{\text{III}}\text{-Ru}^{\text{III}}$ states which is also in progress. Such substances can be possible use in the future as storage materials.

Chapter 9

Zusammenfassung

Mehrkernige Metallkomplexe mit multiplen Redoxprozessen gewinnen wegen ihrer umfangreichen Anwendungsmöglichkeiten von molekularen Schaltern bis hin zu enzymatischen Systemen an Bedeutung. In dieser Dissertation wurde der 1,1'-Bis(diphenylphosphino)ferrocenylkupfer(I)-Baustein $[\text{Cu}(\text{dppf})]^+$ genutzt, um Komplexe mit verschiedenen "non-innocent" Liganden wie 2,2'-Azobispyridin (abpy), Amiden und Estern der Azodicarbonsäure, *o*-Chinonen und Hexaazatrinaphtanlin-derivate zu synthetisieren.

In Kapitel 2 werden die vierkernigen Metallkomplexe des $[\text{Cu}(\text{dppf})]^+$ mit den starken π -Akzeptorliganden Di-tert-butyl- und Di-iso-propylazodicarbonsäureester (adc-OR) beschrieben: $[(\mu\text{-adcO}^t\text{Bu})\{\text{Cu}^{\text{I}}(\text{dppf})\}_2](\text{PF}_6)$ und $[(\mu\text{-adcO}^i\text{Pr})\{\text{Cu}^{\text{I}}(\text{dppf})\}_2](\text{PF}_6)$. Die Verbindungen wurden in ihrer stabilen radikalverbrückten Form isoliert. Der Komplex $[(\mu\text{-adcO}^t\text{Bu})\{\text{Cu}^{\text{I}}(\text{dppf})\}_2](\text{PF}_6)$ wurde kristallographisch charakterisiert (Abb. 8.1). Die Abbildung zeigt zwei $[\text{Cu}(\text{dppf})]^+$ -Bausteine die über den zentralen Brückenliganden Di-tert-butylazodicarbonsäureester verknüpft sind. Die Gegenwart eines Gegenanions bestätigt die radikale Natur der Verbindung.

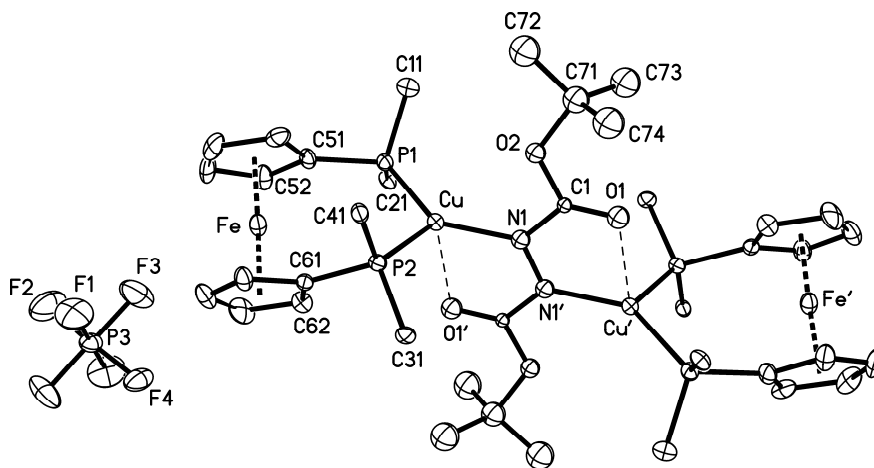


Abb. 8.1: Molekülstruktur des $[(\mu\text{-adcO}^t\text{Bu})\{\text{Cu}^{\text{I}}(\text{dppf})\}_2](\text{PF}_6)$ (P-Phenylgruppen wurden aufgrund der übersichtlicheren Darstellung weggelassen).

Bei 298 K weisen beide Verbindungen teilweise aufgelöste linienreiche ESR-Spektren mit $g_{\text{iso}}=2.011$ beziehungsweise 2.012 auf. Die Verbindungen konnten mit zwei $^{63/65}\text{Cu}$ ($I=3/2$)-, vier ^{31}P ($I=1/2$)- und zwei Azo ^{14}N ($I=1/2$)-Kernen simuliert werden (Abb. 8.2). Bei Hochfeld-ESR-Messungen (285 GHz) in glasartig erstarrter Lösung zeigen die Komplexe ein rhombisches Signal mit einer schmalen g Anisotropie, was auf einen vorwiegend Ligandzentrierten Spin hinweist.

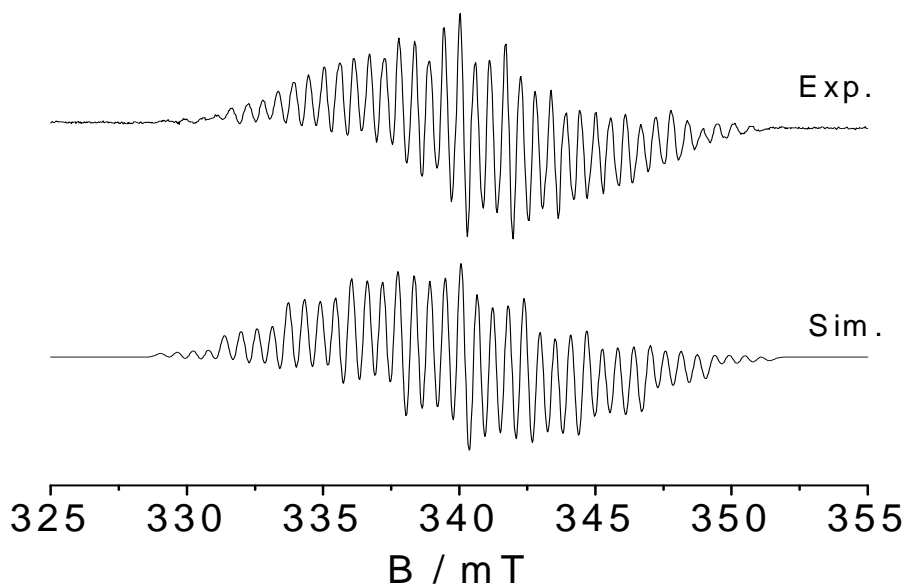


Abb. 8.2: X-Band-ESR-Spektrum von $\{(\mu\text{-adcO}^{\text{t}}\text{Bu})[\text{Cu}(\text{dppf})_2]^+\}$ bei 298 K in CH_2Cl_2 (oben) mit Simulation (unten).

Der blaue Radikalkomplex zeigt langwellige Absorptionen bei ca. 800 nm für die MLCT-Übergänge $d(\text{Cu}^{\text{I}}) \rightarrow \pi^*(\text{adcOR}^{\cdot-})$ verantwortlich sind. Nach der reversiblen Einelektronenoxidation verschiebt sich der MLCT zu höheren Wellenlängen (1100 nm) infolge der Bildung teilweise leerer π^* -Molekülorbitale des adcOR. Nach der reversiblen Einelektronenreduktion $\{(\mu\text{-adcOR})[\text{Cu}(\text{dppf})_2]^{(+)\rightarrow(0)}\}$ verschwindet der MLCT vollständig durch Auffüllen des π^* -Orbitals des $\text{adcOR}^{\cdot-}$. Die Verbindungen können durch eine reversible Zweielektronenoxidation weiter oxidiert werden, dieser Prozess steht im Einklang mit der Oxidation des Ferrocenzentrums. Der große Abstand zwischen den beiden dppf-Einheiten verhindert jegliche elektronische Kommunikation, was sich in der Zweielektronenwelle des Cyclovoltammogramms zeigt.

In Kapitel 3 werden Heterozweikernkomplexe des $[\text{Cu}(\text{dppf})]^+$ mit den Amidinen der Azodicarbonsäuren behandelt. Die Azodicarboxyimide weisen ähnliches Koordinations- und identisches Redoxverhalten wie andere Azocarbonylliganden auf. In diesem Kapitel werden

erstmals die Heterozweikernkomplexe $[\text{Cu}^{\text{I}}(\text{adc-pip})(\text{dppf})](\text{BF}_4)$ und $[\text{Cu}^{\text{I}}(\text{adc-NMe}_2)(\text{dppf})](\text{BF}_4)$ mit einer unreduzierten $\text{N}=\text{N}-\text{C}=\text{O}$ Gruppe vorgestellt, dies wurde durch die Einkristallanalyse (Abb. 8.3) der jeweiligen Verbindungen festgestellt. Die durch Röntgenbeugung erhaltenen Bindungslängen ($d_{\text{N}=\text{N}} = 1.258(7) \text{ \AA}$, $d_{\text{C}-\text{N}} = 1.466(8) \text{ \AA}$, and $d_{\text{C}=\text{O}} = 1.234(7) \text{ \AA}$) legen nahe, dass das $[\text{Cu}(\text{dppf})]^+$ durch die nicht reduzierte $\text{N}=\text{N}-\text{C}=\text{O}$ Gruppe gebunden wird. Offensichtlich ist die π -Rückbindung des d^{10} (Cu) zum π^* (adc-NR_2) für den vollständigen Elektronentransfer nicht stark genug.

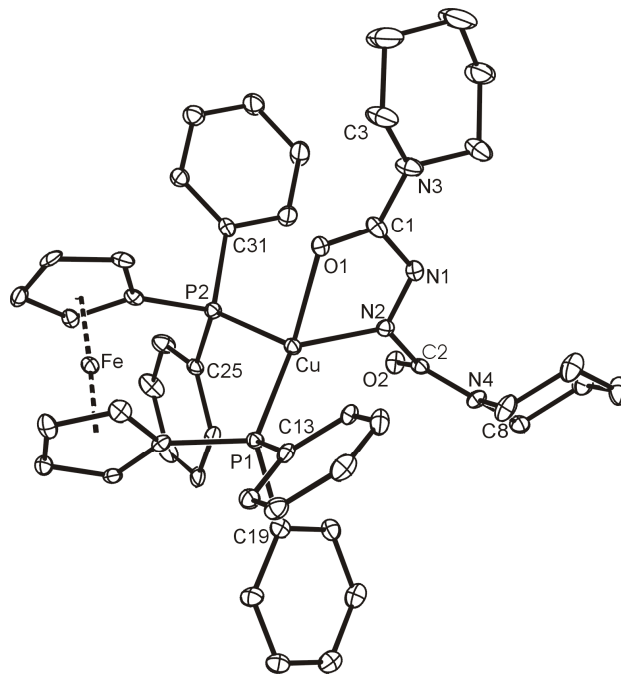


Abb. 8.3: Molekülstruktur des $[\text{Cu}^{\text{I}}(\text{adc-pip})(\text{dppf})]^+$.

Die Verbindungen wurden durch IR-Spektroelektrochemie weiter untersucht. Das IR-Spektrum zeigt zwei $\nu_{\text{C}=\text{O}}$ -Schwingungsbanden für die metallgebundene und die freie Carbonylbande des adc-NR_2 -Liganden. Durch die erste reversible Reduktion verschiebt sich die Bande des metallgebundenen Carbonyls, die der freien hingegen bleibt unverändert. Selbst die zweite Reduktion verändert die Schwingungsbande der freien Carbonylgruppe nicht, was nahelegt, dass die Reduktion des Chelatrings $\text{N}=\text{N}-\text{C}=\text{O}-\text{Cu}$ die freie $\text{C}=\text{O}$ nicht beeinflusst.

Kapitel 4 beschreibt einen weiteren gut bekannten, redoxaktiven Azoliganden, das 2,2'-Azobispyridin (abpy). Abpy wird zur Herstellung eines Heterozweikernkomplexes $[(\text{abpy})\text{Cu}(\text{dppf})](\text{BF}_4)$, eines Heterovierkernkomplex mit neutraler abpy-Brücke $\{(\mu\text{-abpy})[\text{Cu}(\text{dppf})_2]\}(\text{BF}_4)_2$ und der Einelektronenreduzierten radikalische Form $\{(\mu\text{-abpy}^{\cdot-})$

$)[\text{Cu}(\text{dppf})_2](\text{BF}_4)$ verwendet. Das dppf spielt eine wichtige Rolle bei der Isolierung der beschriebenen Komplexe. Die Verbindungen wurden durch Einkristallanalyse charakterisiert, und infolgedessen konnten die N=N-Azobindungsängen der nicht reduzierten Form $[(\text{abpy})\text{Cu}(\text{dppf})](\text{BF}_4)$ ($d_{\text{N}=\text{N}} = 1.274(3) \text{ \AA}$) und die Einelektronenreduzierten Form $\{(\mu\text{-abpy})[\text{Cu}(\text{dppf})_2](\text{BF}_4)\}$ ($d_{\text{N}=\text{N}} = 1.317(5) \text{ \AA}$) (Abb. 8.4) verglichen werden.

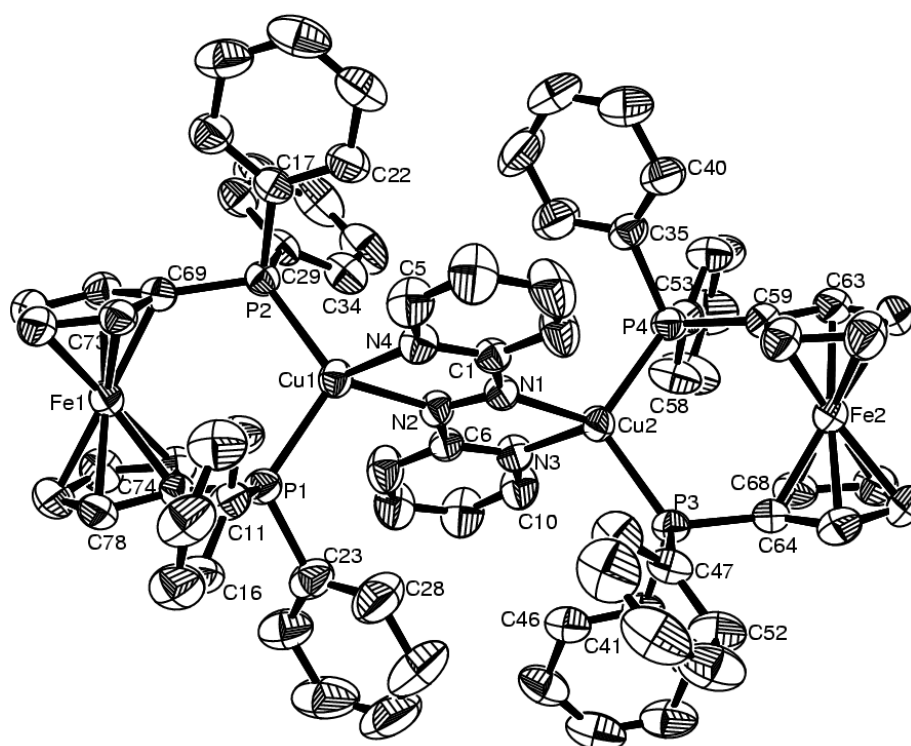


Abb. 8.4: Molekülstruktur des $\{(\mu\text{-abpy})[\text{Cu}^{\text{I}}(\text{dppf})_2]\}^+$.

Die elektronischen Eigenschaften der Komplexe wurden weiter mithilfe der X-Band- und der Hochfeld-ESR-Spektroskopie untersucht. Der paramagnetische Komplex $\{(\mu\text{-abpy})[\text{Cu}(\text{dppf})_2]\}^+$ zeigt ein gut aufgelöstes, linienreiches ESR-Spektrum mit $g_{\text{iso}} = 2.0069$ im X-Band, was unter Verwendung von zwei Azo ^{14}N -, zwei Pyridin ^{14}N -, vier ^{31}P - und zwei $^{63/65}\text{Cu}$ -Kernen simuliert werden konnte (Abb. 8.5). Die in situ generierte Einelektronenreduzierte Spezies des $[(\text{abpy})\text{Cu}(\text{dppf})]^+$ ergab ein zu $\{(\mu\text{-abpy})[\text{Cu}(\text{dppf})_2]\}^+$ identisches ESR-Spektrum, dieses Ergebnis lässt vermuten, dass die Reduktion am Brückenliganden stattfindet. Die Hochfeld-ESR-Messung des $\{(\mu\text{-abpy})[\text{Cu}(\text{dppf})_2]\}^+$ weist

ein rhombisches Signal mit einer kleinen g Anisotropie auf, was auf ein hauptsächlich ligandenzentrierten Spin hindeutet (Abb. 8.5).

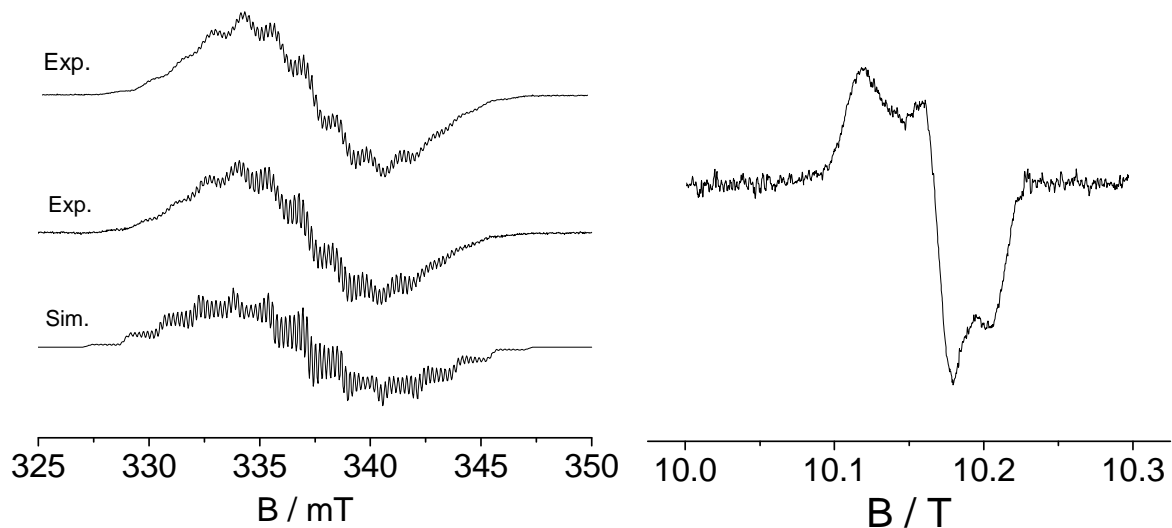


Abb. 8.5: X-Band-ESR-Spektrum des elektrochemisch generierten $\{(\mu\text{-abpy})^-[Cu(dppf)_2]^+\}$ (links oben), erhalten durch in situ-Reduktion des $[(abpy)Cu(dppf)]^+$ (in CH_2Cl_2 / 0.1 M Bu_4NPF_6 bei RT) und für $\{(\mu\text{-abpy})[Cu(dppf)_2](BF_4)\}$ gelöst in CH_2Cl_2 bei RT (links mitte); Simulation (links unten) und 285 GHz ESR-Spektrum des $\{(\mu\text{-abpy})[Cu(dppf)_2](BF_4)\}$ bei 5 K in CH_2Cl_2 / Toluol (4/1) (rechts).

In Kapitel 5 wird ein Cu^I Komplex des 9,10-Phenanthrenchinon = PhenQ beschrieben. Obwohl es viele Veröffentlichungen über Cu^I -Semichinon, Cu^{II} -Semichinon und Cu^{II} -Catechol-Komplexe gibt, ist dies das erste Beispiel einer Chelatverbindung zwischen Cu^I und einem *o*-Chinon. Die *o/p*-Chinone sind redoxaktive Liganden, die durch zwei Einelektronenschritte zum Catechol reduziert werden können. In diesem Kapitel wurde der Heterozweikernkomplex $[(PhenQ)Cu^I(dppf)](BF_4)$ strukturell und spektroskopisch charakterisiert. Die Kristallstrukturanalyse (Abb. 8.6) bestätigt die O,O'-Koordination zu Cu^I in $[(PhenQ)Cu(dppf)](BF_4)$ und belegt den unreduzierten Chinoncharakter des PhenQ durch die C=O-Bindungslängen mit 1.257(11) und 1.244(10) Å (im Vergleich: Semichinone ≥ 1.27 Å) und die (O)C-C(O)-Einfachbindungslänge von 1.499(13) Å (Semichinone ≤ 1.46 Å). Die Cu^I -Koordinationssphäre ist tetraedrisch verzerrt. Die Kristallstruktur zeigt sowohl

intramolekulare als auch intermolekulare π - π -Stapelung welche durch DFT-Rechnung bestätigt wird.

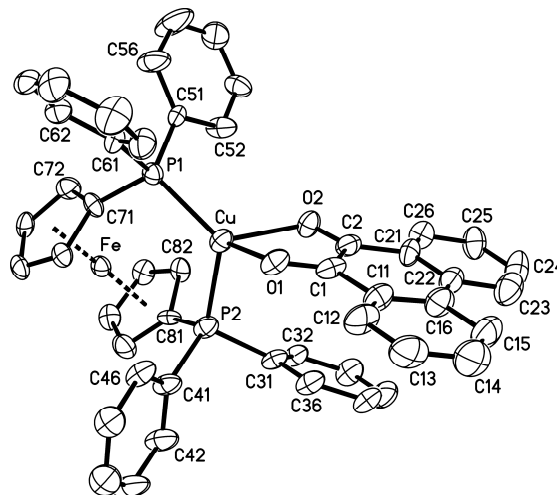


Abb. 8.6: Molekülstruktur des $[(\text{PhenQ})\text{Cu}^{\text{I}}(\text{dppf})]^+$.

Im Cyclovoltammogramm zeigt der Komplex eine reversible Reduktion $[(\text{PhenQ})\text{Cu}^{\text{I}}(\text{dppf})]^+ \rightarrow [(\text{PhenQ}^{\cdot-})\text{Cu}^{\text{I}}(\text{dppf})]$ und eine Einelektronenoxidation der Ferrocengruppe. Das elektrochemisch generierte $[(\text{PhenQ}^{\cdot-})\text{Cu}^{\text{I}}(\text{dppf})]$ wurde mit Hilfe der X-Band-ESR-Spektroskopie untersucht. Infolge der Bildung des PhenSQ-Radikals weist das ESR-Spektrum ein typisches Signal mit Hyperfeinkopplungen von Cu-, P- und H-Isotopen von 1.0 mT (1Cu), 1.4 mT (2P) und 0.15 mT (4H) auf.

In Kapitel 6 werden neue Verbindungen der Art $\{(\mu_3\text{-dqp})[\text{Cu}(\text{dppf})]_3\}(\text{BF}_4)_3$ beschrieben, wobei dqp hexamethyl-, hexachloro- oder unsubstituiertes Diquinoxalino[2,3-a:2'-3'-c]phenazine, auch als Hexaazatrinaphtalen (HATN) bezeichnet, darstellt. Die Komplexe mit BF_4^- und PF_6^- als Gegenionen wurden strukturell, spektroskopisch und elektrochemisch untersucht. Die Molekülstruktur des $\{(\mu_3\text{-dqp})[\text{Cu}(\text{dppf})]_3\}(\text{BF}_4)_3$ weist eine Koordination der drei $[\text{Cu}(\text{dppf})]^+$ -Einheiten an das zentral verbrückende dqp in C_1 -Konformation mit Fehlordnung entlang der Cu-N- und Cu-P-Bindungen (Fig 8.7). In der Kristallstruktur kann das Einfangen der Gegenionen BF_4^- an beiden Seiten des zentralen dqp beobachtet werden.

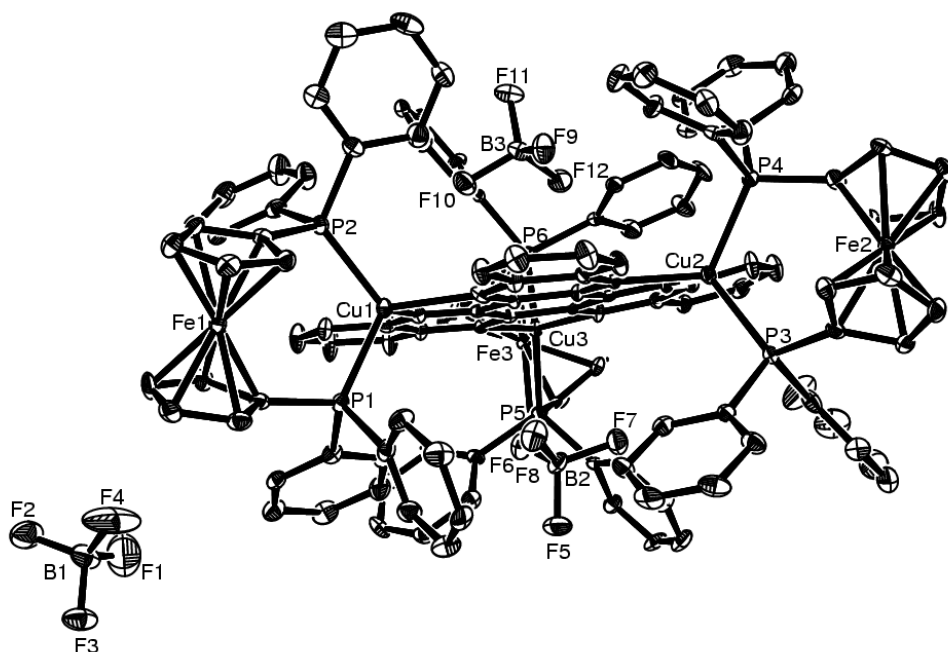


Abb. 8.7: Molekülstruktur des $\{(\mu_3\text{-dqp})[\text{Cu}(\text{dppf})]_3\}(\text{BF}_4)_3$.

Die Verbindung zeigt zwei bis drei reversible ligandenzentrierte Reduktionen und eine reversible Dreielektronenoxidation (Abb. 8.8). Wie auch in allen anderen Fällen ist die Oxidation ein Merkmal der Eisenoxidation im dppf. Dennoch konnte die stufenweise Oxidation der Ferrocenbausteine zusätzlich über UV-vis-NIR- Spektroelektrochemie gezeigt werden. Bei Stufenweiser Reduktion konnten im NIR intra-ligand-Übergänge beobachtet werden.

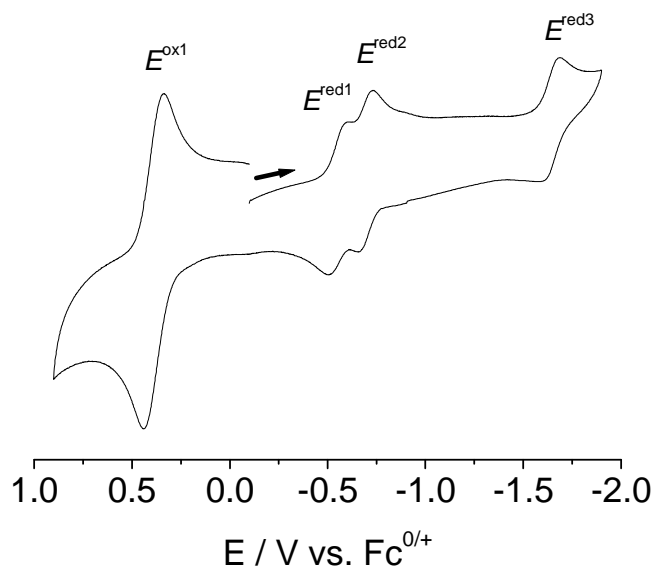


Abb 8.8: Cyclovoltammogramm des $\{(\mu_3\text{-Cl}_6\text{-dqp})[\text{Cu}(\text{dppf})]_3\}(\text{BF}_4)_3$ in CH_2Cl_2 / 0.1 M Bu_4NPF_6 bei RT

Wegen der relativ hohen Stabilität der einelektronenreduzierten Spezies $\{(\mu_3\text{-dqp})^-[\text{Cu}(\text{dppf})]_3\}^{2+}$, konnte Hochfeld-ESR-Spektroskopie bei 95 und 115 GHz durchgeführt werden. Die g-Faktoren zeigen eine axiale Aufspaltung mit kleiner g- Anisotropie, was den Schluss zulässt, dass es sich dabei um Cu^{I} handelt das an ein anionisch radikalischen N-Heterocyclenliganden gebunden ist.

Ausblick.

Die Koordinationschemie der Pteridin- und Iso(alloxazin)-Derivate von Oxidoreduktaseenzymen ist seit vielen Jahren Gegenstand von Untersuchungen. Diese Moleküle gelten als potentielle Liganden für Metalle, welche vorzugsweise an O(4) und N(5) binden, um fünfgliedrige redoxaktive α -Iminoketon-Chelatringe zu ergeben. Bei Betrachtung der biochemischen Bedeutung der Flavin-Metall-Wechselwirkungen wäre es sehr interessant die $[\text{Cu}(\text{dppf})]^+$ -Komplexe der Pteridin- und Iso(alloxazin)- Derivate (Abb. 8.9) zu untersuchen. Diese Arbeit ist momentan in der Entwicklung.

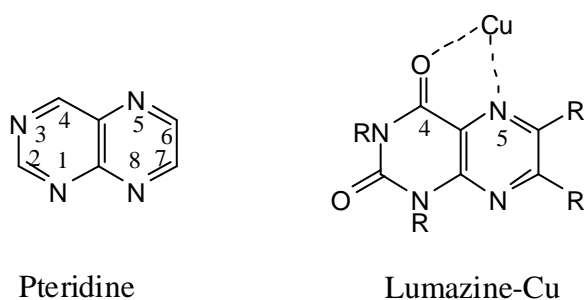


Abb. 8.9: Pteridin Liganden und die Wechselwirkung zwischen Lumazin mit Kupfer.

Die Verwendung von Estern und Amidien der Azodicarbonsäuren in Metallkomplexen mit der nicht reduzierten (adc-R) und der einfach reduzierten Form (adc-R^{\cdot}) wurden innerhalb dieser Arbeit vorgestellt. Die strukturellen sowie spektroskopischen Eigenschaften von Metallkomplexen mit zweifach reduzierten Azodicarbonsäure-derivaten ($\text{adc-R}^{2\cdot}$) sind von großem Interesse, da ein Vergleich mit Komplexen mit denselben Liganden in anderen Oxidationsstufen sehr aufschlussreich wäre. Die Zweikernruthenium(III)komplexe mit Estern

der Azodicarbonsäure (adc-OR)-Brücke wurden dargestellt und die strukturellen und spektroskopischen Eigenschaften untersucht. Die Kristallstrukturanalyse zeigt, dass zwei $[\text{Ru}^{\text{III}}(\text{acac})_2]^+$ -Bausteine an dem ungesättigten fünfgliedrigen Chelatringen mit vollständig reduzierten Azodicarbonyl, in Hydrazidoform (adc-OR^{2-}), mit langem N-N-Abstand von $1.440(5) \text{ \AA}$ und kurzen C-O Abständen von $1.263(4) \text{ \AA}$ und eher kurzen Metall-Metall Abständen von 4.764 \AA (Abb. 8.10), beteiligt sind.

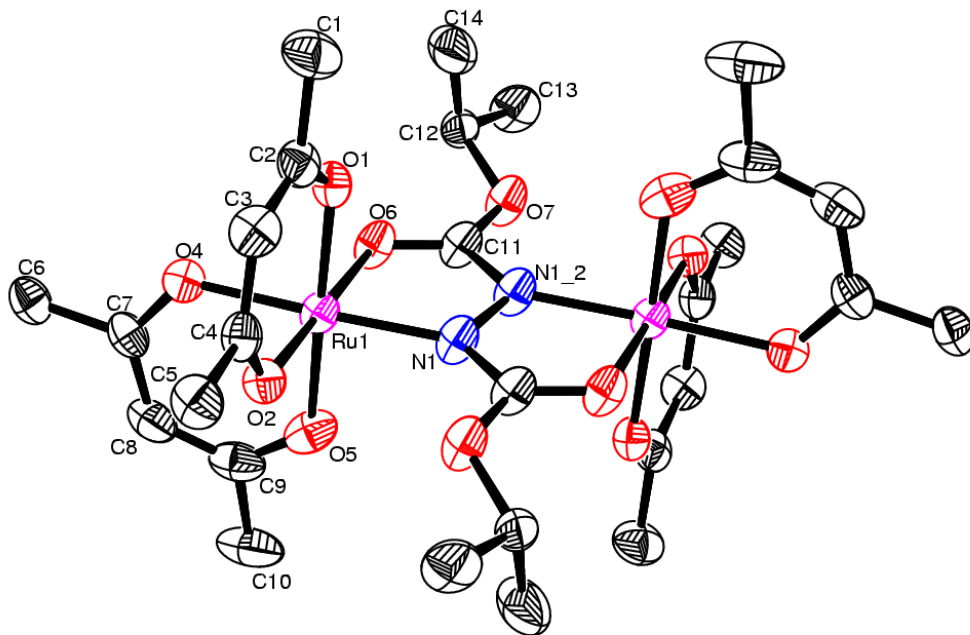


Abb. 8.10: Molekülstruktur von $[(\mu\text{-adc-OR}^{2-})\{\text{Ru}(\text{acac})_2\}_2]$.

Das Auftreten der IVCT-Bande während der Einelektronenreduktion in der NIR-Region bei ca. 2000 nm und die Komproportionierungskonstante $K_c > 10^8$, ermittelt für diesen Fall, weisen auf eine starke elektronische Kommunikation zwischen den Rutheniumzentren im gemischtvalenten Zustand hin. Die magnetischen Messungen der Komplexe, die derzeit durchgeführt werden, sind notwendig, um einen besseren Einblick in die magnetischen Wechselwirkungen zwischen den $\text{Ru}^{\text{III}}\text{-Ru}^{\text{III}}$ -Zuständen zu bekommen. Solche Materialien sind in der Zukunft als Speichermedien denkbar.

Bibliography

- [1] Kaim, W.; Schwederski, B. *Bioinorganic Chemistry*, Wiley, Chichester, **1994**
- [2] Gerdemann, C.; Eicken, C.; Krebs, B. *Acc. Chem. Res.* **2002**, *35*, 183
- [3] (a) Tolman, W. B. *Acc. Chem. Res.* **1997**, *30*, 227; (b) Cramer, C. J.; Tolman, W. B. *Acc. Chem. Res.* **2007**, *40*, 601
- [4] (a) Tyeklar, Z.; Karlin, K. D. *Acc. Chem. Res.* **1989**, *22*, 241;
- [5] Karlin, K. D.; Kaderli, S.; Zuberbühler, A. D. *Acc. Chem. Res.* **1997**, *30*, 139;
- [6] Kim, E.; Helton, M. E.; Wasser, I. M.; Karlin, K. D.; Huang, H-w; Moenne-Loccoz, P.; Incarvito, C. D.; Rheingold, A.; Honecker, M.; Kaderli, S.; Zuberbühler, A. D. *Proc. Nat. Acad. Sci.* **2003**, *100*, 3623;
- [7] Solomon, E. I.; Sarangi, R.; Woertink, J. S.; Augustine, A. J.; Yoon, J.; Ghosh, S. *Acc. Chem. Res.* **2007**, *40*, 581.
- [8] Mirica, L. M.; Ottenwaelder, X.; Stack, T. D. P. *Chem. Rev.* **2004**, *104*, 1013
- [9] (a) Collman, J. P.; Sunderland, C. J.; Berg, K. E.; Vance, M. A.; Solomon, E. I. *J. Am. Chem. Soc.* **2003**, *125*, 6648; (b) Collman, J. P.; Decreau, R. A.; Yan, Y.; Yoon, J.; Solomon, E. I. *J. Am. Chem. Soc.* **2007**, *129*, 5794.
- [10] Malmström, B. G. *Annu. Rev. Biochem.* **1982**, *51*, 21
- [11] Kaim, W. *Dalton Trans.* **2003**, 761-768
- [12](a) Itoh, S.; Fukuzumi, S. *Acc. Chem. Res.* **2007**, *40*, 592;
- [13](a) Jazdzewski, B. A.; Tolman, W. B. *Coord. Chem. Rev.* **2000**, *200-202*, 633; (b) Holland, P. L.; Tolman, W. B. *Coord. Chem. Rev.* **1999**, *190-192*, 855;
- [14] Hatcher, L. Q.; Vance, M. A.; Sarjeant, A. A. N.; Solomon, E. I.; Karlin, K. D. *Inorg. Chem.* **2006**, *45*, 3004;
- [15] Fry, H. C.; Cohen, A. D.; Toscano, J. P.; Meyer, G. J.; Karlin, K. D. *J. Am. Chem. Soc.* **2005**, *127*, 6225.
- [16] Frausto da Silva, J. J. R.; Williams, R. J. P. *The Biological Chemistry of the Elements*, 2nd edn. Oxford University Press, Oxford, **2001**.
- [17] Kaim, W. *Coord. Chem. Rev.* **2001**, *219-221*, 463
- [18] Duine, J. A. *Eur. J. Biochem.*, **1991**, *200*, 271
- [19] Klinman, J. P.; Mu, D. *Annu. Rev. Biochem.*, **1994**, *63*, 299;
- [20] Dooley, D. M. *J. Biol. Inorg. Chem.*, **1999**, *4*, 1
- [21] Wang, S. X.; Nakamura, N.; Murell, M.; Klinman, J. P.; Sanders-Loehr, J. J. *Boil. Chem.* **1997**, *272*, 28841

- [22] Solomon, E. I.; Sundaram, U. M.; Machonkin, T. E. *Chem. Rev.* **1996**, *96*, 2563
- [23] Kitajima, N.; Moro-oka, Y. *Chem. Rev.* **1994**, *94*, 737.
- [24] Rall, J.; Wanner, M.; Albrecht, M.; Hornung, F. M.; Kaim, W. *Chem. Eur. J.* **1999**, *5*, 2802;
- [25] Rall, J.; Kaim, W. *J. Chem. Soc., Faraday Trans.* **1994**, *90*, 2905.
- [26] Kahn, O Prins, R.; Reedijk, J.; Thompson, J. S. *Inorg. Chem.* **1987**, *26*, 3557.
- [27] Berreau, L. M.; Mahapatra, S.; Halfen, J. A.; Houser, R. P.; Young, Jr., V. G.; Tolman, W. B. *Angew. Chem.* **1999**, *111*, 180; *Angew. Chem. Int. Ed.* **1999**, *38*, 207.
- [28] Tapodi, B.; Speier, G.; Giorgi, M.; Reglier, M.; Funabaki, T.; Korecz, L.; Rockenbauer, A. *Inorg. Chem. Commun.* **2006**, *9*, 367
- [29](a) Pierpont, C. G. *Coord. Chem. Rev.* **2001**, *216-217*, 95 ; (b) Pierpont, C. G.; Lange, C. W. *Prog. Inorg. Chem.* **1994**, *41*, 331
- [30](a) Sarma, M. S. P.; Czarnik, A. W. *Synthesis*, **1988**, 72; (b) Rademacher, J. T.; Kanakarajan, K.; Czarnik, A. W. *Synthesis*, **1994**, 378.
- [31] Barlow, S.; Zhang, Q.; Kaafarani, B. R.; Risko, C.; Amy, F.; Chan, C. K.; Domercq, B.; Starikova, Z. A.; Antipin, M. Y.; Timofeeva, T. V.; Kippelen, B.; Bredas, J.; Kahn, A.; Marder, S. R. *Chem. Eur. J.* **2007**, *13*, 3537
- [32] Piglosiewicz, I. M.; Beckhaus, R.; Wittstock, G.; Saak, W.; Haase, D. *Inorg. Chem.* **2007**, *46*, 7610;
- [33](a) Kitagawa, S.; Masaoka, S. *Coord. Chem. Rev.* 2003, **246**, 73; (b) Furukawa, S.; Okubo, T.; Masaoka, S.; Tanaka, D.; Chang, H. -C.; Kitagawa, S. *Angew. Chem. Int. Ed.* **2005**, *44*, 2700;
- [34] Keene, F. R. *Coord. Chem. Rev.* **1997**, *166*, 121;
- [35] Ishi-i, T.; Murakami, K. I.; Imai, Y.; Mataka, S. *J. Org. Chem.* **2006**, *71*, 5752;
- [36] Angeles-Boza, A. M.; Bradley, P. M.; Fu, P.K.L; Shatruk, M.; Hilfiger, M. G.; Dunber, K. R.; Turro, C. *Inorg. Chem.* **2005**, *44*, 7262
- [37](a) Baxter, P.; Lehn, J. -M.; DéCian, A.; Fischer, J. *Angew. Chem. Int. Ed.* **1993**, *32*, 69;
- [38] Bu, X. H.; Biradha, K.; Yamaguchi, T.; Nishimura, M.; Ito, T.; Tanaka, K.; Shinoya, M. *Chem. Commun.* **2000**, 1953;
- [39] Herman, L.; Ghosh, S.; Defrancq, E.; Mesmaeker, A. K. D. *J. Phys. Org. Chem.* **2008**, *21*, 670
- [40](a) Monelli, M. T.; Heinecke, J.; Mayfield, S.; Okeyere, B.; Winkel, B. S. J.; Brewer, K. *J. J. Inorg. Biochem.* **2006**, *100*, 1983;
- [41] Elias, B.; Mesmaeker, A. K-De. *Coord. Chem. Rev.* **2006**, *250*, 1627.

- [42](a) Marquis-Rigault, A. ; Dupont-Gervais, A. ; Baxter, P. N. W. ; Dorselaer, A. V. ; Lehn, J.-M. *Inorg. Chem.* **1996**, *35*, 2307;
- [43] Baxter, P. N. W.; Lehn, J. -M; Knersel, B. O.; Baum, G.; Feske, D. *Chem. Eur. J.* **1999**, *5*, 113;
- [44] Masoka, S.; Furukawa, S.; Chang, H, -C; Mizutani, T.; Kitagawa, S. *Angew. Chem. Int. Ed.* **2001**, *40*, 3817
- [45] Vogler, A.; Kunkely, H. *Coord. Chem. Rev.* **2002**, *230*, 243;
- [46] Che, C-M.; Mao, Z.; Miskowski, V. M.; Tse, M-C.; Chan, C.-K.; Cheung, K.-K.; Phillips, D. L.; Leung, K.-H. *Angew. Chem. Int. Ed.* **2000**, *39*, 4084
- [47](a) Albinati, A.; Fabrizi de Biani, F.; Leoni, P.; Marchetti, L.; Pasquali, M.; Rizzato, S.; Zanello, P. *Angew. Chem. Int. Ed.* **2005**, *44*, 5701; (b) Siemeling, U.; Vor der Brüngen, J.; Vorfeld, U.; Neumann, B.; Stammler, A.; Stammler, H.-G.; Brockhinke, A.; Plessow, R.; Zanello, P.; Laschi, F.; Fabrizi de Biani, F.; Fontani, M.; Steenken, S.; Stapper, M.; Gurzadyan, *Chem. Eur. J.* **2003**, *9*, 2819; (c) Femoni, C.; Iapalucci, M.C.; Longoni, G. Svensson, P.H.; Zanello, P.; Fabrizi de Biani, F. *Chem. Eur. J.* **2004**, *10*, 2318; (d) Hartwig, J.F. *Acc. Chem. Res.* **1998**, *31*, 852; (e) Pawlas, J.; Nakao, Y.; Kawatsura, M.; Hartwig, J.F.; *J. Am. Chem. Soc.* **2002**, *124*, 3669.
- [48](a) Barluenga, J.; Gonzalez, F. J.; Fustero, S.; Gotor, V. *J. Chem. Soc. Chem. Commun.* **1986**, *15*, 1179; (b) Coxon, J. M.; O'Connell, M. J.; Steel, P. J. *J. Org. Chem.* **1987**, *52*, 4726.
- [49] Kolb, H. C.; Finn, M. G.; Sharpless, K. B. *Angew Chem. Int. Ed.* **2001**, *40*, 2004.
- [50](a) Mitsunobu, O.; Yamada, Y. *Bull. Chem. Soc. Japan*; **1967**, *40*, 2380; (b) Grochowski, E.; Hilton, B. D.; Kupper, R. J.; Michejda, C. J. *J. Am. Chem. Soc.* **1982**, *104*, 6876.
- [51](a) Creber, K.A.M.; Ho, T.; Depew, M.C.; Weir, D.; Wan, J.K.S. *Can. J. Chem.* **1982**, *60* 1504; (b) Chen, K.S.; Wan, J.K.S. *Chem. Phys. Lett.* **1979**, *57*, 285.
- [52] Kasack, V.; Kaim, W.; Binder, H.; Jordanov, J.; Roth, E. *Inorg. Chem.* **1995**, *34*, 1924;
- [53] Knödler, A.; Fiedler, J.; Kaim, W. *Polyhedron* **2004**, *23*, 701;
- [54] Kaim, W.; Kasack, V. *Inorg. Chem.* **1990**, *29*, 4696.
- [55] Moscherosch, M.; Field, J.S.; Kaim, W.; Kohlmann, S.; Krejcik, M. *J. Chem. Soc., Dalton Trans.* **1993**, 211.
- [56](a) Kaim, W.; Moscherosch, M. *J. Chem. Soc., Faraday Trans.* **1991**, *87*, 3185.
- [57] Barra, A.-L.; Brunel, L.-C.; Baumann, F.; Schwach, M.; Moscherosch, M.; Kaim, W. *J. Chem. Soc., Dalton Trans.* **1999**, 3855;
- [58] Remenyi, C.; Reviakine, R.; Kaupp, M. *J. Phys. Chem. A* **2006**, *110*, 4021.
- [59] Zanello, P. in *Ferrocenes: From Homogeneous Catalysis to Material Science* (Eds. T.

- Hayashi; A. Togni, VCH, Weinheim, **1995**, Chapter 7.
- [60](a) Sakamoto, R.; Murata, M.; Nishihara, H. *Angew. Chem.* **118** (2006) 4911; *Angew. Chem. Int. Ed.* **2006**, *45*, 4793.
- [61](a) Pawlas, J.; Nakao, Y.; Kawatsura, M.; Hartwig, J.F. *J. Am. Chem. Soc.* **124** (2002) 3669; (b) Hartwig, J.F. *Acc. Chem. Res.* **1998**, *31*, 852;
- [62] Cooke, M. W.; Cameron, T. S.; Robertson, K. N.; Swarts, J. C.; Aquino, M. A. S. *Organometallics* **2002**, *21*, 5962.
- [63] Kaim, W.; Sixt, T.; Weber, M.; Fiedler, J. *J. Organomet. Chem.* **2001**, *637-639*, 167.
- [64] Constable, E.C. *Chem. Ind. (London)* **1994**, 56;
- [65] Steel, P.J. *Acc. Chem. Res.* **2005**, *38*, 243.
- [66] Youinou, M.T.; Ramouni, N.; Fischer, J.; Osborn, J.A. *Angew. Chem.* **1992**, *104*, 771; *Angew. Chem. Int. Ed. Engl.* **1992**, *31*, 733;
- [67] Schwach, M.; Hausen, H.-D.; Kaim, W. *Chem. Eur. J.* **1996**, *2*, 446.
- [68] Nitschke, J.R.; Hutin, M.; Bernardinelli, G. *Angew. Chem.* **2004**, *116*, 6892; *Angew. Chem. Int. Ed.* **2004**, *43*, 6724
- [69] Krejcik, M.; Danek, M.; Hartl, F. *J. Electroanal. Chem.* **1991**, *317*, 179.
- [70] Roy, S.; Sieger, M.; Singh, P.; Niemeyer, M.; Fiedler, J.; Duboc, C.; Kaim, W. *Inorganica Chimica Acta*, **2008**, *361*, 1699.
- [71] (a) Chaudhuri, P.; Verani, C. N.; Bill, E.; Bothe, E.; Weyhermüller, T.; Wieghardt, K. *J. Am. Chem. Soc.* **2001**, *123*, 2213; (b) Ward, M.D.; McCleverty, J. A. *J. Chem. Soc. Dalton Trans.* **2002**, 275.
- [72] A. Modelli, D. Jones, S. Rossini, G. Distefano, *Tetrahedron* **1984**, *40*, 3257.
- [73](a) Roy, S.; Sieger, M.; Sarkar, B.; Schwederski, B.; Lissner, F.; Schleid, T.; Fiedler, J.; Kaim, W. *Angew. Chem. Int. Ed.* **2008**, *47*; (b) Roy, S.; Sieger, M.; Sarkar, B.; Schwederski, B.; Lissner, F.; Schleid, T.; Fiedler, J.; Kaim, W. *Angew. Chem.* **2008**, *120*,
- [74] Díez, J.; Gamasa, M. P.; Gimeno, J.; Aguirre, A.; García-Granda, S. *Organometallics* **1999**, *18*, 662.
- [75] Baldwin, D. A.; Lever, A. B. P.; Parish, R. V. *Inorg. Chem.* **1969**, *8*, 107.
- [76](a) Sarkar, B.; Patra, S.; Fiedler, J.; Sunoj, R. B.; Janadanan, D.; Mobin, S. M.; Niemeyer, M.; Lahiri, G. K.; Kaim, W. *Angew. Chem.* **2005**, *117*, 5800; *Angew. Chem. Int. Ed.* **2005**, *44*, 5655.
- [77] Sarkar, B.; Patra, S.; Fiedler, J.; Sunoj, R. B.; Janadanan, D.; Lahiri, G. K.; Kaim, W. *J. Am. Chem. Soc.* **2008**, *130*, 3532.
- [78] Sarkar, B.; Kaim, W.; Fiedler, J.; Duboc, C. *J. Am. Chem. Soc.* **2004**, *126*, 14706.

- [79] Frantz, S.; Hartmann, H.; Doslik, N.; Wanner, M.; Kaim, W.; Kümmerer, J. –H.; Denninger, G.; Barra, A. –L.; Duboc, C.; Fiedler, J.; Ciofini, I.; Urban, C.; Kaupp, M. *J. Am. Chem. Soc.* **2002**, *124*, 10563; Frantz, S.; Fiedler, J.; Hartenbach, I.; Schleid, T.; Kaim, W. *J. Organomet. Chem.* **2004**, 689, 3031.
- [80] Dogan, A.; Sarkar, B.; Klein, A.; Lissner, F.; Schleid, T.; Zališ, S.; Jain, V. K.; Kaim, W. *Inorg. Chem.* **2004**, *43*, 5973.
- [81](a) Kaim, W.; Kohlmann, S.; Jordanov, J.; Fenske, D. *Z. Anorg. Allg. Chem.* **1991**, *598/599*, 217; (b) Krejcik, M.; Zalis, S.; Klima, J.; Sykora, D.; Matheis, W.; Klein, A.; Kaim, W. *Inorg. Chem.* **1993**, *32*, 3362
- [82] (a) Doslik, N.; Sixt, T.; Kaim, W. *Angew. Chem.* **1998**, *110*, 2521; (b) Doslik, N.; Sixt, T.; Kaim, W. *Angew. Chem. Int. Ed.* **1998**, *37*, 2403.
- [83] Kohlmann, S. *Ph.D. Thesis, University of Stuttgart*, **1988**
- [84] Bock, H.; Dienelt, R.; Schödel, H.; Van, T. T. H. *Struct. Chem.* **1998**, *9*, 279.
- [85] Kaim, W.; Doslik, N.; Frantz, S.; Sixt, T.; Wanner, M.; Baumann, F.; Denninger, G.; Hanns, J.; Duboc, C.; Fiedler, J.; Zalis, S. *J. Mol. Struct.* **2003**, *656(1-2)*, 183
- [86] Barra, A.-L.; Brunel, L.-C.; Baumann, F.; Schwach, M.; Moscherosch, M.; Kaim, W. *J. Chem. Soc. Dalton Trans.* **1999**, 3855
- [87] Kohlmann, S.; Kaim, W. *Inorg. Chem.* **1987**, *26*, 1470
- [88] Doslik, N. *Ph.D. Thesis, University of Stuttgart* **1998**.
- [89] Schwach, M. *Ph.D. Thesis, University of Stuttgart* **1997**.
- [90] Mure, M. *Acc. Chem. Res.* **2004**, *37*, 131.
- [91] McIntire, W. S.; Wemmer, D. E.; Chistoserdov, A.; Lidstrom, M. E. *A. Science*, **1991**, *252*, 817
- [92] Janes, S. M.; Mu, D. ; Wemmer, D.; Smith, A. J.; Kaur, S.; Maltby, D.; Burlingame, A. L.; Klinman, J. P. *Science*, **1990**, *248*, 981;
- [93] Wang, S. X.; Mure, M.; Medzihradzky, K. F.; Burlingame, A. L.; Brown, D. E.; Dooley, D. M.; Smith, A. J.; Kagan, H. M.; Klinman, J. P. *Science*, **1996**, *273*, 1078;
- [94] (a) Matoba, Y.; Kumagai, T.; Yamamoto, H.; Yoshitsu, H.; Sugiyama, M. *J. Biol. Chem.* **2006**, *281*, 8981;
- [95] Decker, H.; Schweikardt, T.; Tuzcek, F. *Angew. Chem. Int. Ed.* **2006**, *45*, 4546;
- [96] Klabunde, T.; Eicken, C.; Sacchettini, J. C.; Krebs, B. *Nat. Str. Biol.* **1998**, *5*, 1084;
- [97] Jazdzewski, B. A.; Tolman, W. B. *Coord. Chem. Rev.* **2000**, *200*, 633;
- [98] (a) Klinman, J. P.; Mu, D. *Annu. Rev. Biochem.* **1994**, *63*, 299;
- [99] Dooley, D. M. *J. Biol. Inorg. Chem.* **1999**, *4*, 1;

- [100] Dove, J. E.; Klinman, J. P. *Adv. Prot. Chem.* **2001**, 58, 141;
- [101] Izumi, Y.; Sawada, H.; Sakka, N.; Yamamoto, N.; Kume, T.; Katsuki, H.; Shimohama, S.; Akaike, A. *J. Neurosci. Res.* **2005**, 79, 849;
- [102](a) Hendrickson, D. N.; Pierpont, C. G. *Top. Curr. Chem.* **2004**, 234, 63;
- [103] Speier, G.; Tyeklár, Z.; Tóth, P.; Speier, E.; Tisza, S.; Rockenhauer, A.; Whalen, A. M.; Pierpont, C. G. *Inorg. Chem.* **2001**, 40, 176;
- [104](a) Rall, J.; Wanner, M.; Albrecht, M.; Hornung, F. M.; Kaim, W. *Chem. Eur. J.* **1999**, 5, 2802; (b) Rall, J.; Kaim, W. *J. Chem. Soc. Faraday Trans.* **1994**, 38, 207; (c) Kaim, W.; Kohlmann, S. *Inorg. Chem.* **1987**, 26, 1469;
- [105] Liu, R.; Goodell, B.; Jellison, J.; Amirbahman, A. *Environ. Sci. Technol.* **2005**, 39, 175 ;
- [106] Tsuruya, S. ; Yonezawa, T. ; Kato, H. *J. Phys. Chem.* **1974**, 78, 811 ;
- [107] Kunkely, H. ; Vogler, A. *J. Photochem. Photobiol. A: Chem.* **2002**, 147, 149;
- [108] Matsuzaki, S. Y.; Gotoh, M.; Kuboyama, A. *Mol. Cryst. Liq. Cryst.* **1987**, 142, 127.
- [109] Poupko, R.; Rosenthal, I. *J. Phys. Chem.* **1973**, 77, 1722.
- [110] Kahn, O; Prins, R.; Reedijk, J.; Thompson, J. S. *Inorg. Chem.* **1987**, 26, 3557;
- [111] Berreau, L. M.; Mahapatra, S.; Halfen, J. A.; Houser, R. P.; Young, Jr. V. G.; Tolman, W. B. *Angew. Chem.* 1999, **111**, 180; *Angew. Chem. Int. Ed.* **1999**, 38, 207;
- [112](a) Uppadine, L. H.; Gisselbrecht, J.-P.; Kyritsakas, N.; Nättinen, K.; Rissanen, K.; Lehn, J.-M. *Chem. Eur. J.* **2005**, 11, 2549;
- [113] Bassani, D. M.; Lehn, J.-M.; Serroni, S.; Puntoriero, F.; Campagna, S. *Chem. Eur. J.* **2003**, 9, 5936;
- [114] Akasaka, T.; Otsuki, J.; Araki, K. *Chem. Eur. J.* **2002**, 8, 130.
- [115] Collman, J. P.; Devaraj, N. K.; Decréau, R. A.; Yang, Y.; Yan, Y.-L.; Ebina, W. Eberspacher, T. A.; Chidsey, C. E. D. *Science* **2007**, 315, 1565.
- [116] Gordon, K. C.; David, G.; Walsh, T. J. *Spectrochim. Acta Part A: Mol. Biomol. Spectrosc.* **2008**, in press, and literature cited; doi: 10.1016/j.saa.2008.07.039
- [117] Kitagawa, S.; Masaoka, S. *Coord. Chem. Rev.* **2003**, 246, 73-88
- [118] Baxter, P. N. W.; Lehn, J. M.; Baum, G.; Fenske, D. *Chem. Eur. J.* **1999**, 5, 102
- [119] Bu, X. -H.; Biradha, K.; Yamaguchi, T.; Nishimura, M.; Ito, T.; Tanaka, K.; Shionoya, M. *Chem. Commun.* **2000**, 1953
- [120] Piglosiewicz, I. M.; Beckhaus, R.; Saak, W.; Haase, D. J. *Am. Chem. Soc.* **2005**, 127, 14190;
- [121] Rutherford, T. J.; Van Gijte, O.; Masmaker, A. K. D.; Keene, R. F. *Inorg. Chem.* **1997**,

36, 4465

[122] Ong, C. W.; Liao, S. C.; Chang, T. H.; Hsu, H. F. *Tet. Lett.* **2003**, *44*, 1477

[123] Crispin, X.; Cornil, J.; Friedlein, R.; Okumudaira, K. K.; Lemaury, V.; Crispin, A.; Kestemont, G.; Lehmann, M.; Fahlman, M.; Lazzaroni, R.; Geerts, Y.; Wendin, G.; Ueno, N.; Bredas, J. -L.; Salaneck, W. R. *J. Am. Chem. Soc.* **2004**, *126*, 11889

[124](a) Barlow, S.; Zhang, Q.; Kaafarani, B. R.; Risko, C.; Amy, F.; Chan, C. K.; Domercq, B.; Starikova, Z. A.; Antipin, M. Y.; Timofeeva, T. V.; Kippelen, B.; Bredas, J.; Kahn, A.; Marder, S. R. *Chem. Eur. J.* **2007**, *13*, 3537;

[125] Alfonso, M.; Stoeckli-Evans, H.; *Acta Crystallogr., Sect. E: Struct. Rep. Online* **2001**, *E57*, o242;

[126] Catalano, V. J.; Larson, W. E.; Olmstead, M. M.; Gray, H. B. *Inorg. Chem.* **1994**, *34*, 4502;

[127](a) Patra, S.; Sarkar, B.; Ghumaan, S.; Fiedler, J.; Kaim, W.; Lahiri, G. K. *Dalton Trans.* **2004**, 754; (b) Ghumaan, S.; Sarkar, B.; Patil, M. P.; Fiedler, J.; Sunoj, R. B.; Kaim, W.; Lahiri, G. K. *Polyhedron* **2007**, *26*, 3409.

[128] Stěpnička, P. *Ferrocenes: Ligands, Materials and Biomolecules*, Wiley, Hoboken, **2008**

[129] Roy, S.; Sarkar, B.; Bubrin, D.; Niemeyer, M.; Zališ, S. Lahiri, G. K. *J. Am. Chem. Soc.* **2008**, *130*, 15230.

[130] Kaim, W.; Lahiri, G. K. *Angew. Chem.* 2007, *119*, 1808; *Angew. Chem. Int. Ed.* **2007**, *46*, 1778.

[131] Kaim, W.; Sarkar, B.; Lahiri, G. K. in *Spectroelectrochemistry*, Kaim, W.; Klein, A.; Royal Society of Chemistry (Cambridge), **2008**, p 68.

[132] Das, N.; Arif, A. M.; Stang, P. J.; Sieger, M.; Sarkar, B.; Kaim, W.; Fiedler, J. *Inorg. Chem.* **2005**, *44*, 5798

[133] Sixt, T.; Fiedler, J.; Kaim, W. *Inorg. Chem. Commun.* **2000**, *3*, 80.

[134] Kaim, W.; Ernst, S.; Kasack, V. *J. Am. Chem. Soc.* **1990**, *112*, 173.

[135](a) Barlow, S.; Zhang, Q.; Kaafarani, B. R.; Risko, C.; Amy, F.; Chan, C. K.; Domercq, B.; Starikova, Z. A.; Antipin, M. Y.; Timofeeva, T. V.; Kippelen, B.; Bredas, J.; Kahn, A.; Marder, S. R. *Chem. Eur. J.* **2007**, *13*, 3537;

[136] Alfonso, M.; Stoeckli-Evans, H.; *Acta Crystallogr., Sect. E: Struct. Rep. Online* 2001, *E57*, o242;

[137] Catalano, V. J.; Larson, W. E.; Olmstead, M. M.; Gray, H. B. *Inorg. Chem.* **1994**, *34*, 4502;

[138] Sheldrick, G. M.; *Programme SHELXS*: Göttingen, **1997**;

- [139] Sheldrick, G. M.; *Programme SHELXL*: Göttingen, **1997**;
- [140] Herrendorf, W.; Bärnighausen, H. *Programme HABITUS*: Giessen, Karlsruhe, **1993**,
Giessen, **1996**;
- [141] CRYSTAL IMPACT *Programme DAIMOND, Version 2.1e*: Bonn, **2001**.

Abbreviations.

| | |
|----------------------------------|--|
| a | Hyperfine coupling constant |
| a_0 | isotropic hyperfine constant |
| A | ampere |
| abb. | Abbildung |
| abcp | azo bis(5-chloropyrimidine) |
| abpy | 2,2'-azobispyridine |
| acac | acetylacetonate |
| adcO ^t Bu | di- <i>tert.</i> -butylazodicarboxylic ester |
| adcO ⁱ Pr | di- <i>iso.</i> -propylazodicarboxylic ester |
| adc-pip | azodicarboxylic dipiperidide |
| adc-NMe ₂ | N,N,N',N'-tetramethylazodicarboxamide |
| av | average |
| b | broad (IR band) |
| B | magnetic field |
| bdph / hexaPhos | 1,5-bis(diphenylphosphino)hexane |
| bdpp / pentaPhos | 1,5-bis(diphenylphosphino)penane |
| bptz | 3,6-bis(2-pyridyl)-1,2,4,5-tetrazine |
| Bu ₄ NPF ₆ | tetrabutylammonium hexafluorophosphate |
| calc. | calculated |
| cm | centimetre |
| Cl | chloro |
| Cp | cyclopentadienyl |
| d | doublet / bond length |
| dd | doublet of a doublet |
| diPhos | 1,2-bis(diphenylphosphino)ethane |
| δ | chemical shift |
| dm | decimetre |
| DMF | dimethylformamide |
| dmsO | dimethylsulfoxide |
| dppf | 1,1'-bis(diphenylphosphino)ferrocene |
| dqp | Diquinoxalino[2,3-a:2',3'-c]phenazine |
| E _{pa} | anodic peak potential |
| E _{pc} | cathodic peak potential |

| | |
|-----------------------|-------------------------------------|
| ϵ | molar extinction coefficient |
| EPR | electron paramagnetic resonance |
| exp | experimental |
| $\text{FeCp}_2^{0/+}$ | ferrocene / ferrocenium |
| fig | figure |
| g | gram |
| GHz | gigahertz |
| HAT | 1,4,5,8,9,12-hexaazatriphenylene |
| HATN | hexaazatriphenylene |
| HOMO | highest occupied molecular orbital |
| Hz | hertz |
| I | nuclear spin |
| IR | infrared |
| irr | irreversible |
| iso | isotropic |
| IVCT | inter valence charge transfer |
| k | rate constant |
| K_c | comproportionation constant |
| L | ligand |
| λ | wavelength |
| LLCT | ligand to ligand charge transfer |
| LMCT | ligand to metal charge transfer |
| LUMO | lowest unoccupied molecular orbital |
| M | molar / metal |
| max | maximum |
| Me | methyl |
| MeOH | methanol |
| MHz | megahertz |
| ml | millilitre |
| MLCT | metal to ligand charge transfer |
| mm | millimeter |
| mmol | millimole |
| MO | molecular orbital |
| mol | mole |

| | |
|------------|---|
| mT | militesla |
| mV | milivolt |
| v | wavenumbers |
| NIR | near infrared |
| nm | nanometer |
| NMR | nuclear magnetic resonance |
| ° | degree |
| °C | degree centigrade |
| <i>o</i> | ortho |
| OTTLE cell | optically transparent thin layer electrochemical cell |
| Ox | oxidized |
| <i>p</i> | para |
| Ph | phenyl |
| PhenQ | 9,10-phenanthrene quinone |
| PhenSQ | 9,10-phenanthrene semiquinone |
| ppm | parts per million |
| red | reduced |
| RT | room temperature |
| s | strong (IR band) / singlet |
| S | electron spin |
| SCE | standard calomel electrode |
| sh | shoulder |
| sim | simulated |
| SOMO | singly occupied molecular orbital |
| t | triplet |
| T | temperature / Tesla |
| Tab | table |
| THF | tetrahydrofuran |
| UV | ultra violet |
| V | volt |
| vs. | very strong (IR band) |
| vs. | versus |
| vis | visible |
| ω | dihedral angle |

Z

atomic number

Curriculum Vitae

Personal profile:

Name: Sayak Roy
Sex: Male
Date of Birth: 27-12-1981
Nationality: Indian
Marital Status: Single
Languages known: English, Bengali, Hindi
Address: Sayak Roy
C/O Prof. Dr. Wolfgang Kaim
Institut für Anorganische Chemie
Universität Stuttgart
Pfaffenwaldring 55
70569 Stuttgart
Germany

Studies:

1992 to 1998: Ramakrishna Vivekananda Mission, Barrackpore, West Bengal, India

1998 to 2000: Sodepur Chandrachur Vidyapith, Kolkata, India

2000 to 2003: *University of Calcutta*, Kolkata, West Bengal
Degree obtained: Bachelor of Science in Chemistry

2003 to 2005: *Indian Institute of Technology, Kharagpur*, West Bengal, India
Degree obtained: Master of Science in Chemistry
Master Thesis was titled as 'Synthesis, characterization, structure and properties of cationic Ruthenium (II) compounds' under the supervision of Prof. Dr. Manish Bhattacharjee.

August 2005 to April 2009: Doctoral work at the *Institut für Anorganische Chemie, Stuttgart* under the guidance of Prof. Dr. Wolfgang Kaim.
Title: Detailed Structural and Spectroscopic Studies on Radical and Non-radical Ferrocenylcopper(I) complexes.

Position Held:

August 2005 to January 2006:
Wissenschaftliche Hilfskraft at the Institut für Anorganische Chemie der Universität Stuttgart

February 2006 to April 2009:
Wissenschaftliche Angestellte at the Institut für Anorganische Chemie der Universität Stuttgart